University of Alberta

Re-Os Geochronology of Oxide Minerals

by

Joshua Davies

A thesis submitted to the Faculty of Graduate Studies and Research
in partial fulfillment of the requirements for the degree of

Master of Science

Earth and Atmospheric Science

©Joshua Davies
Spring 2010
Edmonton, Alberta

Examining Committee

Dr. Rob Creaser, Earth and Atmospheric Science

Dr. Larry Heaman, Earth and Atmospheric Science

Dr. Claire Currie, Physics

Abstract

^{187}Re-^{187}Os analysis of magnetite and other oxide minerals from various well dated geological settings (kimberlites, lamprophyres, Manicouagan impact melt rock, Great Bear magmatic zone iron ore deposits and Laramie Anorthosite complex) worldwide have been used to investigate the potential for precise geochronology. ^{187}Re-^{187}Os isotopes in groundmass oxide minerals from kimberlites and lamprophyres are not suitable for emplacement geochronology due to low Re contents and large quantities of un-radiogenic Os. T_{RD} and T_{MA} ages can be calculated however, and correlate well with previously published depletion ages and large magmatic events in the overlying crust, indicating the effectiveness of this technique. Geochronology using magnetite from the remaining settings is imprecise due to very low Re and Os contents but the ages produced are in the correct area. Young ages produced from the Laramie anorthosite complex indicate that magnetite may have a low closure temperature to Os diffusion (~200-300ºC).

<u>Acknowledgements</u>

I would like to begin by thanking my supervisor Dr Rob Creaser for helping me develop an interesting and diverse thesis, despite the refusal of the Re-Os system in magnetite to date things properly. I would also like to thank Rob for all of the invaluable analytical support he has provided me with, and his availability for help whenever I have needed it. He has always allowed this project to be my own work but has steered me in the right direction whenever I needed it, for this I am extremely grateful.

I would also like to take the opportunity to thank Dr Larry Heaman who has consistently out-performed his role as committee member. He has offered numerous advice and suggestions throughout the project and has always had an open door. I really appreciate the conversations we have had, and always feel more motivated after them.

I also want to acknowledge Dr Tom Chacko for searching for magnetite samples for me with no prior notice, just through his own goodwill, and the same thanks also goes to Dr Andrew Locock, Dr Don Lindsey and Luke Ootes, who are also great people.

The analytical work for this thesis could not have been, or would have taken a lot longer without the help of Gayle Hatchard and Dr Steven Turgeon, their friendship has meant a lot to me throughout my time here.

Finally I would like to thank Emily for putting up with me talking ad nauseam about things she is not entirely interested in. All of the fun times we have together make hard work more manageable. I would also like to thank Annie Mac, for providing entertainment and motivation every week, two things that are essential for getting a thesis done.

Table of Contents

4

List of Figures

List of Tables

Appendix

1.0 Introduction

The application of the ^{187}Rhenuim-^{187}Osmium (^{187}Re-^{187}Os) isotope system to date both crustal and mantle samples has greatly expanded over the past two decades. This expansion has been facilitated by improvements to the analysis and innovations in mass spectrometry. Seminal advancements in the laboratory procedures include those made by Shirey and Walker (1995), who developed the carius tube method for sample digestion ensuring sample spike equilibration, and by Cohen and Waters (1996), who showed that Os could be easily extracted from a sample after acid digestion, without adversely affecting blanks. These improvements were instrumental to permitting sample spike homogenization and their techniques remain largely unchanged today. Innovative mass spectrometry advancements over the past few decades include the development of the negative thermal ionization method (Creaser et al., 1991; Volkening et al., 1991), which allowed for precise analysis of small Os samples and greatly improved ionization efficiency. Current analytical improvements are focused on reducing procedural blanks, and now permit ^{187}Re-^{187}Os geochronology to be determined from sulphide inclusions within diamonds (Richardson and Shirey, 2008; Stachel and Harris, 2008). Further procedural and analytical progress is needed before single sulphide grains (except molybdenite) in the crust can be analyzed, due to their extremely low ^{187}Re-^{187}Os contents.

The ^{187}Re-^{187}Os geochronometer has proven very useful in a variety of crustal settings due to the chalcophilic, siderophilic and organometallic nature of the elements (Selby et al., 2007b). These properties enable the isotope system

to provide information about many samples where other lithosphile systems (e.g., U-Pb, K-Ar, Rb-Sr, Sm-Nd) cannot, such as with ore deposits. Reliable and precise ^{187}Re-^{187}Os ages have been produced for a variety of different sulphide minerals (Morelli et al., 2005; Morelli et al., 2004; Stein et al., 2001; Stein et al., 2000), and also for igneous intrusions (Foster et al., 1996; Mondal et al., 2007). Furthermore, robust depositional ages have been produced for black shales (Kendall et al., 2006; Selby and Creaser, 2005), and progress has been made using the ^{187}Re-^{187}Os system to date hydrocarbon maturation and migration (Selby et al., 2005; Selby et al., 2007a).

Despite similar geochemical affinities, Re and Os behave differently during mantle melting, as Re is mildly incompatible and Os is strongly compatible with the residue (Pearson et al., 2004; Shirey and Walker, 1998). During crustal formation processes, highly contrasting Re/Os ratios are therefore generated between the crust and mantle. The differential partitioning of Re permits Os isotopes to be used as powerful tracers of mantle interactions with crustal rocks (e.g., Turgeon and Creaser, 2008), and it is part of the reason that so much work has been dedicated to the system.

The majority of precise dating work using the ^{187}Re-^{187}Os geochronometer has focused on the chalcophilic and organometallic properties of the elements, but there is also great potential for utilizing the system in other areas. For example, oxide minerals are extremely common within igneous, metamorphic and sedimentary rocks, and there are numerous rock suites in which the ^{187}Re-^{187}Os

9

system in oxides may provide the only method for dating. As the application of this isotope system for dating oxide minerals has not been widely used, verification is needed to prove that ^{187}Re-^{187}Os ages from oxides can be correlated with ages previously determined by U-Pb (or another reliable geochronometer) from the same sample. The research results presented in this thesis address the potential use of ^{187}Re-^{187}Os geochronology applied to the dating of oxide minerals. Specifically, it investigates the production of isochrons using these minerals, in a variety of igneous and ore settings, in samples where the age has been previously established. The main mineral group analyzed is spinel (XY_2O_4), due to its prevalence, its ease of extraction, and its formation under variable oxygen fugacities (fO_2), which may control Re partitioning during crystallization. The following sections outline the experimental reasons for choosing spinel, and discuss previous geochronological work using the ^{187}Re-^{187}Os system in this mineral.

1.1 Experimental work on Re and Os partitioning

Experimental studies investigating the partitioning of Re and Os between minerals and fluids have primarily focused on mantle melting, due to the different compatibilities of Re and Os (e.g., Fonseca et al., 2007; MacKenzie and Canil, 2006; Mallmann and O'Neill, 2007; Righter et al., 2004). There is little agreement in the conclusions drawn from these studies, which can be attributed to the complex behavior of Re. Re and Os are generally accepted to partition into sulphide phases when magmas are sulphur-saturated (Sproule et al., 2002), but there is much controversy over the behavior of Re when sulphur saturation is not reached and when fO_2 varies. Some experimental work has indicated that platinum group

10

elements (PGEs) and Re are compatible with spinel, (Righter and Downs, 2001), especially magnesoferrite ($MgFe_2O_4$). Conversely, recent experiments by Finnigan et al. (2008) suggest that PGEs do not partition into spinel group minerals, but rather, PGE metal nodules form in the locally reduced space around growing chromites, as opposed to partitioning into the mineral itself. These findings suggest that a small number of chromites within a magma could contain the majority of the PGE content of the melt, whereas the rest are relatively PGE free. Element mineral partitioning is extremely difficult to determine experimentally, which is part of the reason that controversy over Re partitioning (D_{Re}) exists. However, experimental work in many cases is the only method for quantifiable testing of elemental partitioning, and therefore is the best technique presently available. Experimental work by Righter et al. (2004) indicates that Re is not compatible with Cr rich spinel (chromite) under reducing conditions, and Re compatibility is controlled primarily by its Fe^{3+} content, indicating its dependence on fO_2. However, Mallmann and O'Neill (2007) suggest that the experimental results from Righter et al. (2004) could also be explained by the unintentional creation of PGE and Re micronuggets and thus question the validity of the Righter et al. (2004) conclusions. In their 2007 study, Mallmann and O'Neill found that Re was mildly incompatible in spinel ($MgAl_2O_4$) under reduced conditions, and became more incompatible with increased fO_2, opposite to the findings that of Righter et al. (2004). It is important to note, however, that Mallmann and O'Neill (2007) did not vary the composition of the spinel to assess the impact of oxidized iron in their study. Fonseca et al. (2007) found oxidized iron to be very influential on Re partitioning, suggesting that, under strongly oxidizing conditions, fO_2 controls Re partitioning rather than sulphur fugacity (fS_2), even in

the presence of sulphur. Righter et al. (2008) studied this finding in more detail by analyzing Re, Os and S contents from basalts in the Trans Mexican Volcanic Belt. Although they did not analyze pure spinel fractions from the basalts, they were able to model partition coefficients for Re into magnetite (Fe_3O_4) under a range of fO_2 values. They found that under oxidizing conditions (FMQ +1 to +3; fayalite-magnetite-quartz buffer), Re had a partition coefficient of 100 strongly favouring partitioning into magnetite, which is the highest for any basaltic mineral. However, under reducing conditions (FMQ -1), Re did not partition into magnetite. Righter et al. (2008) suggested that this behavior was due to the presence of sulphide in the source of the reduced basaltic magma, which caused Re to behave compatibly during melting. Under oxidized conditions, sulphide was no longer stable in the source region, causing Re to behave incompatibly, and to partition into a basaltic mineral, most likely magnetite. Righter et al. (2008) also noted that, under more silica saturated conditions, Re volatility may also be an issue, with up to 20% lost during degassing. These results are in agreement with earlier work done by Righter et al. (1998) on samples from the Galápagos Islands. Analysis of magnetite from these samples showed that Re can strongly partition into magnetite under oxidizing conditions, regardless of the presence of sulphur. Righter et al. (1998) calculated partition coefficients (D_{Re}) of 20-50 into magnetite. These values are smaller than those predicted in their 2008 work, but they represent a significant chemical forcing nonetheless.

Despite the uncertainty regarding the partition coefficients for Re into spinel, there is general agreement in the scientific community that Fe^{3+} and fO_2

12

play an important role in controlling the solubility of Re in spinel, and that under high silica conditions, Re may be lost during magma degassing (Righter et al., 1998). For these reasons, the main mineral focus of this research was chosen to be magnetite, which is the most oxidized, and the most Fe and Fe^{3+} rich of the spinel group minerals. The experimental work suggests that under oxidizing conditions, magnetite is the mineral into which Re is most likely to partition during crystallization from a mantle melt. Even though mantle melting is not identical to crustal melting, similar principles apply. For example, under oxidized conditions, in the absence of sulphide, spinel (magnetite) is expected to be the main source of Re in the crust as well as the mantle.

1.2 Previous geochronology using the ^{187}Re-^{187}Os in oxide magnetite and other oxide minerals

To date, there has been limited ^{187}Re-^{187}Os geochronology performed using magnetite. This is mostly attributable to the low Re and Os content and ratios in magnetite (e.g. Gangopadhyay and Walker, 2003; Gervilla et al., 2005; Mathur et al., 2002; Morgan et al., 2000; Puchtel et al., 1999; Righter et al., 1998) in comparison to sulphide minerals. Morgan et al. (2000) suggest that variations in the Re and Os content and ratio of magnetite grains in the Suwaøki Anorthosite Massif in Poland may be due to micron sized inclusions of sulphide. The Re and Os values presented in Morgan et al. (2000) therefore likely represent maximal contents and ratios, since the presence of putative sulphide minerals would control the results rather than magnetite. If this were the case, precise geochronology using pure magnetite may not be possible due to the Re and Os contents being below detection limits.

13

To test this theory, magnetite geochronology should be performed in areas without co-genetic sulphide to ensure that magnetite is the host, and then the true Re and Os content of magnetite can be assessed. The majority of previous studies analyzing [187]Re-[187]Os isotopes in magnetite (Mathur et al., 2002; Yang et al., 2008) have not taken this interaction into account. Rather, they have analyzed samples that contain both sulphide and magnetite minerals with the assumption that Re and Os isotopes in both mineral groups behave in the same manner, which may not be the case.
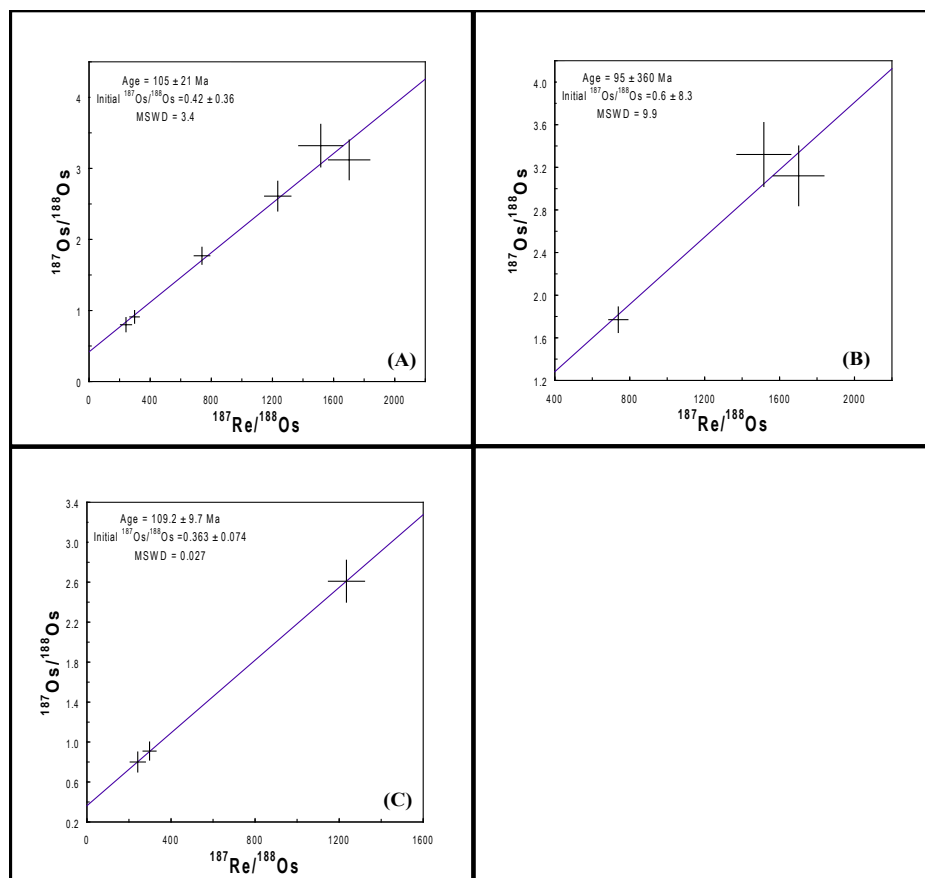
Figure 1

Re-Os diagrams of data from Mathur et al. (2002), created with ISOPLOT Ex3 (Ludwig, 2003) and full error propagation. Diagram (A) combined magnetite and chalcopyrite isochron (B) Chalcopyrite mineral isochron (C) Magnetite mineral isochron.

For example, Mathur et al., (2002) use chalcopyrite and magnetite from a Fe-Cu-Au deposit in Candelaria, Chile, to constrain the age of mineralization at 110±9 Ma. This value was re-calculated in this study to be 105±21 Ma (Figure 1A) using ISOPLOT Ex3 and fully propagated errors (which is how all further geochronological data presented has been processed). The age reported by Mathur et al. (2002), although calculated using 6 data points (3 chalcopyrite, 3 magnetite), is entirely constrained by magnetite (3 point magnetite age of 109.2±9.7 Ma, (Figure 1B)), with the chalcopyrite samples plotting above and below the isochron (3 point chalcopyrite age 95±360 Ma, Figure 1C). This result indicates that magnetite can provide useful age information even in the presence of sulphide, and suggests that magnetite may be a more suitable mineral for geochronology in certain cases. It should be noted however, that Mathur et al. (2002) did not prove the purity of the magnetite and so the ^{187}Re-^{187}Os information may still be controlled by sulphide inclusions similar to the study of Morgan et al. (2000). Magnetite ^{187}Re-^{187}Os data from other local iron oxide deposits is also presented in the Mathur et al. (2002) paper, although no age information can be obtained from these minerals. Mathur et al. (2002) suggest that the lack of age information from these magnetites is attributable to leaching of Re and Os from surrounding sediments during ore genesis. Their explanation suggests that Re and Os age information in magnetite may be compromised during hydrothermal alteration. In a reply to Mathur et al. (2002), Naslund et al. (2003) suggested that the lack of age information obtainable from the magnetite Re and Os data could be due to multiple generations of magnetite rather than ^{187}Re-^{187}Os disturbances from hydrothermal alteration. This alternate conclusion supports the discordant data, but does not provide insight into the possibility of hydrothermal

15

resetting of magnetite. No published work has discussed this possibility directly, although Peucker-Ehrenbrink and Blum (1998) showed that oxidative weathering of magnetite mobilizes Os, but did not evaluate the impact of hydrothermal fluid interaction on the isotope system. Some authors also comment on the possible closure temperature of magnetite for the [187]Re-[187]Os system. For example, Yang et al. (2008) suggest a value of ~500°C due to a pentlandite, pyrrhotite, chalcopyrite and magnetite isochron yielding an apparent age that corresponds approximately with a 500°C disturbance. Also, Lambert et al. (2000) discuss the possibility of [187]Re-[187]Os systematic disturbances in magnetite, whose existence is supported by a chalcopyrite, pentlandite, pyrrhotite, magnetite, ilmenite and whole rock isochron ages that appear to have been reset by a Grenville age event. The authors do not discuss the possible temperature and pressure conditions required for resetting, but do suggest the possibility of hydrothermal alteration mobilizing Re and Os. All of these studies suggest that in order to successfully determine the usefulness of the [187]Re-[187]Os system in magnetite, careful sample selection needs to take place. Samples need to be sourced from rocks which have not experienced medium-high grade metamorphism, or hydrothermal alteration. These processes would add potential sources of error to age determinations, and could compromise the results.

A study of [187]Re-[187]Os isotopes in oxide minerals from kimberlites, melnoites and carbonatites completed by Graham et al. (2004) found that magnetite and chromite preserved accurate and precise [187]Re-[187]Os emplacement ages. In contrast, sulphide minerals from the same rocks showed evidence of recent Re addition, and therefore were compromised for Re-Os geochronology. These findings indicate

16

that oxide minerals may contain accurate age information even in altered rocks, and is further evidence that magnetite contains accurate and precise ^{187}Re-^{187}Os age information. In earlier work, Graham et al. (2002) showed the potential use of the Re-Os system in calculating model ages (T_{CHUR}) in ilmenite, a technique that could be used to help understand the timing of lithospheric enrichment and growth events (Walker et al., 1989). However, the ilmenite minerals were a composite, and may have contained sulphides or other oxide phases. Thus it remains unclear as to exactly which mineral controlled the Re-Os systematics in the material analyzed. The study highlights the possibility of using the ^{187}Re-^{187}Os system to calculate Re model ages (T_{MD}) and Re depletion ages (T_{RD}) (Walker et al., 1989) from mantle oxides. Additional analysis is needed to assess which minerals constrain the age.

The conditions under which magnetite retains ^{187}Re-^{187}Os geochronological information are still unknown. Additional investigative work in this area is necessary to better understand the ^{187}Re-^{187}Os systematics in magnetite, and to ascertain the conditions under which the mineral can and cannot be reliably used for geochronology.

The research presented here addresses the potential for ^{187}Re-^{187}Os magnetite geochronology, in a variety of environments. To minimize avoidable Re and Os loss or gain from magnetite, this study focuses on magnetite with no oxidative weathering, obtained from areas that have not experienced post-crystallization hydrothermal alteration or high grade metamorphism. Focusing on unaltered minerals simplifies the ^{187}Re-^{187}Os systematics, and permits more conclusive

interpretations to be drawn from the results. Additionally, magnetite samples are selected from areas where good age control has already been established, in order to assess the reliability and accuracy of this method.

The analysis presented is divided into the following sections:

2.   A detailed description of the methodology used in this study, including mineral separation techniques, full and procedural blank analysis and other analytical procedures.

3.   A study of Re depletion ages (T_{RD}), calculated using oxide minerals from a range of North American and South African kimberlites and lamprophyres. The reliability of the age information obtained, the controlling minerals and the magma source material are all examined.

4.   A geochronological study of ^{187}Re-^{187}Os isotopes from crustal magnetite in a variety of geological settings: the Manicouagan impact melt rock; the Great Bear Magmatic Zone (GBMZ); and the Sybille Fe-Ti oxide deposit from the Laramie Anorthosite Complex.

These sections will be followed by a concluding discussion of the implications of the findings of this research.

18

1.3 References

Cohen, A.S. and Waters, F.G., 1996. Separation of osmium from geological materials by solvent extraction for analysis by thermal ionisation mass spectrometry. Analytica Chimica Acta, 332(2-3): 269-275.

Creaser, R.A., Papanastassiou, D.A. and Wasserburg, G.J., 1991. Negative thermal ion mass spectrometry of osmium, rhenium and iridium. Geochimica Et Cosmochimica Acta, 55(1): 397-401.

Finnigan, C.S., Brenan, J.M., Mungall, J.E. and McDonough, W.F., 2008. Experiments and models bearing on the role of chromite as a collector of platinum group minerals by local reduction. Journal of Petrology, 49(9): 1647-1665.

Fonseca, R.O.C., Mallmann, G., O'Neill, H.S.C. and Campbell, I.H., 2007. How chalcophile is rhenium? An experimental study of the solubility of Re in sulphide mattes. Earth and Planetary Science Letters, 260(3-4): 537-548.

Foster, J.G., Lambert, D.D., Frick, L.R. and Maas, R., 1996. Re-Os isotopic evidence for genesis of Archaean nickel ores from uncontaminated komatiites. Nature, 382(6593): 703-706.

Gangopadhyay, A. and Walker, R.J., 2003. Re-Os systematics of the ca. 2.7-Ga komatiites from Alexo, Ontario, Canada. Chemical Geology, 196(1-4): 147-162.

Gervilla, F. et al., 2005. Distribution of platinum-group elements and Os isotopes in chromite ores from Mayari-Baracoa Ophiolitic Belt (eastern Cuba). Contributions to Mineralogy and Petrology, 150(6): 589-607.

Graham, S., Lambert, D. and Shee, S., 2004. The petrogenesis of carbonatite, melnoite and kimberlite from the Eastern Goldfields Province, Yilgarn Craton. Lithos, 76(1-4): 519-533.

Graham, S., Lambert, D.D., Shee, S.R. and Pearson, N.J., 2002. Juvenile lithospheric mantle enrichment and the formation of alkaline ultramafic magma sources: Re-Os, Lu-Hf and Sm-Nd isotopic systematics of the Norseman melnoites, Western Australia. Chemical Geology, 186(3-4): 215-233.

Kendall, B., Creaser, R.A. and Selby, D., 2006. Re-Os geochronology of postglacial black shales in Australia: Constraints on the timing of "Sturtian" glaciation. Geology, 34(9): 729-732.

Lambert, D.D., Frick, L.R., Foster, J.G., Li, C.S. and Naldrett, A.J., 2000. Re-Os isotope systematics of the Voisey's Bay Ni-Cu-Co magmatic sulfide system, Labrador, Canada: II. Implications for parental magma chemistry ore genesis, and metal redistribution. Economic Geology and the Bulletin of the Society of Economic Geologists, 95(4): 867-888.

Ludwig, K.R., 2003. User's manual for ISOPLOT/EX, version 3. A geochronological toolkit for Microsoft Excel, Berkeley Geochronology Center. Special Publication 4: 60.

MacKenzie, J.M. and Canil, D., 2006. Experimental constraints on the mobility of Rhenium in silicate liquids. Geochimica Et Cosmochimica Acta, 70(20): 5236-5245.

Mallmann, G. and O'Neill, H.S.C., 2007. The effect of oxygen fugacity on the partitioning of Re between crystals and silicate melt during mantle melting. Geochimica Et Cosmochimica Acta, 71(11): 2837-2857.

Mathur, R. et al., 2002. Age of mineralization of the candelaria Fe oxide Cu-Au deposit and the origin of the Chilean iron belt, based on Re-Os isotopes. Economic Geology and the Bulletin of the Society of Economic Geologists, 97(1): 59-71.

Mondal, S.K., Frei, R. and Ripley, E.M., 2007. Os isotope systematics of mesoarchean chromitite-PGE deposits in the Singhbhum Craton (India): Implications for the evolution of lithospheric mantle. Chemical Geology, 244(3-4): 391-408.

Morelli, R.M., Creaser, R., Selby, D., Kontak, D.J. and Horne, R.J., 2005. Rhenium-osmium geochronology of arsenopyrite in Meguma group gold deposits, Meguma terrane, Nova Scotia, Canada: Evidence for multiple gold-mineralizing events. Economic Geology, 100(6): 1229-1242.

Morelli, R.M. et al., 2004. Re-Os sulfide geochronology of the Red Dog sediment-hosted Zn-Pb-Ag deposit, Brooks Range, Alaska. Economic Geology, 99(7): 1569-1576.

Morgan, J.W., Stein, H.J., Hannah, J.L., Markey, R.J. and Wiszniewska, J., 2000. Re-Os study of Fe-Ti-V oxide and Fe-Cu-Ni sulfide deposits, Suwalki Anorthosite Massif, northeast Poland. Mineralium Deposita, 35(5): 391-401.

Naslund, H.R., Lledo, H. and Henriquez, F., 2003. Age of mineralization of the Candelaria Fe oxide Cu-Au deposit and the origin of the Chilean iron belt, based on Re-Os isotopes - A discussion. Economic Geology and the Bulletin of the Society of Economic Geologists, 98(5): 1047-1049.

Pearson, D.G., Irvine, G.J., Ionov, D.A., Boyd, F.R. and Dreibus, G.E., 2004. Re-

Os isotope systematics and platinum group element fractionation during mantle melt extraction: a study of massif and xenolith peridotite suites. Chemical Geology, 208(1-4): 29-59.

Peucker-Ehrenbrink, B. and Blum, J.D., 1998. Re-Os isotope systematics and weathering of Precambrian crustal rocks: Implications for the marine osmium isotope record. Geochimica Et Cosmochimica Acta, 62(19-20): 3193-3203.

Puchtel, I.S., Brugmann, G.E. and Hofmann, A.W., 1999. Precise Re-Os mineral isochron and Pb-Nd-Os isotope systematics of a mafic-ultramafic sill in the 2.0 Ga Onega plateau (Baltic Shield). Earth and Planetary Science Letters, 170(4): 447-461.

Richardson, S.H. and Shirey, S.B., 2008. Continental mantle signature of Bushveld magmas and coeval diamonds. Nature, 453(7197): 910-913.

Righter, K., Campbell, A.J., Humayun, M. and Hervig, R.L., 2004. Partitioning of Ru, Rh, Pd, Re, Ir, and Au between Cr-bearing spinel, olivine, pyroxene and silicate melts. Geochimica Et Cosmochimica Acta, 68(4): 867-880.

Righter, K., Chesley, J.T., Calazza, C.M., Gibson, E.K. and Ruiz, J., 2008. Re and Os concentrations in arc basalts: The roles of volatility and source region fO(2) variations. Geochimica Et Cosmochimica Acta, 72(3): 926-947.

Righter, K., Chesley, J.T., Geist, D. and Ruiz, J., 1998. Behavior of Re during magma fractionation: an example from Volcan Alcedo, Galapagos. Journal of Petrology, 39(4): 785-795.

Righter, K. and Downs, R.T., 2001. The crystal structures of synthetic Re- and PGE-bearing magnesioferrite spinels: Implications for impacts, accretion

and the mantle. Geophysical Research Letters, 28(4): 619-622.

Selby, D. and Creaser, R.A., 2005. Direct radiometric dating of the Devonian-Mississippian time-scale boundary using the Re-Os black shale geochronometer. Geology, 33(7): 545-548.

Selby, D., Creaser, R.A., Dewing, K. and Fowler, M., 2005. Evaluation of bitumen as a Re-187-Os-187 geochronometer for hydrocarbon maturation and migration: A test case from the Polaris MVT deposit, Canada. Earth and Planetary Science Letters, 235(1-2): 1-15.

Selby, D., Creaser, R.A. and Fowler, M.G., 2007a. Re-Os elemental and isotopic systematics in crude oils. Geochimica Et Cosmochimica Acta, 71(2): 378-386.

Selby, D., Creaser, R.A., Stein, H.J., Markey, R.J. and Hannah, J.L., 2007b. Assessment of the Re-187 decay constant by cross calibration of Re-Os molybdenite and U-Pb zircon chronometers in magmatic ore systems. Geochimica Et Cosmochimica Acta, 71(8): 1999-2013.

Shirey, S.B. and Walker, R.J., 1995. Carius tube digestion for low-blank rhenium-osmium analysis. Analytical Chemistry, 67(13): 2136-2141.

Shirey, S.B. and Walker, R.J., 1998. The Re-Os isotope system in cosmochemistry and high-temperature geochemistry. Annual Review of Earth and Planetary Sciences, 26: 423-500.

Sproule, R.A., Lambert, D.D. and Hoatson, D.M., 2002. Decoupling of the Sm-Nd and Re-Os isotopic systems in sulphide-saturated magmas in the Halls Creek Orogen, Western Australia. Journal of Petrology, 43(2): 375-402.

Stachel, T. and Harris, J.W., 2008. The origin of cratonic diamonds - Constraints

from mineral inclusions. Ore Geology Reviews, 34(1-2): 5-32.

Stein, H.J., Markey, R.J., Morgan, J.W., Hannah, J.L. and Schersten, A., 2001. The remarkable Re-Os chronometer in molybdenite: how and why it works. Terra Nova, 13: 479-486.

Stein, H.J., Morgan, J.W. and Schersten, A., 2000. Re-Os dating of low-level highly radiogenic (LLHR) sulfides: The Harnas gold deposit, southwest Sweden, records continental-scale tectonic events. Economic Geology and the Bulletin of the Society of Economic Geologists, 95(8): 1657-1671.

Turgeon, S.C. and Creaser, R.A., 2008. Cretaceous oceanic anoxic event 2 triggered by a massive magmatic episode. Nature, 454(7202): 323-U29.

Volkening, J., Walczyk, T. and G. Heumann, K., 1991. Osmium isotope ratio determinations by negative thermal ionization mass spectrometry. International Journal of Mass Spectrometry and Ion Processes, 105(2): 147-159.

Walker, R.J., Carlson, R.W., Shirey, S.B. and Boyd, F.R., 1989. Os, Sr, Nd and Pb isotope systematics of Southern African peridotite xenoliths - implications for the chemical evolution of subcontinental mantle. Geochimica Et Cosmochimica Acta, 53(7): 1583-1595.

Yang, S.H. et al., 2008. Origin of the inconsistent apparent Re-Os ages of the Jinchuan Ni-Cu sulfide ore deposit, China: Post-segregation diffusion of Os. Chemical Geology, 247(3-4): 401-418.

2 Methodology

2.1 Introduction

The ^{187}Re-^{187}Os system has provided the geochemist with many intrinsic analytical obstacles, which are partly the reason the system has taken so long to become a commonly used geochronological tool. Osmium is one of earth's least abundant elements and also has an extremely high ionization potential (8.7 eV Volkening et al., 1991) making it extremely difficult to analyze by conventional mass spectrometry. The first attempts to analyze the ^{187}Re-^{187}Os system were made by Naldrett and Libby (1948) who determined that ^{187}Re decayed via beta ($^-\beta$) emission to ^{187}Os. They also were able to estimate the half life of ^{187}Re at 4 ± 1 x10^{12} a^{-1} using direct counting methods. The decay energy of ^{187}Re is very small however, (2.65 keV) making these types of half life determinations extremely difficult. Refinements to the half life of ^{187}Re were made in the 1950's by Herr et al., (1954) who moved away from counting methods and analyzed a molybdenite sample. They were unable to produce an age for the mineral but were able to show that the half life calculated by Naldrett and Libby, (1948) was too long, and estimated a new half life of 5x10^{10} a^{-1}. Precise and accurate geochronology using the ^{187}Re-^{187}Os system was not possible for another 40 years when the negative ion, thermal ionization mass spectrometry (N-TIMS) (Creaser et al., 1991; Volkening et al., 1991), and carius tube methods of sample digestion (Shirey and Walker, 1995) were developed. These techniques negated the problems created by osmium's poor ionization efficiency and incomplete sample spike equilibration, the latter due to

the presence of multiple Os valences. Since the introduction of these analytical methods, ^{187}Re-^{187}Os analyses have flourished and have become the tool of choice for dating sulphide ore systems, and organic rich sedimentary rocks (Creaser et al., 2002; Stein et al., 2001). Standard methods for Re and Os isotopic separation and analysis have now been developed such that procedural blanks can be <1pg for Os and <5pg for Re (using aqua regia digestion) (Morelli et al., 2005; Morelli et al., 2004) which has allowed precise and accurate geochronology from very low level ^{187}Re-^{187}Os samples. These techniques have been fully utilized by this study to allow for a comprehensive investigation of ^{187}Re-^{187}Os geochronology in magnetite. This study uses modified versions of the isotope dilution techniques developed at the Radiogenic Isotope Facility at the University of Alberta to determine Re and Os isotopes (Creaser et al., 2002; Morelli et al., 2004; Selby and Creaser, 2001a; Selby and Creaser, 2001b) and are described below.

The methods for sample preparation will be split into two sections where appropriate due to the different procedures used for two main scopes of this study – 1) attempts at geochronology using magnetite; and 2) a T_{RD} study of oxide minerals from kimberlites, lamprophyres, and carbonatites from North American and South Africa.

2.2 Sample preparation (1)

Massive magnetite and whole rock samples were collected from the Manicouagan impact crater Québec by Dr J. Ramezani of MIT; the Great Bear Magmatic Zone (GBMZ) Northwest Territories by the Northwest Territories Geoscience Office; and

26

the Laramie Anorthosite Complex (LAC) Sybille Pit Wyoming by Dr T. Chacko and brought to the University of Alberta. Massive magnetite was then cut into 4-6 pieces, approximately 5 cm³ volume (30g) using a rock saw in order to remove weathered sections. The samples were then ground to remove any drilling marks. Weathered sections of the minerals were removed to avoid possible loss of Re and Os and subsequent disturbance of the Re-Os isotopic system (Peucker-Ehrenbrink and Blum, 1998). The samples were then coarsely crushed using an agate mill and purified using a hand magnetite before further purified by demagnetization which is explained and described below. Samples from the Manicouagan impact zone were received pre-separated and were inspected for purity before analysis.

2.2.1 Demagnetization

The separation of a pure magnetite fraction (which is required for [187]Re-[187]Os analysis) from other rock forming minerals is surprisingly difficult. Due to its ferromagnetic properties it is the most magnetic mineral and can therefore easily be separated from most other minerals in a rock powder using a hand magnet. However, this causes agglomeration of the magnetite as soon as it enters the magnetic field of the magnet. When the magnetite grains agglomerate, they commonly entrain other surrounding minerals and it is extremely difficult to separate the clumps. Other minerals encased in magnetite can become subsequently magnetized further complicating their separation. For these reasons, it is very difficult to obtain a pure magnetite separate using a hand magnet alone. Franz magnetic separators or magnetic freefall separation systems, which are commonly used to purify other minerals, are not a viable option for producing a pure magnetite separate. Hand

27

picking of minerals is time consuming, and due to the large volume required for ^{187}Re-^{187}Os analysis is not a viable option. In order to reduce the effect of magnetite agglomerates, a demagnetization step has been included in sample preparation for this study.

It has been known for a long time that magnetic materials can become demagnetized after an applied electromagnetic field is slowly removed and that this process occurs quicker under stronger electromagnetic fields. Smith (1961) showed that the use of an AC current is beneficial for demagnetizing magnetite but found that sample size can have an impact on the demagnetization. Work by Hopstock (2000) has taken this further, showing that magnetite fractions of >10μm do not become demagnetized under any electromagnetic field strengths. For this reason the samples collected for analysis by this study were coarsely ground using an agate mill to approximately 210-70μm before demagnetization. After coarse crushing the samples were collected using a hand magnet and added to deionized water in glass beakers. The samples were then placed into a solenoid for demagnetization. Due to the relatively low coercivity of magnetite (Hopstock, 2000), a magnetic field of 500-600 Gauss was applied to the sample for 10 seconds before being slowly moved out of the field. This process successfully separated magnetite agglomerates and the entrained grains and allowed further hand magnet purification. This process was repeated until no foreign minerals were removed from the sample (approximately 10 times total) and produced and extremely pure (>95%) magnetite fraction (although it should be noted that composite grains containing magnetite are not removed using this method). After demagnetization and purification, the

magnetite was ground to powder using an agate mill. The samples were then ready for Re-Os extraction and analysis.

2.3 Sample preparation (2)

Magnetic freefall mineral samples of 210-70μm were provided by Dr. Heaman from the University of Alberta from various kimberlites and lamprophyres from North America and South Africa. The magnetic freefall samples contained groundmass and xenocrystic spinel, ilmenite, perovskite and entrained silicates. The samples had previously been crushed in a steel carbide jaw crusher and consequently also contained flakes of steel from the crusher plates. Steel fragments from the crushing plates were analyzed for Re and Os and were found to contain 50 ppb Re and 1950 ppt Os which represents a serious contaminant, with Re and Os at levels over 1000 times that of some samples. Luckily the Re/Os ratio and Re-Os contents of the steel fragments were significantly different from all of the samples, making contamination easier to detect (Figure 2.1 and 2.2). To ensure that there was no steel contamination, all of the freefall samples were inspected by hand using a binocular microscope and tweezers to extract the steel shards. Figures 2.1 and 2.2 indicate that no samples showed signs of contamination, although sample DBJK2 and PJK3 showed Re-Os contents and Re/Os closest to that of the contaminant. These samples were rechecked before full ^{187}Re-^{187}Os analysis was undertaken. Once all of the contaminants had been removed, the samples were purified and powdered using the same demagnetization, hand magnet extraction and crushing techniques described above.

29
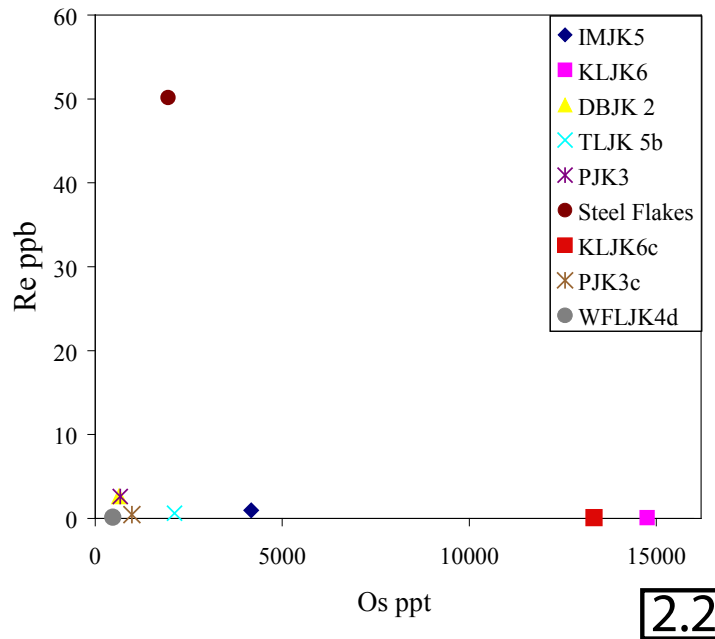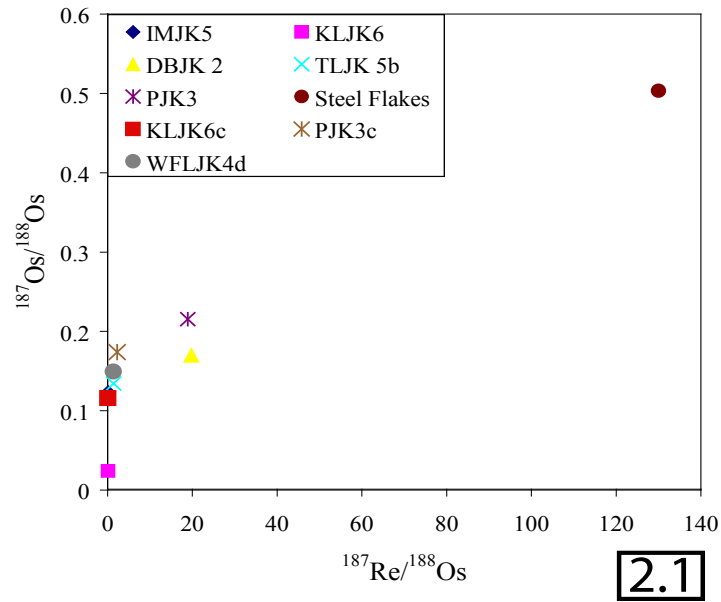
Figures 2.1 and 2.2

Fig 2.1 graph showing $^{187}Os/^{188}Os$ vs $^{187}Re/^{188}Os$ to indicate the difference in isotope ratios between samples and steel contaminant. Fig 2.2 shows a similar graph but total Re and Os contents are plotted

2.4 ^{187}Re-^{187}Os analysis

All ^{187}Re-^{187}Os analysis in this study were carried out using isotope dilution techniques described by Shirey and Walker (1995), Cohen and Waters (1996), Birck et al. (1997) and Selby and Creaser (2001b), with specific modifications relevant to this study described below.

Re tests were carried out on all samples prior to analysis to ensure that the correct sample spike ratios (around a ^{185}Re/^{187}Re ratio of 4 or as low as possible for very Re deficient samples) could be obtained. These were accomplished by dissolving a small amount (0.01g) of powdered sample with a mono ^{185}Re spike. The samples were dissolved using 2ml 12N HCl, Re was then purified using anion exchange chromatography using the normal procedure (Morgan et al., 1991) and then loaded onto a Ni filament and placed into a thermal ionization mass spectrometer and run in negative ion mode. Once the Re content of the sample had been calculated, the full ^{187}Re-^{187}Os analysis could be completed.

For full ^{187}Re-^{187}Os analyses, 0.1 to 1 gram of powdered sample was carefully weighed and added to a thick walled borosilicate Carius tube with a spiked solution of ^{185}Re and ^{190}Os of known concentrations. Dissolution of the magnetite was initially completed using 3ml 12N HCl sealed in the tube at 150ºC for 24 hours. An initial HCl dissolution was used rather than inverse aqua regia due to difficulties in dissolving large quantities of magnetite in this acid (Tarvainen et al., 1996). The tubes were then cooled, frozen and opened with a small hole (~ 2 mm) so that 6 ml of 16N HNO_3 could be added to ensure full sample spike

equilibration. The samples were then sealed and re-heated to 240ºC for 24 hours before being cooled and refrigerated prior to Re and Os extraction. Tests were made using higher volumes of 16N HNO_3 (8ml) in case 6ml was not sufficient to fully oxidize the spike and sample Os. These tests produced identical results to procedures using 6ml of 16N HNO_3 and so the lower volume of acid was chosen for analysis in this study.

Various methods were attempted to avoid re-opening and re-sealing Carius tubes due to the enhanced risk of explosion by weakening the neck or difficulties re-sealing the tube, both of which would result in losing the sample. Attempts were made at dissolving spiked magnetite in sealed Teflon bombs on a hot plate using 3ml 12N HCl with 0.25ml of ethanol to ensure the environment is kept reducing to prevent Os volatilization. After 24 hours the solution was transferred to a Carius tube, frozen, and 6ml 16N HNO_3 added. Samples treated in this way had a >50% chance of explosion due to the reaction between HNO_3 and ethanol forming ethyl nitrate. Tests were conducted without ethanol mixed with the HCl but these resulted in larger blank uncertainties, problems were also expected to occur in transferring the sample from the Teflon bombs to the Carius tubes due to problems ensuring there had been full sample and spike transferal. The double Carius tube method (with initial digestion in HCl then re-opening and adding HNO_3, and re-sealing) was considered the least risky and produced the lowest blank contents and was therefore preferred during this study.

After double Carius tube digestion, OsO_4 was extracted from the sample

32

acid mix using a modified version of the solvent extraction and microdistillation techniques described by Selby and Creaser (2001a), Shirey and Walker (1995) and Birck et al. (1997). The Carius tubes were frozen in a dry ice + alcohol slurry and 3.5ml of chloroform ($CHCl_3$) added. Samples were thawed and placed in a water bath at room temperature for approximately 15 minutes before solvent extraction of OsO_4. The sample chloroform mix was agitated for 1 minute using a centrifuge before the OsO_4 bearing chloroform was decanted to a glass vial containing 3ml of 9N HBr. This process was repeated 3 times, after which, the glass vials were capped and placed on a hotplate (70ºC) for 24 hours to achieve back extraction of the OsO_4 from the chloroform to the HBr. The HBr was subsequently evaporated to a bead and placed on the cap of a Savillex 3ml conical vial before evaporation to dryness. The Os fraction was then purified by microdistillation with the Os fraction oxidized at 80°C using 30μl CrO_3 (this solution contained 0.2g CrO_3 per 7ml H_2SO_4 (Selby and Creaser, 2001a)) and OsO_4 was captured using 20μl HBr. This process was repeated twice with the second time 20μl CrO_3 used, and the HBr was evaporated to dryness under Nitrogen gas at 55°C.

The Re fraction remained in the acid during Os solvent extraction and was evaporated to dryness on a hotplate. Large amounts of Fe can complicate Re chromatography by saturating the available anion resin sites resulting in low Re adsorption and the element of interest passing through the column. Attempts were made to remove Fe from the Re fraction before passing through the anion exchange column. In one method, Fe^{3+} was removed from the Re fraction by

adding 3ml 0.2N HNO_3 and placing the solution on a hotplate for 2 hours. The Fe^{3+} supersaturated solution was easily removed of Fe^{3+} flocculants using a centrifuge and 0.1μm filter. This new solution was then evaporated to dryness and the process repeated 3 times and eventually passed through anion exchange column using conventional techniques (Morgan et al., 1991). Caution was taken using this method due to the high metal adsorption potential onto $Fe(OH)_3$ (Nowack and Sigg, 1996) and potentially Fe^{3+}, although some Re loss was expected, this would not affect the $^{185}Re/^{187}Re$ ratio. Also, removal of Fe was attempted using cation column chemistry prior to the conventional anion column chemistry. Re fractions were dissolved by 3ml 0.2N HCl or HNO_3 and then passed through cation resin. These acid concentrations were chosen due to the large >1000 K_d for Fe^{3+} and $K_d \approx 0$ for Re (Nelson et al., 1964; Strelow, 1960; Strelow et al., 1965). The samples were washed with acid of the same concentration, and all column eluant collected and evaporated to dryness for anion chromatography. Blank testing was also conducted using both Fe separation techniques (Section 2.3, Figure 2.3), and due to the lower blank contribution from the centrifuge and filter method, this became the technique adopted by this study. After anion chromatography, the Re fraction was further purified by single bead chromatography (Selby and Creaser, 2003).

The purified Os and Re fractions were loaded onto Pt and Ni wire using $Ba(OH)_2/NaOH$ and $Ba(NO_3)_2$ as activating solutions, respectively. The samples were analyzed using negative thermal ionization mass spectrometry (Creaser et al., 1991; Volkening et al., 1991) on a Sector 54 mass spectrometer. Os was measured using an ETP multiplier in pulse-counting, peak hopping mode, Re was measured

34

typically using faraday collectors in static mode, however when the Re content of the sample was too low, the ETP multiplier collector was used in peak hopping mode. Re and Os isotope ratios were then corrected for mass fractionation, blank and spike contributions. Long term stability of the mass spectrometer was also tracked throughout the study period analyzing an in house Re and Os standard with every sample turret. Standard results were very consistent, the Os results were $^{187}Os/^{188}Os$ 1.0684 ± 0.0001 1σ (n=64), and the Re results were $^{185}Re/^{187}Re$ 0.5988 ± 0.0005 1σ (n=155).
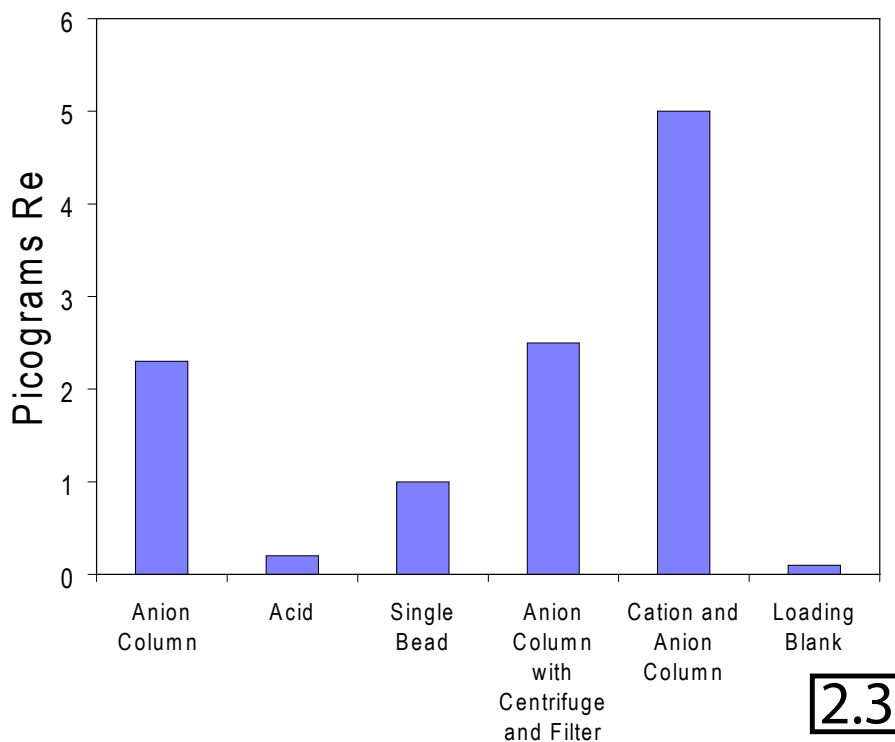
Figure 2.3

Graph showing procedural Re blank content for all Re separation steps. Blanks for different Fe removal techniques are also shown

2.4.1 Blanks and Isochrons

Procedural blanks for both Re and Os were carefully monitored throughout the study. Total Re blanks ranged from 10 to 3pg, Os blanks were on average an order of magnitude lower, ranging from 2 to 0.3pg, individual blank analysis are shown in Figures 2.4 and 2.5. The Os blanks had an average $^{187}Os/^{188}Os$ ratio of 0.49 (n=10). Full procedural blanks were also conducted for Re, due to often low sample/blank ratio for this element, these are shown in Figure 2.3.

Total Re Blank

Total Os Blank
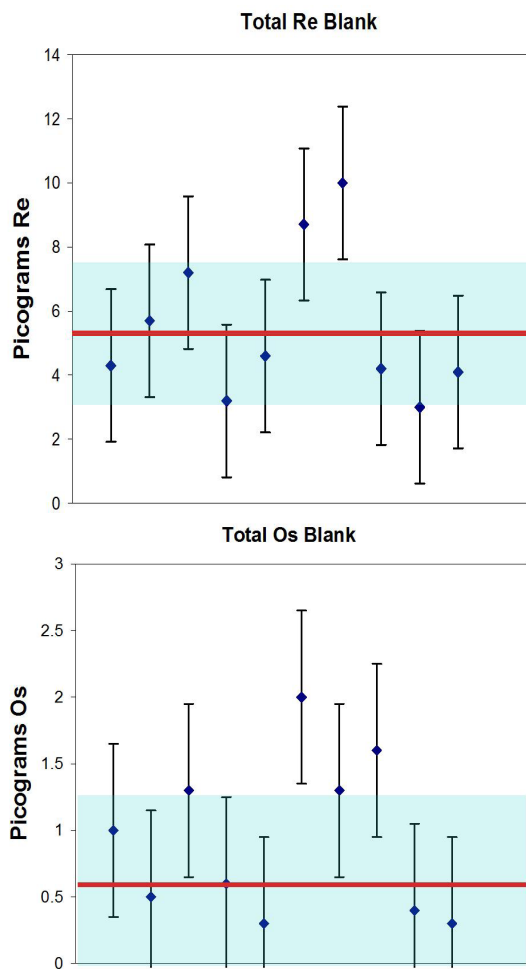
Figures 2.4 and 2.5

Full procedural blank values recorded throughout the study. Figure 2.4 shows Re blanks and Figure 2.5 shows Os blanks and associated errors.

36

The low Re and Os content of many of the samples analyzed in this study meant that blank contributions to the analysis were often the major source of error in the calculated ratios. For this reason it was considered very important to fully understand the blank contribution and to highlight areas where it could be reduced (e.g. using the centrifuge and filter Fe removal method rather than cation column chemistry).

Isochron diagrams were plotted using Isoplot Ex3 (Ludwig, 2003) with all uncertainties plotted at the 2σ level. The program used a $\pm1\%$ uncertainty for regression of $^{187}Re/^{188}Os$ and the measured $2\sigma_m$ uncertainty for $^{187}Os/^{188}Os$. The decay constant of 1.666×10^{-11} a^{-1} (Smoliar et al., 1996) was also used for age calculation.

2.5 Inductively coupled plasma mass spectrometry (ICP-MS)

Trace and major elements in magnetite were analyzed using a Perkin Elmer Elan6000 single collector quadrupole inductively coupled plasma mass spectrometer (ICP-MS) in solution mode. Approximately 30mg of powdered and purified magnetite were dissolved in glass beakers using 6N HCl. The solution was evaporated to dryness and the magnetite re-suspended using 0.2N HNO_3 for analysis as a nitrate species. 63 elements were analyzed and normalized to chondrite for interpretation. ^{56}Fe caused a problem during analysis due to the interference with $^{40}Ar^{16}O$, which is created in abundance by the argon plasma. To correct for this interference, ^{54}Fe was analyzed, and stable isotope ratios applied to calculate ^{56}Fe. Major oxide data were not calculated from the ICP-MS results, only trace element information was used.

37

2.6 Electron microprobe

A JEOL JXA-8900 electron microprobe (EMP) was used to obtain the major element composition of individual oxide minerals, which were analyzed as a bulk for $^{187}Re/^{188}Os$ isotopes. It was a cost efficient tool which provides major element oxide chemistry for discrete grains quickly (<3 minutes per point) and had the added advantage that back scattered electron images of the grains could also be obtained. The only disadvantage of the EMP was that the detection limits for elements were at the 100 ppm level and so analysis of Re and Os were beyond the scope of the machine. For analysis, the oxide minerals were mounted in epoxy pucks with a thickness of ~10mm. After hardening of the epoxy in an oven, the pucks were polished and coated with carbon before analysis.

Two methods of microprobe analysis were utilized in this study. Before quantitative analysis, grains were identified using energy dispersive spectrometry (EDS). This identification method involves recording the x-rays produced from all elements within the sample and displaying the results as a photon energy frequency graph. This method has a low resolution but can provide the bulk chemistry of a mineral quickly (< 10 seconds). This technique was used to identify the differences between ilmenite, perovskite, sulphides and spinel minerals so that spinel minerals and sulphides could be primarily selected for analysis. Once the minerals were identified, wavelength dispersive spectrometry (WDS) was used to quantitatively analyze them (Reed, 2002). The WDS analysis was completed using an accelerating voltage of 20KV and a 10 second scan of background noise before a 20 second scan for each element, the current used was 20nA.

38

2.7 References

Birck, J.L., RoyBarman, M. and Capmas, F., 1997. Re-Os isotopic measurements at the femtomole level in natural samples. Geostandards Newsletter-the Journal of Geostandards and Geoanalysis, 21(1): 19-27.

Cohen, A.S. and Waters, F.G., 1996. Separation of osmium from geological materials by solvent extraction for analysis by thermal ionisation mass spectrometry. Analytica Chimica Acta, 332(2-3): 269-275.

Creaser, R.A., Papanastassiou, D.A. and Wasserburg, G.J., 1991. Negative thermal ion mass spectrometry of osmium, rhenium and iridium. Geochimica Et Cosmochimica Acta, 55(1): 397-401.

Creaser, R.A., Sannigrahi, P., Chacko, T. and Selby, D., 2002. Further evaluation of the Re-Os geochronometer in organic-rich sedimentary rocks: A test of hydrocarbon maturation effects in the Exshaw Formation, Western Canada Sedimentary Basin. Geochimica Et Cosmochimica Acta, 66(19): 3441-3452.

Herr, W., Hintenberger, H. and Voshage, H., 1954. Half life of Rhenium Physical Review, 95(6): 1691-1691.

Hopstock, D.M., 2000. A reexamination of the performance of demagnetizing coils on finely ground natural magnetite. International Journal of Mineral Processing, 59(1): 45-68.

Ludwig, K.R., 2003. User's manual for ISOPLOT/EX, version 3. A geochronological toolkit for Microsoft Excel, Berkeley Geochronology Center. Special Publication 4: 60.

Morelli, R.M., Creaser, R., Selby, D., Kontak, D.J. and Horne, R.J., 2005. Rhenium-osmium geochronology of arsenopyrite in Meguma group gold deposits, Meguma terrane, Nova Scotia, Canada: Evidence for multiple gold-mineralizing events. Economic Geology, 100(6): 1229-1242.

Morelli, R.M. et al., 2004. Re-Os sulfide geochronology of the Red Dog sediment-hosted Zn-Pb-Ag deposit, Brooks Range, Alaska. Economic Geology, 99(7): 1569-1576.

Morgan, J.W., Golightly, D.W. and Dorrzapf, A.F., 1991. Methods for the separation of Rhenium, Osmium and Molybdenum applicable to isotope geochemistry Talanta, 38(3): 259-265.

Naldrett, S.N. and Libby, W.F., 1948. Natural Radioactivity of Rhenium Physical Review, 73(5): 487-493.

Nelson, F., Murase, T. and Kraus, K.A., 1964. Ion exchange procedures 1. Cation exchange in concentrated HCL and $HClO_4$ Solutions. Journal of Chromatography, 13(2): 503-&.

Nowack, B. and Sigg, L., 1996. Adsorption of EDTA and metal-EDTA complexes onto goethite. Journal of Colloid and Interface Science, 177(1): 106-121.

Peucker-Ehrenbrink, B. and Blum, J.D., 1998. Re-Os isotope systematics and weathering of Precambrian crustal rocks: Implications for the marine osmium isotope record. Geochimica Et Cosmochimica Acta, 62(19-20): 3193-3203.

Reed, S.J.B., 2002. Optimization of wavelength daspersive x-ray spectrometry analysis conditions, pp. 497-502.

Selby, D. and Creaser, R.A., 2001a. Late and mid-cretaceous mineralization in the

Northern Canadian Cordillera: Constraints from Re-Os molybdeatite dates. Economic Geology and the Bulletin of the Society of Economic Geologists, 96(6): 1461-1467.

Selby, D. and Creaser, R.A., 2001b. Re-Os geochronology and systematics in molybdenite from the Endako porphyry molybdenum deposit, British Columbia, Canada. Economic Geology and the Bulletin of the Society of Economic Geologists, 96(1): 197-204.

Selby, D. and Creaser, R.A., 2003. Re-Os geochronology of organic rich sediments: an evaluation of organic matter analysis methods. Chemical Geology, 200(3-4): 225-240.

Shirey, S.B. and Walker, R.J., 1995. Carius tube digestion for low-blank rhenium-osmium analysis. Analytical Chemistry, 67(13): 2136-2141.

Smith, F., 1961. Demagnetization of ferromagnetic particles. British Journal of Applied Physics, 12(4): 155-159.

Smoliar, M.I., Walker, R.J. and Morgan, J.W., 1996. Re-Os ages of group IIA, IIIA, IVA, and IVB iron meteorites. Science, 271(5252): 1099-1102.

Stein, H.J., Markey, R.J., Morgan, J.W., Hannah, J.L. and Schersten, A., 2001. The remarkable Re-Os chronometer in molybdenite: how and why it works. Terra Nova, 13: 479-486.

Strelow, F.W.E., 1960. An Ion Exchange Selectivity Scale of Cations Based on Equilibrium Distribution Coefficients. Analytical Chemistry, 32(9): 1185-1188.

Strelow, F.W.E., Rethemey.R and Bothma, C.J.C., 1965. Ion Exchange Selectivity Scales for Cations in Nitric Acid and Sulfuric Acid Media with a Sulfonated

Polystyrene Resin. Analytical Chemistry, 37(1): 106-&.

Tarvainen, T., Aatos, S. and Raisanen, M.L., 1996. A method for determining the normative mineralogy of tills, pp. 117-120.

Volkening, J., Walczyk, T. and G. Heumann, K., 1991. Osmium isotope ratio determinations by negative thermal ionization mass spectrometry. International Journal of Mass Spectrometry and Ion Processes, 105(2): 147-159.

3 Depleted Mantle Model Ages from Oxide Minerals

3.1. Introduction

The ^{187}Re-^{187}Os system has widely been used in mantle sulphide minerals and osmium alloys to date melt depletion events in the mantle (e.g. Alard et al., 2002; Aulbach et al., 2004; Griffin et al., 2004; Pearson et al., 2007; Simon et al., 2007; Xu et al., 2008). During partial melting of the mantle, Re behaves moderately incompatibly and is removed by the melt whereas Os is strongly compatible and remains in the depleted residue, commonly as a trace phase in sulphide minerals (Lorand and Alard, 2001; Shirey and Walker, 1998). Once Re has been removed, the radiogenic growth of ^{187}Os is strongly retarded, arresting the evolution of ^{187}Os/^{188}Os compared to undepleted mantle. If the melt-depleted mantle is subsequently sampled by kimberlitic (or other) magmatism, the ^{187}Os/^{188}Os ratio of the magma can be used to back calculate the timing of the original depletion event (Walker et al., 1989). Mantle depletion ages, calculated in this way have been shown to broadly correlate with overlying crustal growth (Pearson, 1999; Pearson et al., 2007) and, until recently, represented one of the only ways to study evolutionary processes combining continental lithospheric mantle (CLM) and overlying crust. Recent work involving Pb-Pb and Lu-Hf dating of mantle xenoliths have expanded the available isotopic proxies for studying the lower crust and continental lithospheric mantle (e.g., Dai et al. 2008), however this study focuses entirely on the Re-Os system.

The melt depletion ages are typically constrained by sulphide minerals, and osmium alloys, which are the dominant hosts for Os in the mantle often containing ppm to weight percent concentrations of the element. The abundance of Os within these minerals, and the compatibility of Os during mantle melting, had previously led people to believe that the $^{187}Os/^{188}Os$ isotopic composition was robust and not effected by processes such as metasomatism. Detailed analysis on the effects of metasomatism and other mantle processes has shown that Os may be more mobile than previously thought (Brandon et al., 1996; Ionov et al., 2006; Reisberg et al., 2004; Reisberg et al., 2005). Despite the mobility of Os, Xu et al. (2008) show that the $^{187}Os/^{188}Os$ ratio of individual sulphide minerals can remain unchanged during metasomatism and record pre-alteration events. However, information regarding melt depletion events becomes much more complicated and difficult to extract from the whole rock ratios if multiple generations of sulphide are present, such as with xenocrystic material.

The major drawback of obtaining melt depletion ages from sulphide minerals is the paucity of the mineral within mantle rocks, and the limited abundance of mantle xenoliths from mantle derived magmas. Partial melting of >12-15% and variable pressure conditions can remove sulphur entirely from the mantle source (Luguet et al., 2003; Luguet et al., 2007), forcing Os into alternative mineral phases. Experimental and physical evidence suggests that spinel group minerals, which are a common phase in many mantle rocks, are a major host to Os and other Platinum Group Metals (PGMs) (Finnigan et al., 2008; Walker et al., 2002). It is not clear whether PGMs partition into spinel crystal structure or form micronuggets around

44

the mineral as it grows, although the presence of micronuggets is the currently favored hypothesis (Luguet et al., 2007; Finnigan et al., 2008).

^{187}Re-^{187}Os geochronology using spinel group minerals has previously been established (e.g. Gangopadhyay and Walker, 2003) and research by Nagler et al. (1997) has also shown that mantle-derived chromite can retain depleted mantle model ages (T_{MA}). Following the study of Nagler et al. (1997), chromites have repeatedly been used to calculate mantle depletion or enrichment events. However, there has been some suggestion that Re and Os isotopes within chromites may be prone to disturbance during metasomatism, as Chesley et al. (1999) showed that metasomatized rims of chromites from xenoliths in the East African rift were more radiogenic than the core. Studies such as Chesley et al. (1999) indicate the importance of detailed compositional analysis of the samples in conjunction with ^{187}Re-^{187}Os analysis to fully understand the results. The dominant host rocks for chromite studies so far have been ophiolites and ultramafic chromite ores (Kocks et al., 2007; Mondal et al., 2007) whereas, small degree ultramafic mantle melts such as kimberlites have not been extensively investigated. These types of magmas are useful in that they are found throughout geological time from the Proterozoic onwards, and over all cratons giving a wide spatial and temporal coverage of the Earth. Graham et al. (2004) have shown that ^{187}Re-^{187}Os ages from spinel group minerals can give emplacement ages as well as information regarding mantle depletion for 2025 Ma kimberlites, melnoites and carbonatites from the Yilgarn craton. It is not clear, however from the Graham et al. (2004) study whether crustal contamination and weathering affected the results. Compositionally pure kimberlitic

spinel separates are extremely difficult to obtain due to the constantly evolving composition of the magma, and progressive crystallization of the oxide phase. However, it is evident from the Graham et al. (2004) study that Re-Os isotopes from spinel minerals can contain useful information regarding the formation of kimberlites and related magmas.

In order to better constrain the hosts for ^{187}Re-^{187}Os depletion model ages within ultramafic magmas, ^{187}Re-^{187}Os analysis has been conducted on groundmass spinel minerals from a variety of kimberlites and lamprophyres from cratons and Paleoproterozoic domains in North America and South Africa. Microprobe analysis of the oxide minerals has also been used to investigate the presence of micronugget PGM phases, and to constrain the composition and origin of the oxide minerals. This work also provides insight into the osmium budget of the upper mantle and spinel minerals and the source region for kimberlites and lamprophyres.

3.2. Samples and previous work

Emplacement ages for the samples used in this study and location maps have been previously published in Heaman et al. (2003), Heaman et al. (2004), Tappe et al. (2008) and Richardson, (1986). The samples cover 4 cratons; Slave, Superior, Wyoming and Kaapvaal, and the Torngat Orogen, and they range in age from 1180 to 408 Ma. Average spinel compositions and percentage mineral abundance for the samples are listed in Tables 3.1 and 3.2. The spinel minerals are classified using similar techniques to Mitchell and Clarke, (1976) and Tompkins and Haggerty, (1985) although end-member compositions were not calculated due to the order

46

of calculation affecting the final composition (Locock 2008). The minerals were plotted on end projections of the spinel prism (Roeder and Schulze, 2008) and on TiO_2 vs FeO_t plots in order to group into similar chemical compositions. Seven spinel groups were identified: aluminous magnesian chromite (AMC), titanian magnesian aluminous chromite (TMAC), titanian magnesian chromite (TMC), magnesian ulvöspinel magnetite (MUM), titanomagnetite (TM), and magnetite (M).

Sample	Mineral											
	AMC	TMAC	TMC	MUM	ATM	TM	M	Ilmenite	Perovskite	Sulphide	Silicate	Total
IM	9	22		30					36		3	100
KL	22	4				74						100
P		13			48	13		25	3			100
WFL					33	40		27				100
DB								100				100
TL		7	3		3	62		13	13		6	100
Prem	10	2	2		8		2	54	6	t	17	100

Spinel Crystalization trend ⟶   3.1

Table 3.1

Table showing mineralogy of each sample as a percentage. IM = Iron Mountain, KL = Kyle Lake, P = Pele, WFL = Whitefish Lake, DB = Drybones, TL = Torngat Lamprophyre, Prem = Premier. AMC = aluminous magnesian chromite, TMAC = titaniferous magnesian aluminous chromite, TMC = titaniferous magnesian chromite, MUM = magnesian ulvöspinel magnetite, ATM = aluminous titano-magnetite, TM = titaniferous magnetite, M = magnetite, t = trace

Table 3.2

Mineral	AMC			TMAC			TMC		MUM				ATM				TM				M
Sample	KL-4	IM-6-2	Prem-3-4	P-22	TL-2	IM-3-2	TL-29	Prem 9-3	IM-4-3	IM-5-4	IM-2	IM-18	WFL-12	P-3	P-31	Prem 5-6	WFL-17	KL-5	P-19	TL-36	Prem 5-5
SiO₂	0.14	0.07	0.10	0.14	0.05	0.17	0.08	0.82	0.17	0.11	0.18	4.00	0.04	0.07	0.09	0.27	0.02	0.07	0.08	0.05	0.65
TiO₂	2.89	0.18	0.24	6.57	4.24	4.66	14.88	6.00	5.70	7.25	12.74	5.78	21.62	19.47	20.07	14.90	19.77	8.99	15.77	14.26	1.83
Al₂O₃	8.87	17.26	12.21	17.29	7.99	6.56	2.49	2.79	3.43	5.90	7.95	5.46	4.21	9.26	9.33	10.87	2.92	2.01	4.02	1.67	0.81
Cr₂O₃	49.25	43.27	46.50	31.45	26.17	38.92	22.41	25.57	0.52	0.34	1.86	0.36	1.06	0.86	0.54	8.79	1.47	5.68	0.85	1.18	1.48
Fe₂O₃	5.45	9.88	10.77	11.04	28.71	19.55	18.04	23.02	59.41	54.42	42.91	47.47	23.96	21.58	18.90	18.80	28.98	47.46	34.06	42.93	61.49
FeO	19.79	13.71	21.68	21.35	25.64	13.83	31.25	31.54	18.46	19.07	17.95	20.61	40.47	39.76	45.41	37.94	36.43	26.74	39.52	32.01	32.44
FeOₜ	25.24	23.59	32.46	32.39	54.35	33.38	49.28	54.56	77.87	73.49	60.86	68.08	64.44	61.34	64.30	56.74	65.41	74.20	73.58	74.94	93.92
MnO	0.54	0.37	0.39	0.29	0.38	0.79	0.80	1.63	0.72	0.77	0.72	0.64	1.22	1.21	1.19	1.69	1.39	0.51	0.76	0.93	0.42
MgO	9.56	13.06	7.78	12.55	7.03	14.46	8.59	5.92	11.62	12.40	17.01	13.42	6.32	6.00	2.76	4.20	7.48	8.11	3.79	7.73	0.27
CaO	0.02	0.05	0.03	0.04	0.03	0.06	0.00	2.05	0.07	0.09	0.07	0.09	0.17	0.05	0.10	0.36	0.04	0.05	0.04	0.05	0.30
ZnO	0.14	0.16	0.13	0.09	0.09	0.11	0.07	1.02	0.06	0.06	0.04	0.06	0.07	0.11	0.00	0.14	0.20	0.00	0.02	0.06	0.05
Total	98.84	98.01	99.83	101.15	100.73	99.11	99.08	100.35	100.17	100.41	101.44	97.88	99.50	98.65	98.69	97.94	99.03	99.78	99.23	101.07	99.74
Fe³⁺ᵃ	3.81	6.91	7.53	7.72	20.07	13.67	12.61	16.09	41.53	38.04	29.99	33.18	16.75	15.09	13.21	13.14	20.26	33.17	23.81	30.01	42.98
Fe²⁺ᵃ	15.38	10.66	16.86	16.60	19.93	10.75	24.29	24.51	14.35	14.82	13.96	16.02	31.46	30.91	35.30	29.49	28.32	20.79	30.72	24.88	25.21
Cr	30.48	26.78	28.78	19.47	16.20	24.09	13.87	15.83	0.32	0.21	1.15	0.22	0.66	0.53	0.33	5.44	0.91	3.51	0.52	0.73	0.91
Al	4.70	9.13	6.46	9.15	4.23	3.47	1.32	1.48	1.82	3.12	4.21	2.89	2.23	4.90	4.94	5.75	1.55	1.06	2.13	0.88	0.43
Mg	5.76	7.87	4.69	7.57	4.24	8.72	5.18	2.36	7.01	7.48	10.26	8.09	3.81	3.62	1.66	2.53	4.51	4.89	2.29	4.66	0.16
Ti	1.72	0.11	0.14	3.91	2.52	2.77	8.84	1.78	3.39	4.31	7.57	3.44	12.85	11.57	11.93	8.85	11.75	5.34	9.37	8.48	1.09
Fe²⁺ #	0.73	0.58	0.78	0.69	0.82	0.55	0.82	0.91	0.67	0.66	0.58	0.66	0.89	0.90	0.96	0.92	0.86	0.81	0.93	0.84	0.99
Fe³⁺ #	0.10	0.16	0.18	0.21	0.50	0.33	0.45	0.48	0.95	0.92	0.85	0.91	0.85	0.74	0.71	0.54	0.89	0.88	0.90	0.95	0.97
Ti#	0.05	0.00	0.00	0.12	0.11	0.09	0.37	0.09	0.61	0.56	0.59	0.52	0.82	0.68	0.69	0.44	0.83	0.54	0.78	0.84	0.45
Cr #	0.87	0.75	0.82	0.68	0.79	0.87	0.91	0.91	0.15	0.06	0.22	0.07	0.23	0.10	0.06	0.49	0.37	0.77	0.20	0.45	0.68
Mg/(Mg+Feₜ)	0.23	0.31	0.16	0.24	0.10	0.26	0.12	0.06	0.11	0.12	0.19	0.14	0.07	0.07	0.03	0.06	0.08	0.08	0.04	0.08	0.00

Representative chemical composition of the spinel minerals in each of the assigned spinel groups.

a= calculated assuming stoichiometry, Fe^{2+} # = $Fe^{2+}/(Fe^{2+}+Mg)$, Fe^{3+} # = $Fe^{3+}/(Fe^{3+}+Al+Cr)$, Ti # =

$Ti/(Ti+Al+Cr)$, Cr # = $Cr/(Cr+Al)$, Spinel groups and sample ID are the same as Table 3.1. Full data

for all samples is in the Appendix

48

Figure 3.1

North American geological map of Archean Cratons and some Proterozoic orogens with location of samples. Insert showing South African geology and sample location is also shown. North American map is modified from (Whitmeyer and Karlstrom, 2007)

3.2.1. Slave craton

The Drybones Bay (DB) kimberlite dated at 441.4 Ma (U-Pb zircon), is located in the SW margin of the Slave Craton and intrudes plutons of the Archean Defeat Plutonic Suite (2620 Ma). This kimberlite has been the focus of cratonic evolutionary studies due to its close proximity to the Yellowknife telesismic array (YKA), and deep seismic reflection surveys carried out in the area (Carbno and Canil, 2002). Oxide minerals from the DB kimberlite are monomineralic comprising MgO-rich (>5 wt%) picroilmenite. This is consistent with the findings of Northwest Territories Geoscience Office (NTGO) who conducted till sampling in the area and found that kimberlitic oxide minerals were composed of >97% ilmenite (Kerr et al., 2000). The ilmenite crystals are inclusion free and relatively fresh with some minor alteration. Zoning is minor, and limited to minor MgO- and TiO_2-rich segments, generally the crystals show no zoning. This kimberlite also contains abundant mantle xenoliths. Carbno and Canil (2002) have suggested that the trace element chemistry of garnets from xenoliths entrained by the DB kimberlite indicate a large depletion event occurred in the subcontinental lithosphere.

3.2.2. Superior Craton

Kyle Lake (KL) (1076±3.8 Ma, U-Pb perovskite) is from a group of 5 kimberlite intrusions near the Attawapiskat River in Northern Ontario, Canada. They are located northwest of the Attawapiskat kimberlite field, beneath Paleozoic cover. The KL oxide minerals are comprised of two chromite varieties (AMC, and TMAC) and titanium-rich magnetite (TM). These spinel compositions are similar to those published for the much younger Victor North kimberlite from the Attawipiskat

50

kimberlite field (van Straaten et al., 2008) although the Kyle Lake samples are more titanium- and Fe^{3+}-rich. The KL spinels show some evidence of alteration and post emplacement fracturing. The zoning ranges from complex Fe-Ti exsolution to more typical chromite core - magnetite rim.

Two additional samples from the Superior craton are located on the north shore of Lake Superior in the Wawa district.   Whitefish Lake (WFL) (1035±13 Ma, Rb-Sr phlogopite) and Pele (P) (1172.3±4.6 Ma, U-Pb perovskite) are ultramafic lamprophyres. Oxide minerals from these are dominated by spinel chromites and magnetites but also contain ~30% ilmenite. The spinels are characterized by high-TiO_2 magnetite (TM), and relatively low chromite abundance. The Pele samples are dominated by complexly zoned crystals, often with high-Al_2O_3 close to the core of the mineral and more Fe_3O_4-rich towards the rim, TiO_2 content is consistently high throughout the zoning however. The Whitefish Lake oxide minerals show a similar trend.

Together, these 3 samples are from 2 of the 3 Mesoproterozoic kimberlite/ lamprophyre intrusions in North America, the third is the Lac Tac cluster in Québec (Heaman et al., 2004). These Mesoproterozoic intrusions have been interpreted as precursors to an aborted rift event in the Laurentian supercontinent at 1106-1087 Ma (Heaman and Machado, 1992).   Numerous ultramafic lamprophyre (UML) intrusions have been dated to the northeast of Lake Superior in the Wawa subprovince all of which have been linked to the onset of the 1.1 Ga rifting, although the UML intrusions are typically 1150-1130 Ma, ~40-20 Ma older than the rift magmatism

51

(Queen et al., 1996; Heaman et al., 2007). Prior to the kimberlite and lamprophyre intrusions, the Superior craton was intruded by numerous large mafic dyke swarms, for example, the 2473-2446 Ma Hearst and Matachewan dykes (Heaman, 1997) the 1267 Ma Mackenzie event (Lecheminant and Heaman, 1989), the Senneterre and Nipissing dykes at 2214-2217 Ma (Buchan et al., 1993) and the Lac Esprit dyke swarm at 2069 Ma (Buchan et al., 2007), all of which may have affected the Superior craton subcontinental mantle.

3.2.3 Torngat Orogen

The Torngat lamprophyre sample (K35; 584.0±3.6 Ma, U-Pb perovskite) is located within the Torngat Orogen, southeast of the Churchill Province. The sample is located on the East coast of Northern Labrador and Northeastern Québec and was formed during the collision of the Superior and the Nain (North Atlantic) cratons at 1.9 – 1.8 Ga (Hoffman, 1990). The lithospheric mantle beneath the Torngat Orogen therefore may contain traces of both cratons. Tappe et al. (2008) have suggested that the Torngat lamprophyres and related magmas, may sample a progressively metasomatized mantle beneath the area which was possibly formed during Neoproterozoic rifting associated with the opening of the Iapetus ocean basin at 615 Ma (Kamo et al., 1989). Oxide minerals from this sample are chromite and magnetite-rich spinels with ~20% picroilmenite. The spinel minerals range in composition from chromite to magnetite but all show strong TiO_2 enrichment, which is consistent with the findings of Tappe et al. (2008). The Torngat oxide minerals show the least alteration out of all the samples investigated in this study, however minor complex zoning and composite grains are present. The mineralogy

52

is dominated by titaniferous magnetite with little evidence of zoning, however small Fe_2O_3-rich spinels are common around the edges of the grains.

3.2.4. Wyoming Craton

The Iron Mountain kimberlite (408.4±2.6 Ma, U-Pb perovskite) is located in the Laramie Range district of southeastern Wyoming, just north of the Wyoming/Colorado state line. The Iron Mountain kimberlite field occurs north of the Cheyenne Belt, which marks the border between the Wyoming craton in the north and Proterozoic rocks to the south. It is composed of 3 main domains with the Iron Mountain kimberlite located within the youngest southern domain. The domains were cratonized during a period of subduction accretion and magmatism at 2.9-2.5 Ga (Mueller and Frost, 2006). Once the craton had been established, it remained relatively quiescent, with activity dominated by the accretion of Proterozoic domains to the east and south until the onset of the Laramide orogeny at ~80 Ma (Carlson et al., 2004). The oxide minerals from this kimberlite contain the most unevolved spinels analyzed, characterized by chromites high in MgO and Al_2O_3 and low in TiO_2. The spinel minerals analyzed range in composition from chromites to Mg-rich ulvöspinel; the spinels are relatively Fe-poor with no observed pure magnetite. The oxide minerals from Iron Mountain contain spinels with atoll textures where a chromite core is surrounded by a hydrous unidentified silicate phase and an MgO-rich ulvöspinel rim, this is identical to the compositions identified by Roeder and Schulze, (2008) from the same kimberlite. Reverse zoning is also present in the Iron Mountain spinels with Fe^{3+}-rich cores surrounded by chromite-rich rims, and the kimberlite also contains the highest perovskite abundance of up to 36% (in the

53

magnetic mineral separate).

3.2.5. Kaapvaal Craton

The Premier kimberlite (1180±30 Ma Rb-Sr phlogopite and Sm-Nd garnet) is located in the northern section of the Witwatersrand block of the Kaapvaal craton. The Kaapvaal craton is the most exposed and well-studied of the Archean cratons in Southern Africa and comprises of the Kimberly and Witwatersrand blocks. These blocks amalgamated at ~2.9 Ga by subduction and continent-continent accretion (Simon et al., 2007). The craton subsequently collided with the Zimbabwe craton to the north forming the Limpopo belt between 2.7-2.5 Ga (Simon et al., 2007). Previous depleted mantle model ages from $^{187}Os/^{188}Os$ isotope ratios for the Kaapvaal craton have a median at 3.1 Ga but a mode of 2.5 Ga with a tail towards older ages (Simon et al., 2007). In terms of spinel composition, the Premier mine provided the second most spinel poor magnetic separate (after Drybones) with 70% of the minerals analyzed comprising picroilmenite, Mn-rich ilmenite and perovskite. Spinel minerals occur as inclusions within silicates and are generally euhedral, often with chromite to magnetite core to rim zoning. Sulphide minerals were found as inclusions within Mn-rich ilmenite from the Premier mine. These inclusions are small (<5μm) and were therefore difficult to analyze in isolation, they were the only such inclusions found from the whole sample set.

3.3 Samples and Analytical techniques

Magnetic freefall mineral separates of sampled kimberlites and lamprophyres were

54

checked for purity using a binocular microscope before being crushed in an agate mill and analyzed by isotope dilution for Re and Os isotopes. Table 3.1 indicates the mineralogy of each sample, along with modal percentages for each of the minerals. Further mineral purification techniques are described in Chapter 2 Section 2.2

Re and Os isotopic characteristics of the samples were calculated using isotope dilution negative thermal ionization mass spectrometry (ID-NTIMS) at the University of Alberta Radiogenic Isotope Facility according to the procedures described by Creaser et al. (2002) and Selby and Creaser (2001) with modifications described below. 35-500 μg of finely ground sample powder was accurately weighed and added to borosilicate Carius tubes along with an accurately weighed spike of isotopically enriched ^{190}Os and ^{185}Re of known composition. Sample digestion was conducted using a technique similar to that of Chesley et al. (1999) where the sample powder and spike were first dissolved using 3 ml of 12N HCl in sealed Carius tubes at 150ºC for 24 hours. The tubes were then frozen and opened and 6 ml of 16N HNO_3 added before resealing and digesting at 240ºC for a further 24 hours. Following sample digestion, Re and Os were chemically separated from the sample acid mix. Re was extracted using conventional anion chromatography techniques described in Morgan et al. (1991) and purified using single bead anion chromatography described in Selby and Creaser (2003). Os was extracted from the sample using modified versions of the solvent extraction and microdistillation procedures described in Cohen and Waters (1996), Birck et al. (1997) and Selby and Creaser (2001). Chloroform ($CHCl_3$) was used for solvent extraction of Os rather than carbon tetrachloride (CCl_4) for safety and cost reasons, analytical blanks

were not affected by this switch.

The purified Re and Os fractions were loaded onto Ni and Pt filaments, respectively and analyzed using a Micromass Sector 54 mass spectrometer in negative ion mode (Creaser et al., 1991; Volkening et al., 1991). Re isotopic analysis was typically achieved using static Faraday collectors, when Re ion counts were below Faraday cup detection limits, a single collector ETP electron multiplier, peak hopping in pulse counting mode was used. The ETP analyzing method was used for all Os isotopic determinations. Metal oxide ratios produced by the mass spectrometer were corrected for isobaric interferences from oxygen isotopes and also mass fractionation using stable isotope ratios. Corrections were also applied to the data for spike and blank contributions. Total procedural blanks ranged from 10 to 3 pg for Re and 2 to 0.3 pg for Os, the average $^{187}Os/^{188}Os$ ratio of the blank was 0.49.

Re depletion (T_{RD}) ages were calculated with the assumption that a melt depletion event removed all Re from the source and hence terminating the growth of ^{187}Os at that time, therefore all measured Re was secondary (Shirey and Walker, 1998). Re model ages (T_{MA}) were calculated assuming that the $^{187}Re/^{188}Os$ ratio of the sample reflected its long-term radiogenic in-growth in the mantle and was therefore representative of the source (Shirey and Walker, 1998). Under these assumptions, T_{RD} ages represent minimum ages of melt extraction. Primitive upper mantle (PUM) values of $^{187}Os/^{188}Os = 0.1296$ and $^{187}Re/^{188}Os = 0.422$ (Brandon et al., 2006) and chondrite uniform reservoir (CHUR) values of $^{187}Os/^{188}Os = 0.12705$ and $^{187}Re/^{188}Os$

= 0.40076 (Walker et al., 1994) were used to calculate Re depletion and Re model ages. Due to the uncertainty in the true composition of PUM, calculated errors below 0.4 Ga were considered to be an under-representation of the true error and were rounded up to this value (Pearson et al., 2007). γOs values, which represent the percentage difference of the calculated initial ^{187}Os/^{188}Os value for the sample at emplacement from the average mantle at that time (Shirey and Walker, 1998), were also calculated using CHUR for comparison with other studies. A value of 1.6668e^{-11} a^{-1} was used for the ^{187}Re decay constant (Selby et al., 2007).
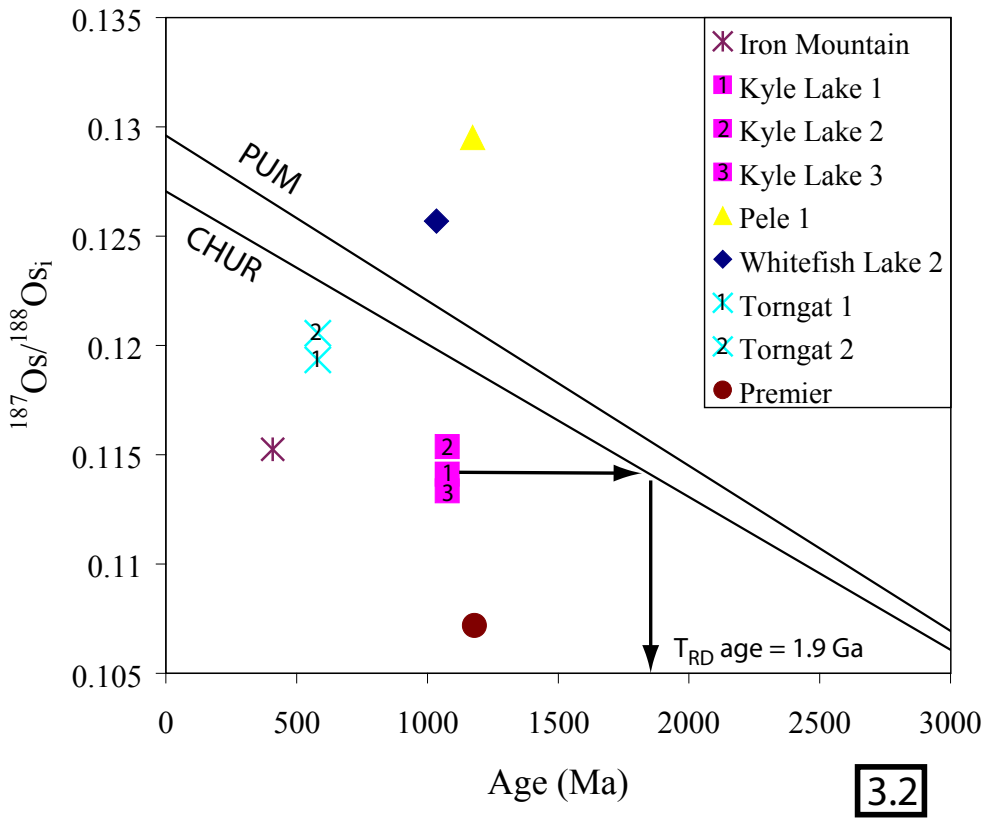
Figure 3.2

Re-Os data for the samples plotted relative to chondrite (CHUR) and primitive upper mantle (PUM) evolution over time. An example of a T_{RD} age for sample KL1 is shown. All of the samples plotted on the graph are corrected for ^{187}Os addition since emplacement.

57

Major element oxide compositions of the minerals in this study were analyzed at the University of Alberta using a JEOL JXA-8900 electron microprobe operating in wavelength dispersive mode. 50-200 grains from each sample were mounted and polished in epoxy pucks and coated with carbon before analysis. An accelerating voltage of 20KV, a spot size of >1μm and a conducting current of 20nA were used. A 10 second scan of background noise before a 20 second analytical scan for each element was conducted. Fe_2O_3 contents of the minerals were calculated assuming stoichiometry.

3.4 Results

Major element and Re-Os isotopic data are provided in Tables 3.2 and 3.3 and are plotted in Figures 3.1-3.8. Os content in the samples range from 14 ppb to 0.4 ppb with KL oxides consistently containing the highest Os abundance and WFL samples the lowest. The Re content of the samples is generally below 1 ppb with 3 exceptions, P2, WFL1 and DB, which all have Re contents of ~2 ppb (Figure 3.1). Interestingly these samples also contain the highest ilmenite abundance (excluding the Prem sample), which has previously been shown to partition Re into its structure (Lambert et al., 2000). Os contents for the oxide minerals span the Os content published for kimberlite magma 0.1-2 ppb (Graham et al., 2004), which indicates that oxide minerals may not be the dominant host for Os in kimberlite magma although the KL samples have 7-140 times the kimberlite value indicating that Os may be controlled by spinel in some instances.

58

Sample	Craton	Age of emplacement (Ma)	Re (ppb)	Os (ppb)	$^{187}Re/^{188}Os$	±2σ	$^{187}Os/^{188}Os$	±2σ	$^{187}Os/^{188}Os_i$	γOs	PUM T_{RD} (Ga)	±2σ	T_{MA} (Ga)	±2σ	CHUR T_{RD} (Ga)	±2σ	T_{MA} (Ga)	±2σ
Iron Mountain (IM)	Wyoming	408.4	0.960	4.168	1.110	0.065	0.122	0.001	0.115	-7	2.01	0.40	-0.59	0.66	1.74	0.22	-0.36	0.61
Kyle Lake -3 (KL-3)	Superior	1076.2	0.073	14.758	0.024	0.001	0.113	0.001	0.113	-5	2.27	0.40	2.34	0.40	2.02	0.08	2.08	0.02
Kyle Lake (KL-2)	Superior	1076.2	0.086	13.341	0.031	0.007	0.115	0.001	0.115	4	1.99	0.40	2.06	0.40	1.72	0.12	1.78	0.07
Kyle Lake (KL-1)	Superior	1076.2	0.115	11.197	0.049	0.005	0.115	0.001	0.114	-5	2.16	0.40	2.31	0.40	1.91	0.09	2.02	0.01
Pete (P-2)	Superior	1172.3	2.607	0.672	18.920	0.393	0.215	0.009	-0.157	-233	31.17	1.42	0.28	1.18	32.22	1.47	0.29	1.18
Pete (P-1)	Superior	1172.3	0.457	0.982	2.255	0.104	0.174	0.002	0.129	9	0.01	0.64	1.44	1.28	-0.37	0.68	1.50	1.26
Whitefish Lake (WFL-2)	Superior	1035.0	0.132	0.469	1.364	0.099	0.149	0.002	0.125	5	0.55	0.54	1.25	1.26	0.20	0.57	1.38	1.21
Whitefish Lake (WFL-1)	Superior	1035.0	2.626	0.581	21.851	0.162	0.150	0.002	-0.229	-292	36.95	0.35	0.06	1.07	38.19	0.36	0.07	1.07
Dry Bones (DB)	Slave	441.4	2.607	0.639	19.766	0.226	0.169	0.002	0.023	-81	13.42	0.46	0.12	0.44	13.75	0.48	0.13	0.44
Torngat (TL-2)	Torngat Orogen	581.4	0.616	2.121	1.400	0.013	0.134	0.001	0.120	-2	1.27	0.40	0.28	0.77	0.96	0.17	0.43	0.75
Torngat (TL1)	Torngat Orogen	581.4	0.590	2.007	1.417	0.018	0.133	0.001	0.119	-3	1.44	0.40	0.21	0.80	1.14	0.12	0.36	0.78
Premier (Prem)	Kaapvaal	1180.0	0.375	0.871	2.079	0.040	0.148	0.001	0.107	-10	3.10	0.40	0.68	1.44	2.90	0.31	0.76	1.41

3.3

Table 3.3

Re-Os data for all of the samples with 2σ absolute errors. Large uncertainties are observed for KL Re and Os abundances, this is due the small amount of spike added and to uncertainties in the absolute composition of the spike. The calculations for T_{RD} and T_{MA} are provided in the text, as well as the values used for CHUR and PUM.

59

Samples from the same kimberlite/lamprophyre show relatively good consistency in terms of Os content but Re contents fluctuate greatly between samples, which contributes to the large range in measured $^{187}Os/^{188}Os$ compositions (Table 3.3). For some samples, there is large Os isotopic inter-sample variation. For example, the γOs values for the two oxide fractions selected from Pele are +9 and -233, a range that indicates a more complex scenario than variable Re-addition during magma genesis and subsequent radiogenic ^{187}Os growth. The samples in which the Re content does not fluctuate (KL and TL) show good consistency in terms of $^{187}Os/^{188}Os$ and $^{187}Os/^{188}Os_i$. Only IM and KL samples have present day $^{187}Os/^{188}Os$ ratios which are below PUM, all other samples show significant isotopic enrichment above the upper mantle average which is strongly suggestive of Re-addition or possibly crustal contamination. Independent emplacement ages using the Re-Os isochron technique or model age calculation from individual samples assuming that all ^{187}Re was added at the time of eruption could not be obtained for any of the samples in this study. A possible explanation for this is that the individual minerals in the sample aliquots contain different initial Os isotopic compositions; this is indicated by the inter-sample variation in γOs. Model ages can also be calculated for individual samples but are only reliable when Re/Os ratios are high due to the large error created by estimating the $^{187}Os/^{188}Os_i$ when Re/Os values are low, the Re/Os ratios are too low for accurate crystallization age information in this study.
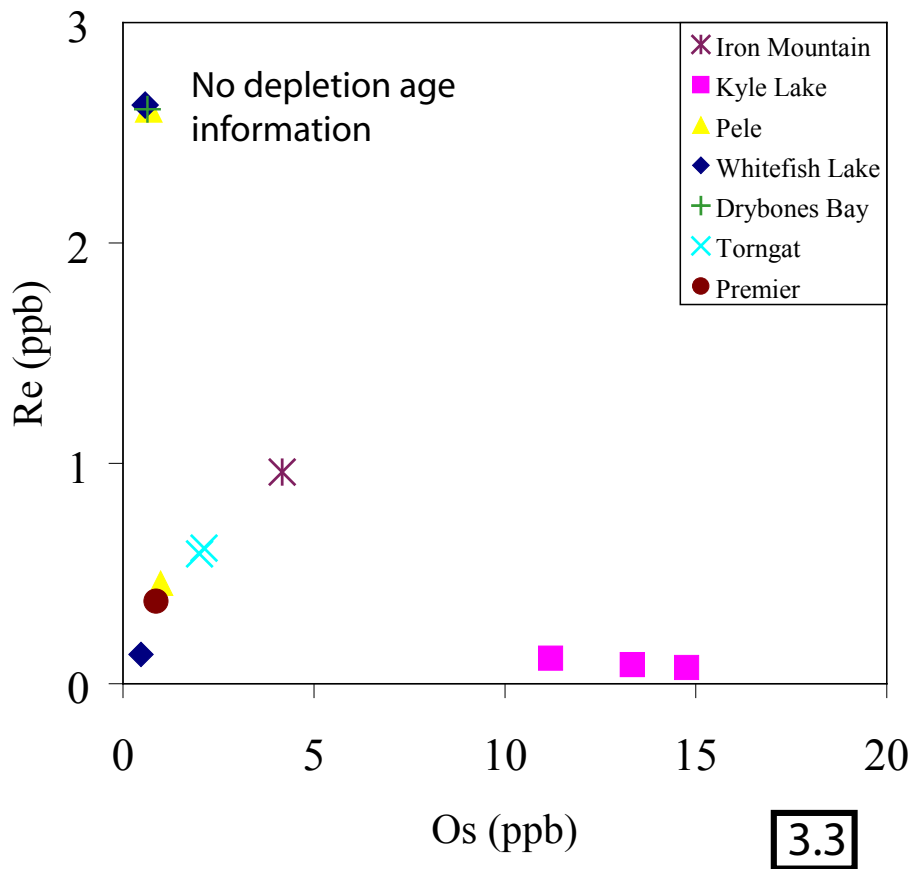
Figure 3.3

Re vs Os abundance. Samples which plot in the upper left corner of the graph did not produce meaningful depletion age information where as samples with Re/Os = ≤1 produced depletion age information.

Major element data for the samples indicate that the dominant spinel minerals are MgO-TiO$_2$-Al$_2$O$_3$ rich chromites (TMAC) and TiO$_2$ rich magnetite (TM). These compositions are similar to spinels of comparable origin worldwide (Roeder and Schulze, 2008), although they are relatively uniformly TiO$_2$-enriched. Lamprophyric spinels (WFL, P and TL) have the highest TiO$_2$ contents although P and TL also contain TiO$_2$-poor, Cr$_2$O$_3$-rich spinels. The TiO$_2$ enrichment may

be due to a sampling bias, as these minerals were separated using a magnetic free fall separator which preferentially concentrates Fe_2O_3-rich minerals, and TiO_2 content is directly proportional to Fe_2O_3 in spinels (Roeder and Schulze, 2008). A strong connection between chromite content, low Re/Os ratios and unradiogenic $^{187}Os/^{188}Os_i$ is also shown by the data. P1 and P2 oxides are the only exception to this as they contain 13 wt % chromite and γOs of 9 and -233 respectively. All of the other samples which contain a chromite-rich spinel phase constrain realistic T_{RD} ages and have low negative γOs values. The T_{RD} ages calculated for all of the samples have relatively low errors which are largely due to low $^{187}Re/^{188}Os$ ratios for the oxide minerals even though the age correction for calculating γOs and T_{RD} is large (Sambridge and Lambert, 1997).

The most interesting feature of the major element data is seen when the spinel samples are compared to published spinel data from mantle xenocrysts (Fig 3.3 and 3.4). All of the data points in Figures 3.4 and 3.5 fall outside of the mantle spinel domain (green field) indicating that the samples are unlikely to contain mantle xenocrysts. Overlap is shown between some IM and KL samples and metasomatized spinel (grey field), indicating that the analyzed spinel could contain metasomatic mantle xenocrysts. It is also possible that some spinel minerals represent crustal-derived xenocrysts, entrained during magma emplacement, although dominantly negative γOs values do not support this theory.
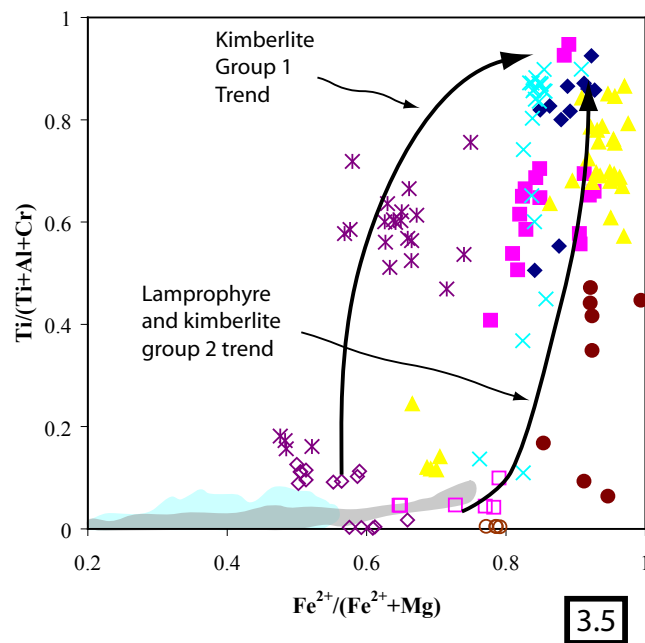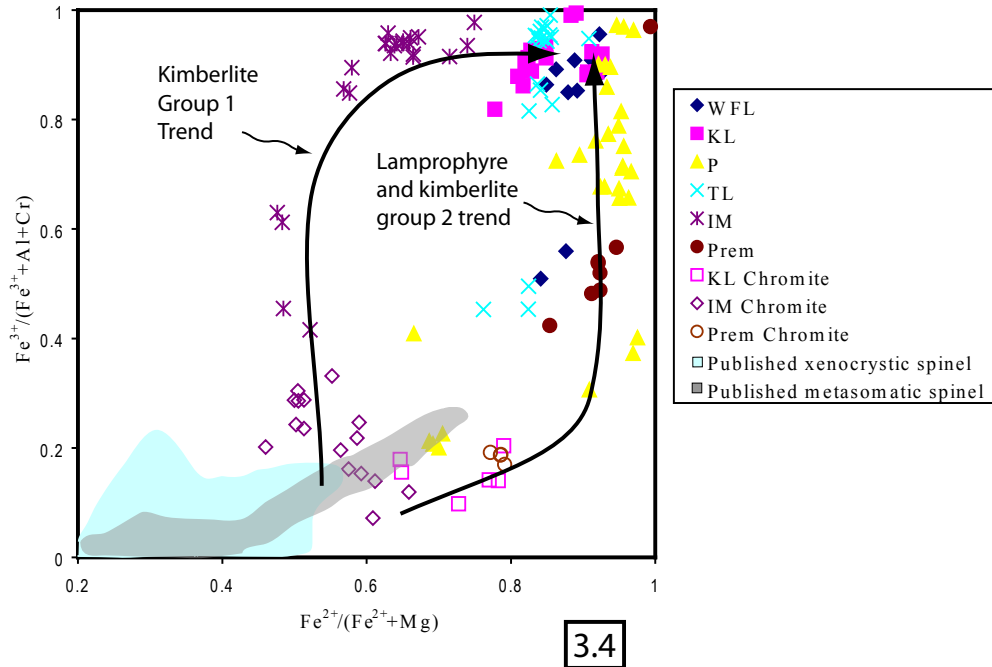
Figure 3.4 and 3.5

Spinel geochemistry data plotted on the oxidized (fig 3.4) and reduced (fig 3.5) spinel prism. Data

fields for mantle xenocrysts and metasomatized mantle xenocrysts from Roeder and Schultz (2008).

Raw data in Appendix, legend is the same for both figures
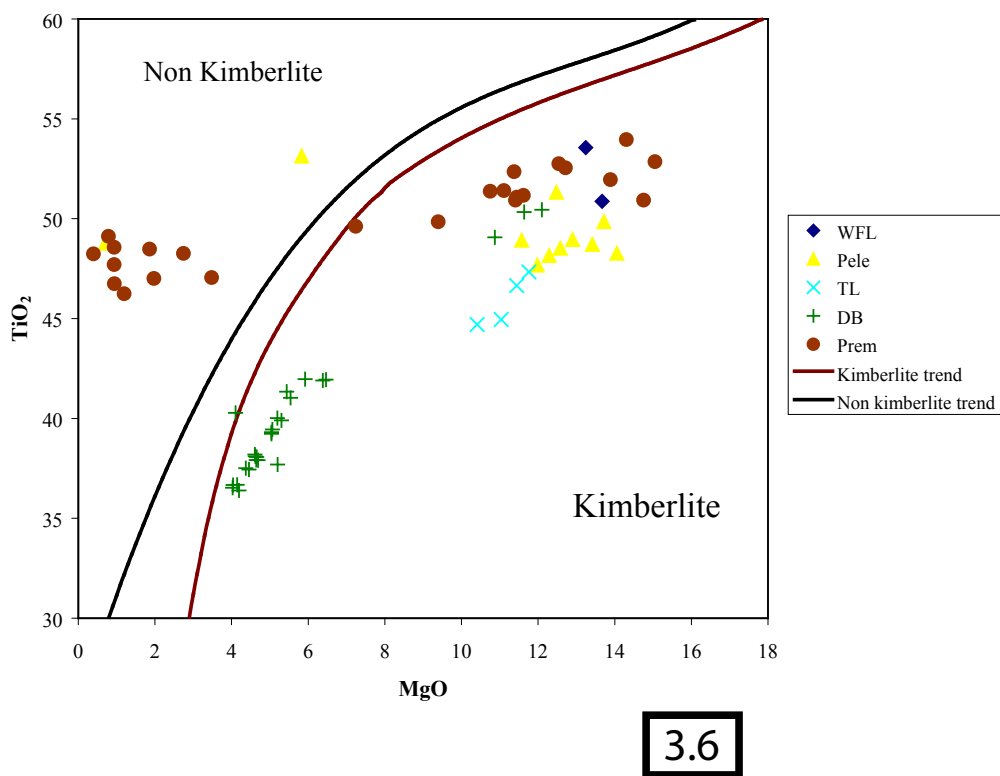
Figure 3.6

Ilmenite geochemistry data plot of TiO_2 vs MgO. Kimberlite and non kimberlite trends are taken from Wyatt et al. (2004). Raw data in Appendix

Except for spinel, ilmenite is the most common oxide phase present in these samples. Almost all of the grains analyzed were of picroilmenite composition with the exceptions composed of MnO-rich ilmenite from Prem and P. Compositional zoning was also seen in back scattered electron pictures of DB ilmenite, this zoning corresponds to variations in Fe_2O_3 content of the mineral, representing crystallization at different times during magma emplacement. Despite compositional zoning in the DB samples, most of the ilmenite samples plot within the kimberlite and lamprophyre field, Figure 3.6. The only samples which do not plot within this field

are MnO-rich ilmenites with low-MgO contents. Ilmenite compositions with MnO enrichment have been previously identified from the Premier mine (Wyatt et al., 2004) and have been interpreted as alteration of primary kimberlitic ilmenite post-emplacement or late stage interaction of ilmenite with carbonate. Wyatt et al. (2004) found Mn-rich ilmenites as rims around ilmenites of normal composition. The Mn-rich zones retain high-Cr_2O_3 (>0.5 wt.%) which is characteristic of kimberlitic ilmenite. Therefore, these ilmenites are interpreted as alteration products of a primary magmatic phase. The Premier mine ilmenites also contain tiny sulphide mineral grains associated with the Mn-rich zones, and was the only sample where sulphide minerals were observed. The sulphides can not be precisely classified due their small size ~1-2μm, (i.e. similar to the analysis spot size of the electron microprobe) and the lack of data for Co which can be a major component of mantle sulphides (Aulbach et al., 2004). The minerals appear to represent an Fe-rich Ni mineral (possibly millerite) and an Fe-rich mineral (possibly pyrrhotite).

3.4 Discussion

3.4.1. T_{RD} ages from kimberlite and lamprophyre oxides

T_{RD} ages from kimberlitic and lamprophyric oxides have rarely been calculated. The reason for this is probably due to uncertainties in obtaining primary magmatic mineral separates and problems associated with recent Re-addition. In order for the T_{RD} ages to be meaningful, all of the above concerns need to be addressed as well as links between calculated depletion ages and independent age estimates presented. If these conditions can be met, the benefit would be opening up an extremely wide

possible dataset for studying the source of kimberlitic and related magmas. There are numerous kimberlite, lamproite, lamprophyre and other deeply sourced alkaline mafic rocks worldwide, for which no mantle xenoliths are available. Oxide minerals are a dominant phase in all of these rocks, and therefore drill core samples may provide enough material to allow detailed study of the mantle source for these magmas.

3.4.2. Origin of the oxide minerals and Re-Os isotopes

Figures 3.4 and 3.5 indicate that the spinel minerals analyzed are not mantle xenocrysts. It does not however negate the possibility that the spinels were entrained from the crust during magma emplacement or were affected by Re-Os addition during assimilation of crustal xenoliths. Three different contamination possibilities are investigated below.

1) Contamination by average continental crust assimilated during magma emplacement. Figure 3.7 investigates this possibility by showing mixing trends between average continental crust and the analyzed data for KL-3 and Prem samples. The crustal contaminant end-member represents the average Re and Os concentrations reported by Shirey and Walker (1998) which is likely to be representative for all of the different cratons covered by this study. Figure 3.7 clearly shows that the Os systematics of the analyzed spinel separate are robust, and require >30% continental crustal contamination to affect the Os content and γOs of Prem (representative of most samples in this study), and >60% contamination for KL. The data also assumes that the Re and Os, liberated by assimilating average continental crust is subsequently entirely taken up by the spinel phase, which has

66

been shown not to be the case (Luguet et al., 2007). The risk of contamination by Re and Os from average continental crust is therefore minimal, however ultramafic magmas can have much higher Re-Os contents (Shirey and Walker, 1998) and therefore pose a greater threat in terms of contamination.
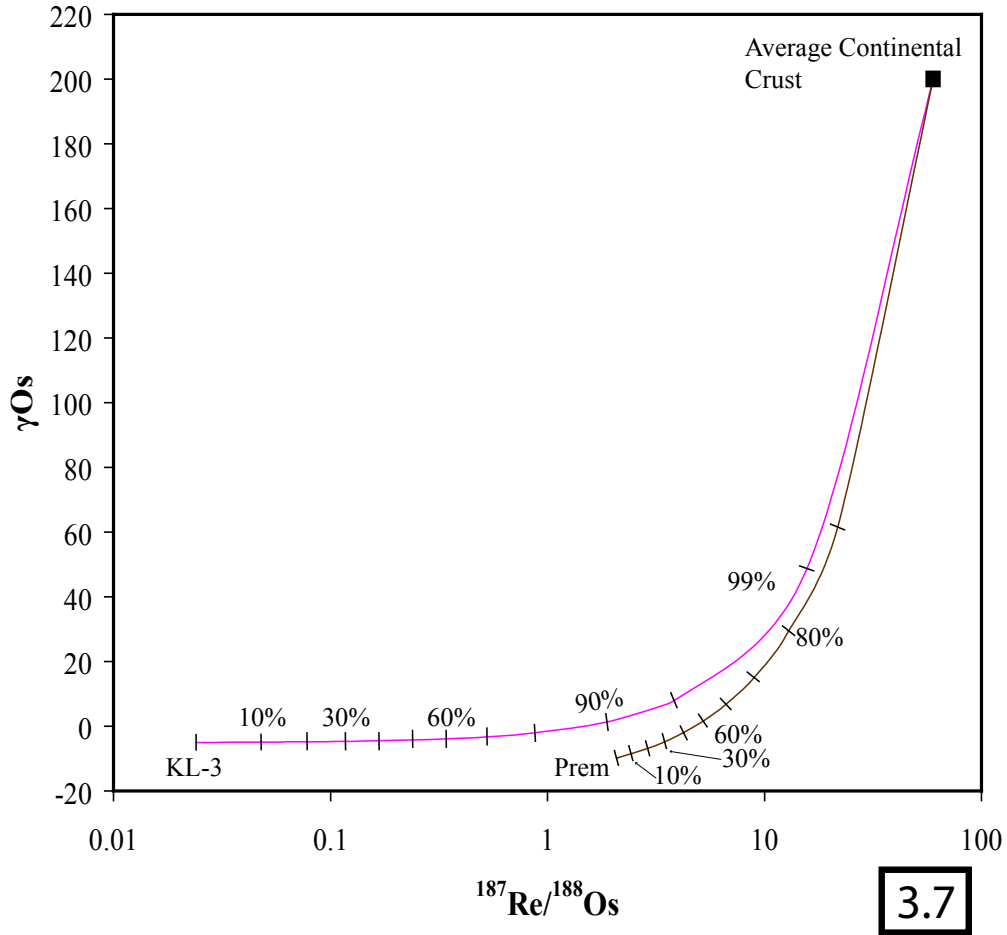
Figure 3.7

Plot of theoretical mixing between average continental crust with a $^{187}Re/^{187}Os$ ratio of 50 and a γOs value of 200 (Shirey and Walker, 1998). The values for Kyle Lake and Premier kimberlite are used to determine the effect of Re-Os addition from average continental crust.

2) Contamination by addition of chromite spinels from komatiite basalts.

This process may be applicable when magmas have erupted though Archean greenstone terrains which commonly contain large komatiite bodies e.g. the Superior Craton in the James Bay area in which KL, WFL and P are all located. Figure 3.8 suggests that very small (<1%) addition of chromite from a komatiite basalt could significantly affect the observed γOs and Os content values. The Re-Os composition of komatiitic chromite is similar to that of chromite from kimberlites and lamprophyres (Barnes, 1998) it may therefore be difficult to rule out contamination from a basaltic source. However, backscattered electron imaging of the samples suggests that analyzed chromite is found included within silicate minerals or as the core of gradationally zoned spinels. No obvious magnetite overgrowths on foreign spinels were seen, or isolated chromite xenocrysts which would be expected from this type of contamination.

3) Contamination by assimilation of ultramafic rocks during magma emplacement. Re and Os released from partial melting of ultramafic xenoliths may greatly affect the composition of the spinels (again assuming that the contaminant Re and Os strongly partition into the magmatic spinel). Re is most likely to be the major contaminant (as with the assimilation of continental crust), due to its moderately incompatible nature during melting (Righter et al., 1998). The increase in Re, added this way would correspond to an increase in radiogenic ^{187}Os over time. The addition of Re during magma emplacement is accounted for by the T_{RD} calculation and therefore would not affect T_{RD} ages, or conclusions drawn from back corrected data. Os addition from the assimilation of ultramafic basalts would be difficult to constrain, but would almost certainly have a detrimental effect on the

68

results. Although mafic/ultramafic intrusions and komatiites are relatively common within Archean cratons, and xenoliths in kimberlites can make up a very large volume of the melt, the analyzed spinel minerals are considered primary magmatic phases, and the initial Os isotopes representative of the source.
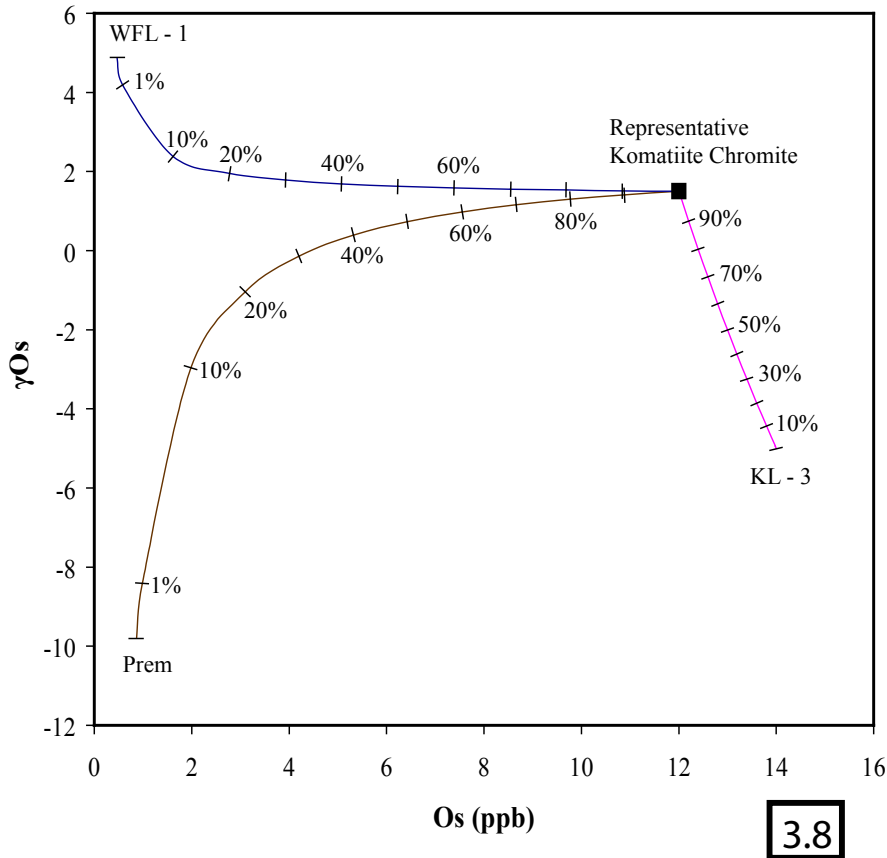
Figure 3.8

Plot of theoretical mixing between average chromite from komatiitic basalt (Gangopadhyay and Walker 2003) and three of the samples analyzed in this study. The results suggest that small amounts of komatiite chromite could greatly influence the kimberlite and lamprophyre Re-Os oxide compositions.

The samples where the initial Os isotopic composition is not considered primary are WFL and P, these samples have variable and high Re contents and

meaningless T_{RD} ages. They are both dominated by highly magnetite-rich spinel and contained no chromites. Figure 3.8 shows that these samples have elevated FeO and Al_2O_3 relative to normal spinel values, indicating post emplacement alteration. FeO enrichments have been shown to affect Re content of the samples (Chesley et al., 1999), and for this reason, the γOs and T_{RD} values for P and WFL are considered compromised. Some spinels from Prem also show evidence for post-emplacement alteration, but it is not thought to affect the γOs and T_{RD} values because Re and Os are thought to be contained within the sulphide phases, and unaltered chromite inclusions contained in and buffered by silicate phases. Also the T_{RD} age calculated for the DB sample is meaningless. The major element data (Figure 3) suggests that the ilmenite is not altered, but the very low calculated initial Os suggests that the sample has suffered post emplacement mobility of Re or Os. For this reason the DB sample was not investigated further.

3.4.3. Do the depletion ages relate to anything?

The oldest T_{RD} ages from xenolith suites have previously been shown to broadly correlate with the age of overlying crustal formation events (Carlson et al., 2005) although it is not feasible to link the depletion events to exact crustal assemblages or intrusions. If links between T_{RD} ages calculated in this study and published ages are to be drawn, they should be either with previously published xenolith T_{RD} ages, or large crustal magmatic processes and should also be treated with caution due to the infancy of this technique.
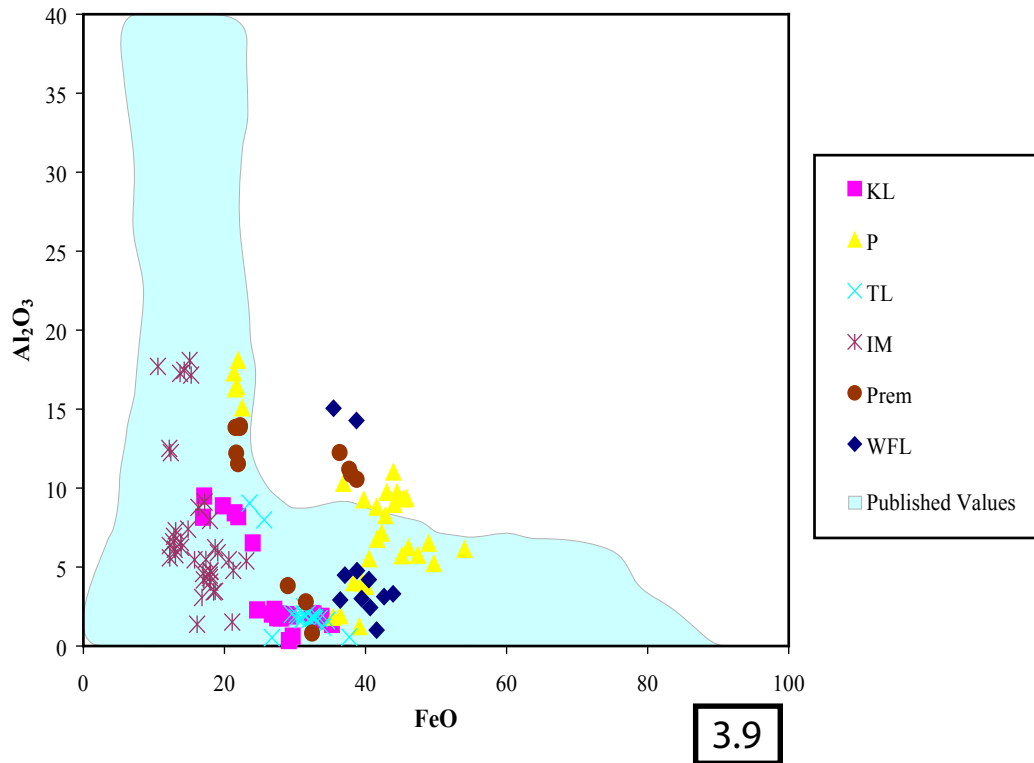
Figure 3.9

Graph showing P, WFL and Prem major element values outside the field of published kimberlitic

spinel values (Roeder and Schulze, 2008). Published spinel field incorporates >95% of all values,

published spinels also trend to higher Al_2O_3 but stay within a low FeO range. Raw data in Appendix

The samples from which depletion ages can be reliably calculated are,

KL, IM, TL and Prem, and of these, KL is clearly the most reliable, with the

smallest errors and greatest consistency. T_{MA} and T_{RD} ages for KL are similar,

and a total range in ages of 0.3 Ga is very small compared with published ages

from xenoliths and sulphides (Xu et al., 2008) suggesting the effectiveness of the

technique. No previous depletion ages have been conducted for this kimberlite

negating the possibility of comparison, although the maximum age (T_{MA} 2.34±0.4 Ga) for the sample is very similar to a proposed 2.22 Ga Superior Province break up event (Buchan et al., 1998), which suggests that the mantle under the Kyle Lake kimberlite was depleted during the breakup. The depletion age of 1.87±0.42 Ga for the IM sample is also identical to Re, Hf and Nd depletion ages found for xenoliths from the Sloan kimberlite (Carlson et al., 2004), which is located close to the Iron Mountain kimberlite in the southern Wyoming craton. The IM depletion age is also identical to the dominant age of the 1.8 Ga overlying Proterozoic crust.

The TL sample has a maximum T_{RD} age of 1.44±0.4 Ga, which is not in agreement with the major lithospheric depletion events for the NAC suggested by Tappe et al. (2007) but is identical to the Mesoproterozoic age of lamproite magmatism in the area (1.2-1.4 Ga). The Mesoproterozoic lamproites were sourced from a long-term enriched lithosphere ($\varepsilon Nd_{(i)}$=−8.4 to −5.4 and $\varepsilon Hf_{(i)}$=−11 to −7.8 Tappe et al., 2007) which does not suggest depletion at 1.44 Ga. The generation of the Mesoproterozoic magmas would be likely to reduce source isotopic enrichment at this time, especially in the Re-Os system, which is highly sensitive to magma generation. However, the generation of lamproite magma in the CLM is unlikely to create the 12-15% partial melting needed to remove all Re from the source, which would be needed, especially if it is as strongly enriched as the Nd and Hf isotopes suggest. Tappe et al. (2008), indicate that the isotopic enrichment recorded in xenoliths from the lamproites relates to metasomatism, similar to MARID metasomatism observed in the Kaapvaal craton rather than a fertile undepleted mantle source. The Re-Os system has been shown to be unaffected by MARID

metasomatism (Hopp et al., 2008) which could explain the lack of enrichment seen in γOs, but if the insensitivity of the Re-Os system to metasomatism is used to explain lack of enrichment, a T_{RD} age corresponding to some older melt depletion event would be expected. Similar T_{RD} ages (~1.8 Ga) have been found in kimberlitic xenoliths from Greenland by Wittig et al. (2008). These mantle rocks indicate initial depletion below the NAC around 3 Ga and subsequent Re depletion at 2.8 and 1.8 Ga. Wittig et al. (2008) suggest that these ages correspond to crustal formation events in the NAC. The 1.8 Ga depletion age is within error of the age calculated by this study from TL-1 supporting the conclusion of Witting et al, (2008) although it is difficult to explain the long term isotopic enrichments shown by the lithophile elements using this model.

The calculated depletion age of 3.1 Ga for the Prem sample is consistent with the dominant 3.0 Ga published T_{RD} and T_{MA} ages throughout the Kaapvaal craton (Pearson 1999; Carlson et al., 2005; Simon et al., 2007) adding further evidence that calculating depletion ages in this manner provides meaningful results.

3.4.4. What controls the T_{RD} ages

Re and Os are commonly enriched in sulphide phases within mantle derived rocks. In the absence of sulphide, Re and Os are thought to partition between the other phases available; Re, in particular commonly choosing olivine and orthopyroxene, whereas Os partitioning is more variable (Luguet et al., 2007). Relative distribution coefficients determined in this study show that Os compatibility in chromite is variable, ranging from $0.2 < D_{Os} > 20$ for WFL and KL respectively (Table 4).

73

The abundance of chromite in the sample has a strong control on Os partitioning, but it is unclear weather the Os is hosted within the chromite crystal structure, or located in PGM grains incorporated in, or around the mineral. Simple mass balance calculations suggest that the entire Os budget for the most Os rich sample (KL-3) could be accounted for by ~30 x 2μm Os rich alloys, and the Os budget of the sample poorest in Os (WFL-2) could be accounted for by 1 such grain (Table 4). These PGM grains are difficult to identify using microprobe back scattered electron imaging, especially when surrounded by oxide minerals with high Fe_2O_3 content. For this reason, and the very small expected diameter for such grains, it is possible that these alloys constrain the Os budget of the samples rather than a major oxide phase and were not identified during imaging. Re is not compatible in the structure of PGM phases (Luguet et al., 2003) and therefore, most Re should be hosted in primary magmatic minerals whereas the PGM grains are more likely to be micro xenocrysts. The decoupling of Re and Os is shown most noticeably in KL samples where Os content seems inversely correlated with Re (Figure 3.2). TL oxides however retain relatively consistent Re and Os concentrations between the two analysis and do not show evidence of decoupling. One explanation for this could be the higher abundance of ilmenite within the TL sample. Puchtel et al. (1999) have suggested that ilmenite may have a partition coefficient of up to 12 for Re in ultramafic magmas, possibly explaining the relative Re abundance in TL, over KL, which contains no ilmenite and is extremely Re poor. There also doesn't appear to be evidence for significant Re or Os partitioning into magnetite, which is shown by the low Re and high magnetite content of KL samples. Prem is the only sample in which Re and Os abundance can not be explained by variable

74

chromite (and PGM grains) and ilmenite contents and is the only sample with sulphide minerals present. Sulphide was only identified as a trace phase, and was contained within a Mn-rich ilmenite, which has been shown to be related to post emplacement alteration. Despite the occurrence of sulphide minerals within altered minerals, the high Re-Os distribution coefficients for sulphides indicate that they are most likely the major host for Re and Os within the Prem sample. Sulphide is known to be affected by metasomatism and alteration during magma emplacement (e.g. Aulbach et al. 2004; Xu et al. 2008), and the location of the grains within altered ilmenite suggests that the sulphides have experienced alteration. The high Re content of Prem indicates that the sulphides may have been affected by Re addition. The affects of Re addition are removed during T_{RD} calculations, allowing seemingly meaningful T_{RD} ages to be calculated.

Sample	Number of Os alloy grains (2μm diameter)	D_{Os}
IM	8.8	5.17
KL-3	31.2	21.83
KL-2	28.2	19.74
KL-1	23.7	16.56
P-2	1.4	1.99
P-1	2.1	2.91
WFL-2	1.0	0.18
WFL-1	1.2	0.22
DB	1.3	0.25
TL-2	4.5	8.16
TL1	4.2	7.72
Prem	1.8	3.35

Table 3.4

3.4

Number of Os alloys calculated assuming RuOs composition (Luguet et al., 2007) and 2μm diameter, number of alloy grains needed to satisfy the Os budget decreases exponentially as the diameter is increases. D_{Os} calculated assuming an average Os content of PUM = 2.3 ng/g (Meisel et al, 2001)

3.4.5. Mantle source region

The location and nature of the source region for kimberlites and lamprophyres is poorly understood. Numerous locations for the source of such magmas have been proposed, ranging from the core-mantle boundary (Haggerty, 1994) to the CLM (Becker and Le Roex, 2006) and all of the mantle in between. The Re-Os oxide data from the kimberlites and lamprophyres analyzed here does not allow constraints to be placed on an exact location for the source region, but can be used to infer the nature of the source.

All of the Os isotopic data presented here for oxide minerals that produce meaningful T_{RD} or T_{MA} ages and have not been affected by post emplacement alteration, have negative γOs values (Figure 3.9, Table 3.3). The negative γOs indicate that the source region for these magmas has experienced $^{187}Os/^{188}Os$ depletion relative to average mantle at least 1Ga prior to magma genesis. The source region for kimberlites and lamprophyres must therefore be dominated by a depleted lithology, and has likely remained isolated from the convective mixing of the asthenosphere for a long time. Depleted lithologies within the mantle are most typically harzburgite or dunite (Griffin et al., 2009) and as a result these lithologies would be expected to make up the largest component of the source. Recent studies have shown that mantle-derived isotopically depleted magmas may be more depleted than the isotopic ratios suggest due to mixing and assimilation of enriched (isotopically normal) magmas during ascent to the surface (Stracke and Bourdon, 2009). Therefore the negative γOs values obtained in this study strongly indicate a depleted source. This observation is consistent with experimental and

76

observational results which suggest that kimberlites and lamprophyres require re-fertilized, melt-depleted sources to account for their major and trace element abundances (Brey et al., 2008; Tainton and McKenzie, 1994).
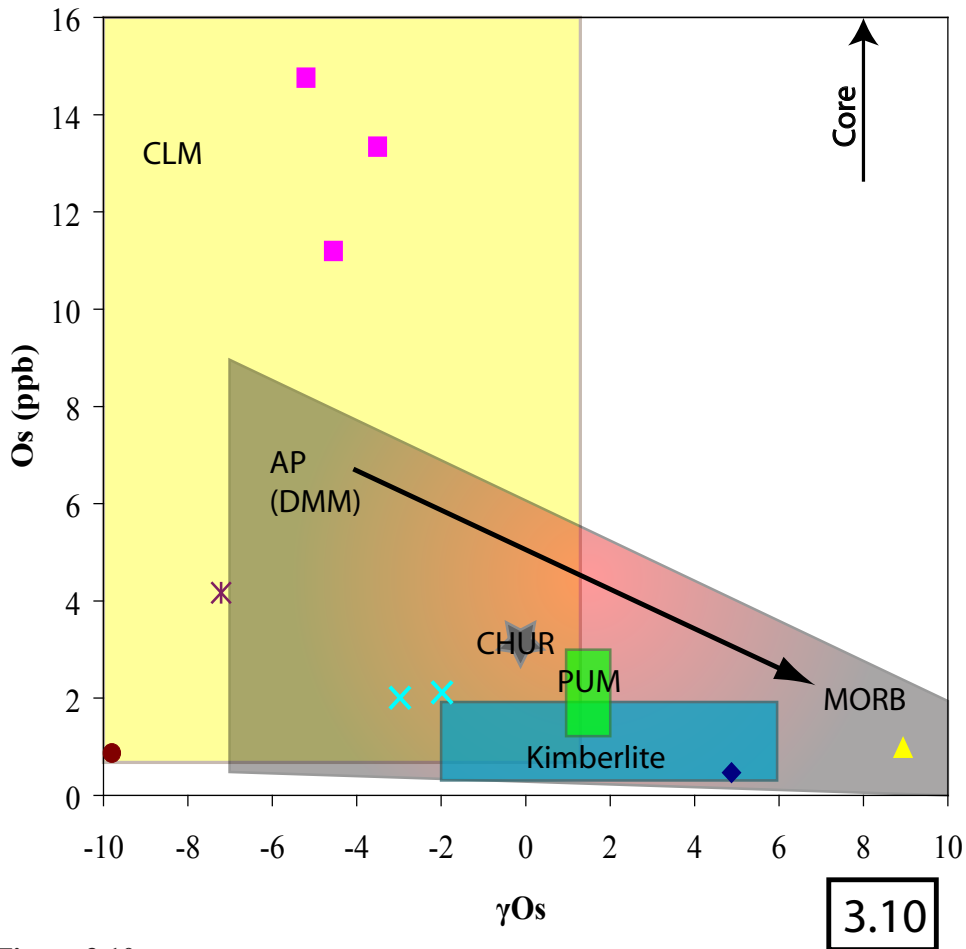
Figure 3.10

Samples plotted against various mantle reservoirs in γOs vs Os space. The symbols are the same as used in all previous diagrams. Continental lithospheric mantle (CLM) values were taken from Brandon et al., (2006) and Shirey and Walker, (1998), Abyssal peridotites (AP) values are used to represent depleted MORB mantle (DMM), AP values represent a continuum towards MORB which plots off the diagram to the bottom right, values were taken from Alard et al. (2005). CHUR and PUM values were obtained from Shirey and Walker, (1998) and Meisel et al. (2001). Average kimberlite values were obtained from Graham et al. (2004) and Aulbach (2009 unpublished data).

As indicated previously the location of these depletion events can not be constrained from the Re-Os data, but some elements of the kimberlite and lamprophyre source can be discussed. For example, Haggerty (1994) and more recently Sim and Agterberg (2006) suggested that kimberlites may be formed by interaction between the core and the mantle at the core-mantle boundary. Modeling using the outer core compositions of Walker et al. (1995) indicates that the total Os budget of the most Os-rich sample (KL3) could be accounted for by adding a 0.012% core component to CHUR, but the resulting γOs would be +4 compared to the observed value of -5 suggesting that even a very small core component in the magmas is very unlikely.

Similar calculations can be conducted to assess the possible influence of subducted oceanic crust in the source of the melts. Oceanic crust subducted to the transition zone has often been suggested as the origin for metasomatic melts which enrich the source regions of kimberlites (Ringwood et al., 1992; Nowell et al., 2004; Paton et al., 2009). Using Re = 0.05 ppb and $^{187}Re/^{188}Os$ = 0.045 (Shirey and Walker, 1998; Meibom et al., 2002) to represent the depleted mantle source and Re = 0.9 and $^{187}Re/^{188}Os$ = 150 (Walker et al., 2002) to represent subducted oceanic crust, mixing models can be created. If the depleted source is enriched by addition of a 0.3% melt from oceanic crust, a conservative estimate of the melt volume required to create isotopic enrichments recorded in kimberlitic HREE and LREE (Becker and Le Roex, 2006), the Re and $^{187}Re/^{188}Os$ content of the mixture (Re = 0.8 ppb and $^{187}Re/^{188}Os$ = 0.49) does not fit any of the data particularly well. The Re content, and subsequently the $^{187}Re/^{188}Os$ of subducted oceanic crust are not very

78

well constrained due to uncertainties in the original content of the basalt, and the Re lost due to dehydration during subduction. Variations of up to 40% in the Re content and $^{187}Re/^{188}Os$ of the modeled subducted crust still do not sufficiently fit any of the observed data even when the amount of melting is increased up to 1%. Also the Os content and isotopic composition of subducted oceanic crust is unlikely to fit the data because of the high $^{187}Re/^{188}Os$ ratio, and therefore γOs of MORB (Figure 3.9). The oceanic lithosphere is a more likely source for the Os because it is the depleted residue after the formation of MORB. Fig 3.9 shows that the γOs of the samples are more negative than that of abyssal peridotites, but if the subducted lithosphere is shielded from recycling in the mantle, over time (e.g. Pearson and Nowell, 2002), the γOs of the AP will become more negative, potentially overlapping with that of the samples. The Os contents of the KL samples are conspicuously higher than the AP field, but the values can not be directly compared because the KL samples are mineral separates, rather than whole rock analysis.

The γOs and Os content of the samples suggest a CLM origin for the Os (Figure 3.9), which has often been proposed as the source for kimberlite and lamprophyre magmas (e.g. Becker and La Roex 2006; Tappe et al., 2007). The variations in the γOs values suggest that the CLM maybe heterogeneous in terms of Os isotopic composition, which is probably related to previous melt depletion events. Heterogeneity has also been documented in other isotopic systems, e.g. Argon (Hopp et al., 2007), but the values are consistently depleted relative to PUM or CHUR. A CLM origin for the Os does not seem surprising because the depletion events documented by the oxide minerals indicate a coupled history between the

79

source of the magmatism and the overlying crust.

The depleted Os isotopes found within the spinel minerals in general support a two-stage model of kimberlite formation where long-term depleted mantle residue is enriched by incompatible elements (and possibly Re) before magma generation but no practical information can be obtained regarding the location of the source. The very negative γOs and modeling results suggest that either metasomatic enrichment occurs just prior to melting which is also a suggestion from other isotopic studies, e.g. Nd and Sr (McCulloch et al., 1983) or that Re is not significantly mobilized by the event.

The results also suggest that calculating T_{RD} or T_{MA} ages using oxide minerals from kimberlites and lamprophyres is a viable alternative to the currently used method of calculating the ages using sulphides from mantle xenoliths or using the mantle xenoliths themselves. Rock core samples containing oxide minerals from kimberlite and related magmas are relatively common whereas large xenolith samples are not. Further study is needed to confirm the findings as this contribution only analyzed 7 intrusions across North America and South Africa with 4 producing meaningful results.

3.5. Summary

^{187}Re-^{188}Os isotopes have been investigated in kimberlitic and lamprophyre groundmass spinel. Chromite, which is associated with early stages of spinel evolution during magma genesis and eruption, controls Os abundance within the

80

spinel group minerals, although the role of PGM grains included in chromites is not clear. Re shows some evidence of preferential partitioning into ilmenite, but magnetite-rich spinels do not significantly partition Re or Os from the host magma. Depletion and model ages calculated from the spinel data using known emplacement ages for the magmas show broad correlation with previously published depletion ages, and large scale crustal magmatic events. Initial Os isotopes for KL, TL, IM and Prem samples suggest that the magmas were sourced from domains in the mantle which have experienced long-term depletion and isolation from the convecting mantle. Information regarding the location of the source can not be ascertained from the data, but the Os isotopes are consistent with a two-stage kimberlite and lamprophyre formation, where an initially depleted source is enriched in incompatible elements via metasomatism prior to magma generation. Strongly negative γOs values suggest that this metasomatic event occurred temporally close to melt generation, or did not involve Re and Os isotopes. The results of this study suggest that Re-Os isotopes in magmatic oxide minerals may provide an easy alternative to mantle xenoliths and mantle sulphides for assessing the lithospheric mantle, especially when the crystallization age of the magma is known.

3.6 References

Alard, O., Griffin, W.L., Pearson, N.J., Lorand, J.P. and O'Reilly, S.Y., 2002. New insights into the Re-Os systematics of sub-continental lithospheric mantle from in situ analysis of sulphides. Earth and Planetary Science Letters, 203(2): 651-663.

Alard, O., Luguet, A., Pearson, N. J., Griffin, W. L., Lorand, J. P., Gannoun, A., Burton, K. W., and O'Reilly, S. Y., 2005. In situ Os isotopes in abyssal peridotites bridge the isotopic gap between MORBs and their source mantle. Nature, 436(7053): 1005-1008.

Aulbach, S., Griffin, W. L., Pearson, N. J., O'Reilly, S. Y., Kivi, K. D., and Buddy J., 2004. Mantle formation and evolution, Slave Craton: constraints from HSE abundances and Re-Os isotope systematics of sulfide inclusions in mantle xenocrysts. Chemical Geology, 208(1-4): 61-88.

Barnes, S.J., 1998. Chromite in komatiites, 1. Magmatic controls on crystallization and composition. Journal of Petrology, 39(10): 1689-1720.

Becker, M. and Le Roex, A.P., 2006. Geochemistry of South African on- and off-craton, Group I and Group II kimberlites: Petrogenesis and source region evolution. Journal of Petrology, 47(4): 673-703.

Birck, J.L., RoyBarman, M. and Capmas, F., 1997. Re-Os isotopic measurements at the femtomole level in natural samples. Geostandards Newsletter-the Journal of Geostandards and Geoanalysis, 21(1): 19-27.

Brandon, A.D., Creaser, R.A., Shirey, S.B. and Carlson, R.W., 1996. Osmium recycling in subduction zones. Science, 272(5263): 861-864.

Brandon, A.D., Walker, R.J. and Puchtel, I.S., 2006. Platinum-osmium isotope

evolution of the Earth's mantle: Constraints from chondrites and Os-rich alloys. Geochimica Et Cosmochimica Acta, 70(8): 2093-2103.

Brey, G.P., Bulatov, V.K., Girnis, A.V. and Lahaye, Y., 2008. Experimental melting of carbonated peridotite at 610 GPa. Journal of Petrology, 49(4): 797-821.

Buchan, K.L., Mortensen, J.K. and Card, K.D., 1993. Northeast - trending early Proterozoic dykes of southern Superior province - multiple episodes of emplacement recognized from integrated paleomagnetism and U-Pb geochronology. Canadian Journal of Earth Sciences, 30(6): 1286-1296.

Buchan, K.L., Mortensen, J.K., Card, K.D. and Percival, J.A., 1998. Paleomagnetism and U-Pb geochronology of diabase dyke swarms of Minto block, Superior Province, Quebec, Canada. Canadian Journal of Earth Sciences, 35(9): 1054-1069.

Buchan, K.L., Goutier, J., Hamilton, M.A., Ernst, R.E. and Matthews, W.A., 2007. Paleomagnetism, U-Pb geochronology, and geochemistry of Lac Esprit and other dyke swarms, James Bay area, Quebec, and implications for Paleoproterozoic deformation of the Superior Province. Canadian Journal of Earth Sciences, 44(5): 643-664.

Carbno, G.B. and Canil, D., 2002. Mantle structure beneath the SW Slave craton, Canada: Constraints from garnet geochemistry in the Drybones Bay kimberlite. Journal of Petrology, 43(1): 129-142.

Carlson, R.W., Irving, A.J., Schulze, D.J. and Hearn, B.C., 2004. Timing of Precambrian melt depletion and Phanerozoic refertilization events in the lithospheric mantle of the Wyoming Craton and adjacent Central Plains Orogen, pp. 453-472.

Carlson, R.W., Pearson, D.G. and James, D.E., 2005. Physical, chemical, and chronological characteristics of continental mantle. Reviews of Geophysics, 43(1): 24.

Chesley, J.T., Rudnick, R.L. and Lee, C.T., 1999. Re-Os systematics of mantle xenoliths from the East African Rift: Age, structure, and history of the Tanzanian craton. Geochimica Et Cosmochimica Acta, 63(7-8): 1203-1217.

Cohen, A.S. and Waters, F.G., 1996. Separation of osmium from geological materials by solvent extraction for analysis by thermal ionisation mass spectrometry. Analytica Chimica Acta, 332(2-3): 269-275.

Creaser, R.A., Sannigrahi, P., Chacko, T. and Selby, D., 2002. Further evaluation of the Re-Os geochronometer in organic-rich sedimentary rocks: A test of hydrocarbon maturation effects in the Exshaw Formation, Western Canada Sedimentary Basin. Geochimica Et Cosmochimica Acta, 66(19): 3441-3452.

Dai, B.Z., Jiang, S.Y., Jiang, Y.H., Zhao, K.D. and Liu, D.Y., 2008. Geochronology, geochemistry and Hf-Sr-Nd isotopic compositions of Huziyan mafic xenoliths, southern Hunan Province, South China: Petrogenesis and implications for lower crust evolution. Lithos, 102(1-2): 65-87.

Finnigan, C.S., Brenan, J.M., Mungall, J.E. and McDonough, W.F., 2008. Experiments and models bearing on the role of chromite as a collector of platinum group minerals by local reduction. Journal of Petrology, 49(9): 1647-1665.

Gangopadhyay, A. and Walker, R.J., 2003. Re-Os systematics of the ca. 2.7-Ga komatiites from Alexo, Ontario, Canada. Chemical Geology, 196(1-4): 147-

162.

Graham, S., Lambert, D. and Shee, S., 2004. The petrogenesis of carbonatite, melnoite and kimberlite from the Eastern Goldfields Province, Yilgarn Craton. Lithos, 76(1-4): 519-533.

Griffin, W.L., Graham, S., O'Reilly, S.Y. and Pearson, N.J., 2004. Lithosphere evolution beneath the Kaapvaal Craton: Re-Os systematics of sulfides in mantle-derived peridotites. Chemical Geology, 208(1-4): 89-118.

Griffin, W.L., O'Reilly, S.Y., Afonso, J.C. and Begg, G.C., 2009. The Composition and Evolution of Lithospheric Mantle: a Re-evaluation and its Tectonic Implications. Journal of Petrology, 50(7): 1185-1204.

Haggerty, S.E., 1994. Superkimberlites - A geodynamic diamond window to the Earths core. Earth and Planetary Science Letters, 122(1-2): 57-69.

Heaman, L.M., 1997. Global mafic magmatism at 2.45 Ga: Remnants of an ancient large igneous province? Geology, 25(4): 299-302.

Heaman, L.M., Kjarsgaard, B.A. and Creaser, R.A., 2003. The timing of kimberlite magmatism in North America: implications for global kimberlite genesis and diamond exploration. Lithos, 71(2-4): 153-184.

Heaman, L.M., Kjarsgaard, B.A. and Creaser, R.A., 2004. The temporal evolution of north American kimberlites. Lithos, 76(1-4): 377-397.

Heaman, L. M., Easton, R. M., Hart, T. R., Hollings, P., MacDonald, C. A., and Smyk, M., 2007. Further refinement to the timing of Mesoproterozoic magmatism, Lake Nipigon region, Ontario. Canadian Journal of Earth Sciences, 44(8): 1055-1086.

Heaman, L.M. and Machado, N., 1992. Timing and origin of mid-continent

rift alkaline magmatism, North America: evidence from the Coldwell Complex.. Contributions to Mineralogy and Petrology, 110: 289-303.

Hopp, J., Trieloff, M., Buikin, A. I., Korochantseva, E. V., Schwarz, W. H., Althaus, T., and Altherr, R., 2007. Heterogeneous mantle argon isotope composition in the subcontinental lithospheric mantle beneath the Red Sea region. Chemical Geology, 240(1-2): 36-53.

Hopp, J., Trieloff, M., Brey, G. P., Woodland, A. B., Simon, N. S. C., Wijbrans, J. R., Siebel, W., and Reitter, E., 2008. Ar-40/Ar-39-ages of phlogopite in mantle xenoliths from South African kimberlites: Evidence for metasomatic mantle impregnation during the Kibaran orogenic cycle. Lithos, 106(3-4): 351-364.

Hoffman, P.F., 1990. Dynamics of the tectonic assembly of northeast Laurentia in geon-18 (1.9-1.8-GA). Geoscience Canada, 17(4): 222-226.

Ionov, D.A., Shirey, S.B., Weis, D. and Brugmann, G., 2006. Os-Hf-Sr-Nd isotope and PGE systematics of spinel peridotite xenoliths from Tok, SE Siberian craton: Effects of pervasive metasomatism in shallow refractory mantle. Earth and Planetary Science Letters, 241(1-2): 47-64.

Kamo, S.L., Gower, C.F. and Krogh, T.E., 1989. Birthdate for the Iapetus Ocean - a precise U-Pb Zircon and baddeleyite age for the long-range dikes, southeast Labrador. Geology, 17(7): 602-605.

Kerr, D.E., Smith, D. and Wilson, P., 2000. Anomalous kimberlite indicator mineral and gold grain abundances, Drybones Bay and Yellowknife area, Northwest Territories. Open File D3861, Geological Survey of Canada.

Lambert, D.D., Frick, L.R., Foster, J.G., Li, C.S. and Naldrett, A.J., 2000. Re-

Os isotope systematics of the Voisey's Bay Ni-Cu-Co magmatic sulfide system, Labrador, Canada: II. Implications for parental magma chemistry ore genesis, and metal redistribution. Economic Geology and the Bulletin of the Society of Economic Geologists, 95(4): 867-888.

Lecheminant, A.N. and Heaman, L.M., 1989. Mackenzie igneous events, Canada: Middle Proterozoic hotspot magmatism associated with ocean opening Earth and Planetary Science Letters, 96(1-2): 38-48.

Locock, A.J., 2008. An Excel spreadsheet to recast analyses of garnet into end-member components, and a synopsis of the crystal chemistry of natural silicate garnets. Computers & Geosciences, 34(12): 1769-1780.

Lorand, J.P. and Alard, O., 2001. Platinum-group element abundances in the upper mantle: New constraints from in situ and whole-rock analyses of Massif Central xenoliths (France). Geochimica Et Cosmochimica Acta, 65(16): 2789-2806.

Lorand, J.P., Pattou, L. and Gros, M., 1999. Fractionation of platinum-group elements and gold in the upper mantle: a detailed study in Pyrenean orogenic lherzolites. Journal of Petrology, 40(6): 957-981.

Luguet, A., Lorand, J.P. and Seyler, M., 2003. Sulfide petrology and highly siderophile element geochemistry of abyssal peridotites: A coupled study of samples from the Kane Fracture Zone (45 degrees W 23 degrees 20N, MARK Area, Atlantic Ocean). Geochimica Et Cosmochimica Acta, 67(8): 1553-1570.

Luguet, A., Shirey, S.B., Lorand, J.P., Horan, M.F. and Carlson, R.W., 2007. Residual platinum-group minerals from highly depleted harzburgites of the

87

Lherz massif (France) and their role in HSE fractionation of the mantle. Geochimica Et Cosmochimica Acta, 71(12): 3082-3097.

McCulloch, M.T., Jaques, A.L., Nelson, D.R. and Lewis, J.D., 1983. Nd and Sr isotopes in kimberlites and lamproites from Western-Australia - an enriched mantle origin. Nature, 302(5907): 400-403.

Meibom, A., Sleep, N. H., Chamberlain, C. P., Coleman, R. G., Frei, R., Hren, M. T., and Wooden, J. L., 2002. Re-Os isotopic evidence for long-lived heterogeneity and equilibration processes in the Earth's upper mantle. Nature, 419(6908): 705-708.

Meisel, T., Walker, R.J., Irving, A.J. and Lorand, J.P., 2001. Osmium isotopic compositions of mantle xenoliths: A global perspective. Geochimica Et Cosmochimica Acta, 65(8): 1311-1323.

Mitchell, R.H. and Clarke, D.B., 1976. Oxide and sulfide mineralogy of Peuykuk kimberlite, Somerset Island, NWT Canada. Contributions to Mineralogy and Petrology, 56(2): 157-172.

Morgan, J.W., Golightly, D.W. and Dorrzapf, A.F., 1991. Methods for the separation of Rhenium, Osmium and Molybdenum applicable to isotope geochemistry Talanta, 38(3): 259-265.

Mueller, P.A. and Frost, C.D., 2006. The Wyoming Province: a distinctive Archean craton in Laurentian North America. Canadian Journal of Earth Sciences, 43(10): 1391-1397.

Nagler, T.F., Kramers, J.D., Kamber, B.S., Frei, R. and Prendergast, M.D.A., 1997. Growth of subcontinental lithospheric mantle beneath Zimbabwe started at or before 3.8 Ga: Re-Os study on chromites. Geology, 25(11): 983-986.

Nowell, G.M., Pearson, D. G., Bell, D. R., Carlson, R. W., Smith, C. B., Kempton, P.D., and Noble, S. R., 2004. Hf isotope systematics of kimberlites and their megacrysts: New constraints on their source regions. Journal of Petrology, 45(8): 1583-1612.

Paton, C., Hergt, J.M., Woodhead, J.D., Phillips, D. and Shee, S.R., 2009. Identifying the asthenospheric component of kimberlite magmas from the Dharwar Craton, India. Lithos, In Press, Accepted Manuscript.

Pearson, D.G., 1999. The age of continental roots. Lithos, 48(1-4): 171-194.

Pearson, D.G. and Nowell, G.M., 2002. The continental lithospheric mantle: characteristics and significance as a mantle reservoir. Philosophical Transactions of the Royal Society of London Series a-Mathematical Physical and Engineering Sciences, 360(1800): 2383-2410.

Pearson, D.G., Parman, S.W. and Nowell, G.M., 2007. A link between large mantle melting events and continent growth seen in osmium isotopes. Nature, 449(7159): 202-205.

Pearson, D.G. and Wittig, N., 2008. Formation of Archaean continental lithosphere and its diamonds: the root of the problem. Journal of the Geological Society, 165: 895-914.

Puchtel, I.S., Brugmann, G.E. and Hofmann, A.W., 1999. Precise Re-Os mineral isochron and Pb-Nd-Os isotope systematics of a mafic-ultramafic sill in the 2.0 Ga Onega plateau (Baltic Shield). Earth and Planetary Science Letters, 170(4): 447-461.

Queen, M., Heaman, L.M., Hanes, J.A., Archibald, D.A. and Farrar, E., 1996. Ar-40/Ar-39 phlogopite and U-Pb perovskite dating of lamprophyre dykes

from the eastern Lake Superior region: Evidence for a 1.14 Ga magmatic precursor to Midcontinent Rift volcanism. Canadian Journal of Earth Sciences, 33(6): 958-965.

Reisberg, L., Lorand, J.-P. and Bedini, R.M., 2004. Reliability of Os model ages in pervasively metasomatized continental mantle lithosphere: a case study of Sidamo spinel peridotite xenoliths (East African Rift, Ethiopia). Chemical Geology, 208(1-4): 119-140.

Reisberg, L., Zhi, X. C., Lorand, J. P., Wagner, C., Peng, Z. C., and Zimmermann, C., 2005. Re-Os and S systematics of spinel peridotite xenoliths from east central China: Evidence for contrasting effects of melt percolation. Earth and Planetary Science Letters, 239(3-4): 286-308.

Richardson, S.H., 1986. Latter-day origin of diamonds of eclogitic paragenesis. Nature, 322(6080): 623-626.

Righter, K., Chesley, J.T., Geist, D. and Ruiz, J., 1998. Behavior of Re during magma fractionation: an example from Volcan Alcedo, Galapagos. Journal of Petrology, 39(4): 785-795.

Ringwood, A.E., Kesson, S.E., Hibberson, W. and Ware, N., 1992. Origin of kimberlites and related magmas. Earth and Planetary Science Letters, 113(4): 521-538.

Roeder, P.L. and Schulze, D.J., 2008. Crystallization of groundmass spinel in kimberlite. Journal of Petrology, 49(8): 1473-1495.

Sambridge, M. and Lambert, D.D., 1997. Propagating errors in decay equations: Examples from the Re---Os isotopic system. Geochimica et Cosmochimica Acta, 61(14): 3019-3024.

Selby, D. and Creaser, R.A., 2001. Re-Os geochronology and systematics in molybdenite from the Endako porphyry molybdenum deposit, British Columbia, Canada. Economic Geology and the Bulletin of the Society of Economic Geologists, 96(1): 197-204.

Selby, D. and Creaser, R.A., 2003. Re-Os geochronology of organic rich sediments: an evaluation of organic matter analysis methods. Chemical Geology, 200(3-4): 225-240.

Selby, D., Creaser, R.A., Stein, H.J., Markey, R.J. and Hannah, J.L., 2007. Assessment of the 187Re decay constant by cross calibration of Re-Os molybdenite and U-Pb zircon chronometers in magmatic ore systems. Geochimica et Cosmochimica Acta, 71(8): 1999-2013.

Shirey, S.B. and Walker, R.J., 1998. The Re-Os isotope system in cosmochemistry and high-temperature geochemistry. Annual Review of Earth and Planetary Sciences, 26: 423-500.

Sim, B.L. and Agterberg, F.P., 2006. A conceptual model for kimberlite emplacement by solitary interfacial mega-waves on the core mantle boundary. Journal of Geodynamics, 41(5): 451-461.

Simon, N.S.C., Carlson, R.W., Pearson, D.G. and Davies, G.R., 2007. The origin and evolution of the Kaapvaal cratonic lithospheric mantle. Journal of Petrology, 48(3): 589-625.

Stracke, A. and Bourdon, B., 2009. The importance of melt extraction for tracing mantle heterogeneity. Geochimica Et Cosmochimica Acta, 73(1): 218-238.

Tainton, K.M. and McKenzie, D., 1994. The generation of kimberlites, lamproites, and their source rocks. Journal of Petrology, 35(3): 787-817.

Tappe, S., Foley, S. F., Stracke, A., Romer, R. L., Kjarsgaard, B. A., Heaman, L. M., and Joyce, N., 2007. Craton reactivation on the Labrador Sea margins: Ar-40/Ar-39 age and Sr-Nd-Hf-Pb isotope constraints from alkaline and carbonatite intrusives. Earth and Planetary Science Letters, 256(3-4): 433-454.

Tappe, S., Foley, S. F., Kjarsgaard, B. A., Romer, R. L., Heaman, L. M., Stracke, A., and Jenner, G. A., 2008. Between carbonatite and lamproite - Diamondiferous Torngat ultramafic lamprophyres formed by carbonate-fluxed melting of cratonic MARID-type metasomes. Geochimica Et Cosmochimica Acta, 72(13): 3258-3286.

Tompkins, L.A. and Haggerty, S.E., 1985. Groundmass oxide minerals in the Koidu kimberlite dikes, Sierra-Leone, West Africa. Contributions to Mineralogy and Petrology, 91(3): 245-263.

van Straaten, B.I., Kopylova, M.G., Russell, J.K., Webb, K.J. and Smith, B.H.S., 2008. Discrimination of diamond resource and non-resource domains in the Victor North pyroclastic kimberlite, Canada. Journal of Volcanology and Geothermal Research, 174: 128-138.

Walker, R.J., Carlson, R.W., Shirey, S.B. and Boyd, F.R., 1989. Os, Sr, Nd and Pb isotope systematics of Southern African peridotite xenoliths - implications for the chemical evolution of subcontinental mantle. Geochimica Et Cosmochimica Acta, 53(7): 1583-1595.

Walker, R.J., Morgan, J. W., Horan, M. F., Czamanske, G. K., Krogstad, E. J., Fedorenko, V. A., and Kunilov, V. E., 1994. Re-Os isotopic evidence for an enriched-mantle source for teh Norilsk-type, ore-bearing intrustions,

Siberia. Geochimica Et Cosmochimica Acta, 58(19): 4179-4197.

Walker, R.J., Morgan, J.W. and Horan, M.F., 1995. Osmium-187 Enrichment in Some Plumes: Evidence for Core-Mantle Interaction? . Science, 269(5225): 819-822.

Walker, R.J., Prichard, H.M., Ishiwatari, A. and Pimentel, M., 2002. The osmium isotopic composition of convecting upper mantle deduced from ophiolite chromites. Geochimica Et Cosmochimica Acta, 66(2): 329-345.

Whitmeyer, S.J. and Karlstrom, K.E., 2007. Tectonic model for the Proterozoic growth of North America. Geosphere, 3(4): 220-259.

Wittig, N., Pearson, D. G., Webb, M., Ottley, C. J., Karina, K. S., Jensen, S. M., and Nowell, G. M., 2008. Evolution of the mantle root beneath the North Atlantic Craton, Extended Abstracts 9th International Kimberlite Conference Frankfurt.

Wyatt, B.A., Baumgartner, M., Anckar, E. and Grutter, H., 2004. Compositional classification of "kimberlitic" and "non-kimberlitic" ilmenite. Lithos, 44(1-4): 819-840.

Xu, X.S., Griffin, W. L., O'Reilly, S. Y., Pearson, N. J., Geng, H. Y., and Zheng, J. P., 2008. Re-Os isotopes of sulfides in mantle xenoliths from eastern China: Progressive modification of lithospheric mantle. Lithos, 102(1-2): 43-64.

4 ^{187}Re-^{187}Os geochronology in magnetite: Case studies from the Manicouagan impact melt rock, Great Bear Magmatic Zone, and Laramie Anorthosite Complex

4.1 Introduction

The ^{187}Re-^{187}Os system in chromium spinel $FeCr_2O_4$ has been used to date the formation of chromite deposits (Marques et al., 2003; Mondal et al, 2007) and chromite bearing ultramafic igneous rocks (Walker et al., 2002; Walker and Nisbet 2002). However, other minerals in the spinel group have received limited attention with regards to ^{187}Re-^{187}Os geochronology, likely a result of their very low Re and Os abundances. Current analytical blanks can be as low as <10 femto grams (fg) for Os and <100 fg for Re, allowing analysis of extremely small Re-Os rich samples (e.g. single sulphide inclusions in diamonds (Aulbach et al., 2009; Richardson and Shirey 2008)), or samples with very low Re and Os concentrations. With reductions in analytical blanks, accurate and precise geochronology using other spinel minerals may now be possible. The spinel group mineral selected for investigation in this study is magnetite.

Magnetite is a common igneous, metamorphic and sedimentary mineral, and the ability to date its formation would provide age control for many rock types previously thought un-dateable. Its crystallization is known to be controlled by fO_2 and thus fS_2, both of which are extremely important in controlling Re and Os partitioning between minerals in a magma (Fonesca et al., 2007; Mallman and

O'Neil 2007; Righter et al., 2008). In oxidized magmas (high fO_2), experimental and observational evidence suggests that Re is incompatible during melting and is likely to be partitioned into spinel (magnetite) in the absence of sulphide minerals (Mallman and O'Neil 2007; Righter and Downs 2001; Righter et al., 1998; 2008). If a magma, or magmatic fluid is sufficiently oxidized and fractionated (e.g. the Vanuatu arc magmas from Eggins (1993) FMQ +4) it can contain high Re contents (~2ppb e.g. Sun et al., 2003), which may be entirely contained within magnetite. Previous work using chromite has shown that the spinel structure is not susceptible to Os loss even through greenschist facies metamorphism (Gangopadhyay and Walker, 2003), further supporting the investigation of magnetite as a geochronometer.

Previous work has indicated the potential for ^{187}Re-^{187}Os geochronology using magnetite in the absence of sulphide (Brauns et al., 2000; Hart et al., 2002; 2003; Jicha et al., 2009; Zhou et al., 2005), although only Brauns et al. (2000) and Zhou et al. (2005) were able to produce a ^{187}Re-^{187}Os age using magnetite. The other studies used Os isotopes in magnetite from volcanics associated with subduction under western North America to address the crustal contamination of mantle derived magmas. Brauns et al. (2000) and Zhou et al. (2005) used magnetite from flood basalts to create an isochron, which they were able to achieve because their magnetite had ~100 times more Os and ~10 times more Re than the magnetite from the subdution zone studies. Even in the presence of sulphide, Mathur et al. (2002) have shown that Re-Os isotopes in magnetite from an Fe-oxide Cu-Au ore deposit have a Re-Os age controlled by magnetite rather than co-precipitated sulphides. Mathur et al. (2000) however, do not prove the purity of the magnetite,

95

which could be of considerable importance due to the presence of molybdenite associated with the ore, which is known to concentrate Re and Os. Studies such as Mathur et al. (2000), Brauns et al. (2000) and Zhou et al. (2005) indicate that magnetite may in some cases be less vulnerable to Re and Os mobility than some sulphide minerals and therefore provide more accurate and precise ages. Graham et al. (2004) have also shown that groundmass magnetite in kimberlites and related magmas can be used to constrain the age of emplacement, further indicating that magnetite could be useful for providing age control in a variety of environments.

These studies show that ^{187}Re-^{187}Os geochronology using magnetite is possible in some instances although the most favorable conditions are presently unknown. It is also unclear whether the ages produced using the ^{187}Re-^{187}Ossystem in magnetite are geologically meaningful. They are consistent with other minerals in some cases (Mathur et al., 2002; Graham et al., 2004), although the ages are not supported by other independent techniques (the ^{187}Re-^{187}Os system was typically chosen due to the dearth of other methods). A comprehensive study of ^{187}Re-^{187}Os isotopes in magnetite is therefore essential before this tool can be efficiently and reliably used for geochronology and isotope tracing.

This study investigates Re and Os isotopic and trace element composition of magnetite from three different geological settings, all with well constrained ages, in an attempt to examine the robustness of the geochronometer, and its ability to provide age information in these settings. The areas chosen for research are; Manicouagan Impact melt rock (MIM); massive magnetite veins from the Great

Figure 4.1

North America Archean and Proterozoic geology map showing the location of the samples for this study. Samples are labeled using white initials in black boxes, GBMZ = Great Bear Magmatic Zone (64º51'90"N 114º19'70"W), MIM = Manicouagan impact melt rock (51º22'30"N 68º41'50"W), LAC = Laramie anorthosite complex (41º34'30"N 105º11'80"W). The location of the mid continent rift, Cheyenne belt and Wopmay orogen are also shown. Map is modified from Whitmeyer and Karlstrom, (2007).

Bear Magmatic Zone (GBMZ); and magnetite dykes from the Sybille intrusion, which is part of the Laramie Anorthosite Complex (LAC).

4.2 Samples, geological setting and previous work

Independent ages and geological maps for all of the samples have been published previously in Floran et al. (1978), Ramezani et al. (2005), Gandhi et al. (2001), Ootes et al. (2008), and Scoats and Chamberlain, (2003). The trace element compositions of the analyzed magnetite used for ^{187}Re-^{187}Os geochronology are given in Table 4.1. The Re-Os isotopic data from all of the samples is provided in Table 4.2

4.2.1 Manicouagan Impact Melt Rock (MIM)

The MIM, dated at 215.5 Ma (U-Pb zircon and ^{40}Ar-^{39}Ar K-feldspar Ramezani et al. 2005) is located in central Québec and is part of one of the largest impact related structures in the Canadian Shield. The most prominent feature of the impact structure is a water filled trough which is 5-10 km wide and ~150 km in diameter and is thought to represent the outer most structural expression of the impact crater. Inside the peripheral trough is a central uplift zone which mostly comprises anorthosites of Labradorian age (~1.65 Ga) of the Lelukuau terrain (Jordan et al., 2006) and a layer of MIM rock. The MIM is divided into three units based on grain size and distribution of basement inclusions (Floran et al., 1978). The lower most unit has the finest grain size (<0.2mm) and the most abundant basement xenoliths, whereas the uppermost

Table 4.1 (first half)

Zone	Sample	Li	Na	Mg	Al	P	K	Ca	Ti	V	Cr	Mn	Co	Ni	Cu	Zn	Ga	As	Se	Rb	Sr	Y	Zr	Nb	Mo	Pd
Great Bear Magmatic Zone	08VJ04b	5.91	1538	1729	5363	9795	1068	21483	137	990	0.46	1047	39.32	105	121	167	75.46	24.22	3.82	12.04	8.84	121	4.19	2.11	0.58	0.81
	08VJ04c	6.07	1462	1610	5228	8477	1386	18541	229	1026	1.36	1603	42.53	94.29	93.87	158.39	91.15	26.38	3.65	17.54	8.72	118	5.15	3.92	0.67	0.84
	08VJ04d	7.47	1789	1571	6022	8286	1690	18504	252	1083	1.67	1481	40.75	90.18	96.16	193.22	90.96	20.83	3.27	19.67	9.69	105	5.03	3.69	0.37	0.77
	08VJ04e	5.91	1133	1483	5551	6245	1520	13938	208	1084	0.52	1333	40.21	104	136	176	92.10	14.47	3.41	18.48	6.58	85.45	3.85	3.75	0.50	0.59
	08VJ04e RPT	5.92	1128	1464	5603	6192	1521	13832	207	1084	0.49	1243	37.91	99	129	168	88.02	14.24	3.23	17.88	6.40	76.48	3.58	3.61	0.44	0.58
	08VJ04f	5.58	1989	1610	5985	5966	1491	12785	202	1072	0.81	1369	40.53	107	128	153	92.78	23.08	3.45	17.88	9.14	72.64	6.26	2.54	0.54	0.70
	08VJ20a1	5.61	1253	3924	6086	268	2775	1689	363	841	0.30	288	14.68	72.16	2.87	12.80	50.70	11.18	2.17	36.22	11.02	12.92	2.92	1.46	4.87	0.36
	08VJ20a2	4.83	1048	3801	5763	213	2602	1545	344	835	0.38	289	15.17	74.89	3.25	14.15	54.75	8.17	2.28	38.18	10.56	13.06	2.93	1.12	7.14	0.25
	08VJ20a3	5.89	1278	4139	6316	2373	2428	6860	327	828	1.00	262	14.39	75.95	6.07	14.19	46.60	14.45	2.35	29.44	12.22	32.69	3.15	1.49	5.48	0.37
	08VJ20b1	4.15	1161	3623	27106	3947	2712	33769	1278	959	17.00	295	9.93	28.84	89.81	10.30	37.77	24.44	46.78	34.78	130	547	16.89	1.00	0.89	3.05
	08VJ20b2	4.68	1189	3578	24648	4156	2711	32033	1272	913	18.57	316	11.05	32.40	91.06	12.16	41.61	24.18	43.76	34.90	143	516	19.04	1.36	7.59	3.07
	08VJ20b3	4.02	1231	2993	32089	3046	1507	38351	1121	839	15.94	336	9.86	28.20	75.08	9.74	43.94	33.09	64.46	22.50	151	704	16.67	0.85	1.28	3.91
Laramie Anorthosite Complex	LACIa	0.87	1131	8647	13767	1206	252	3669	68478	4357	509.35	2270	145	110.05	41.39	290	56.47	2.91	2.64	0.73	12.66	3.84	17.90	0.48	0.69	0.70
	LACIb	1.05	1358	11065	13406	1183	275	3971	69739	3939	501.14	2355	304	321.97	52.69	301	55.54	2.22	2.63	0.88	14.61	4.27	23.86	0.48	0.32	0.89
	LACIIa	1.20	1518	10634	14299	1171	456	4691	60674	3847	471.35	2267	138	99.60	31.54	256	51.23	2.96	2.76	0.97	19.93	4.79	20.76	0.45	1.15	1.15
	LACIIb	1.23	1714	10605	14020	1125	525	3981	76784	4208	472.22	2258	140	109.26	37.95	278	53.26	5.93	2.42	1.11	19.40	3.81	28.53	0.62	0.69	1.15

Table 4.1 (second half)

Zone	Sample	Ag	Sn	Cs	Ba	La	Ce	Pr	Nd	Sm	Eu	Gd	Tb	Dy	Ho	Er	Tm	Yb	Lu	Hf	Ta	Au	Pb	Th	U
Great Bear Magmatic Zone	08VJ04b	0.82	3.30	1.01	297	11.73	36.54	4.14	24.44	11.95	2.22	15.81	2.62	16.12	3.21	9.17	1.28	8.35	1.26	0.11	0.03	0.24	131	8.64	349
	08VJ04c	0.51	6.61	1.71	309	11.81	34.63	3.59	21.60	11.18	2.12	15.49	2.57	16.05	3.28	9.56	1.35	8.84	1.33	0.13	0.02	0.32	238	15.74	392
	08VJ04d	0.52	5.90	1.67	367	10.61	33.64	3.19	19.05	9.92	1.91	13.50	2.27	14.16	2.89	8.42	1.20	7.70	1.17	0.11	0.02	0.21	217	14.54	367
	08VJ04e	0.59	5.17	1.47	220	9.21	25.14	2.65	15.40	7.49	1.41	10.01	1.69	10.46	2.15	6.31	0.90	5.95	0.89	0.07		0.10	220	14.71	422
	08VJ04e RPT	0.60	4.96	1.46	219	8.34	23.69	2.54	14.90	7.47	1.40	9.73	1.66	10.34	2.13	6.26	0.90	5.89	0.90	0.06		0.10	227	15.06	434
	08VJ04f	0.55	7.27	1.54	364	8.00	28.77	2.43	14.60	7.38	1.42	10.15	1.70	10.72	2.24	6.56	0.94	6.25	0.94	0.14	0.02	0.34	247	15.88	473
	08VJ20a1	0.05	10.82	2.21	231	6.93	21.10	1.52	5.74	1.44	0.29	1.79	0.28	1.73	0.35	0.99	0.13	0.86	0.13	0.14	0.07	1.20	0.92	0.40	1.41
	08VJ20a2	0.04	8.53	2.34	203	7.44	21.07	1.61	6.07	1.48	0.28	1.75	0.26	1.67	0.34	0.96	0.13	0.85	0.13	0.08		0.20	0.85	0.27	1.32
	08VJ20a3	0.04	5.77	1.98	232	14.27	35.47	3.33	12.64	3.16	0.52	3.84	0.62	4.10	0.89	2.67	0.37	2.30	0.35	0.11	0.04	0.36	10.64	1.56	17.33
	08VJ20b1	0.04	12.63	1.46	189	9622	16191	1506	4489	568	49.87	346	25.43	112	16.90	40.72	4.55	28.59	3.72	0.47		0.18	23.90	53.15	64.55
	08VJ20b2	0.05	22.24	1.47	213	8639	14592	1350	4014	522	47.67	331	21.54	108	16.06	38.79	4.34	26.99	3.51	0.48		0.16	24.61	56.59	64.10
	08VJ20b3	0.05	14.52	0.96	252	13389	22620	2100	6234	795	72.36	496	36.88	160	23.31	56.43	6.28	39.63	5.10	0.48		0.26	32.02	54.87	95.21
Laramie Anorthosite Complex	LACIa	0.03	0.52	0.06	220	3.53	16.64	1.22	5.63	1.18	0.25	1.09	0.11	0.59	0.10	0.24	0.03	0.15	0.02	0.72	0.04	0.54	0.61	0.12	0.04
	LACIb	0.03	0.47	0.07	257	3.82	18.69	1.34	6.22	1.30	0.29	1.21	0.12	0.67	0.11	0.27	0.03	0.17	0.02	0.81	0.04	0.38	0.55	0.12	0.05
	LACIIa	0.04	0.61	0.07	267	4.12	19.75	1.44	6.82	1.43	0.33	1.36	0.14	0.76	0.13	0.32	0.04	0.20	0.03	0.86	0.08	2.64	0.56	0.22	0.05
	LACIIb	0.04	0.55	0.07	305	3.23	18.53	1.11	5.28	1.12	0.29	1.07	0.11	0.62	0.11	0.26	0.03	0.18	0.02	1.04	0.07	0.96	0.62	0.14	0.04

4.1

Table 4.1

Trace element data for magnetite samples from the Great Bear magmatic zone and Laramie anorthosite complex. All values are ppm.

99

	Sample	Re ppb	Os ppt	$^{187}Re / ^{188}Os$	+/- 2σ	$^{187}Os / ^{188}Os$	+/- 2σ	187Os / 188Os$_i$
Manicouagan Impact Melt Rock								(t=215 Ma)
	Mgt 1	3.50	33.45	1107.60	45.89	9.31	0.39	5.3360
	Mgt 2	3.64	32.56	1183.16	52.00	9.28	0.42	5.0302
	Mgt 3	3.32	30.90	1126.71	78.51	9.17	0.64	5.1205
	Mgt 4	3.44	31.70	1128.39	59.52	9.03	0.48	4.9742
	Mgt 5	3.42	32.54	1071.47	54.03	8.68	0.44	4.8353
	Pyx 1	0.46	5.85	707.95	65.74	6.89	0.65	4.3442
	Pyx 2	0.48	5.96	792.82	42.76	8.01	0.44	5.1674
	Pyx 3	0.45	6.51	599.54	25.88	6.19	0.27	4.0336
	Pyx 4	0.49	5.89	793.61	41.99	7.55	0.40	4.6983
	Pyx 5	0.34	4.50	717.27	123.68	7.72	1.33	5.1454
	WR-A	0.17	7.83	155.38	9.55	3.90	0.24	3.3433
	WR-B	0.15	7.06	158.22	11.14	4.17	0.29	3.6034
	WR-A2	0.21	7.20	215.90	16.44	4.26	0.32	3.4891
	WR-B2	0.20	15.60	73.87	2.26	1.58	0.05	1.3121
Great Bear Magmatic Zone								(t=1875 Ma)
	08VJ04a	0.11	3.93	426.6	105.5	16.04	3.95	2.4971
	08VJ04b	0.09	3.48	356.0	91.8	14.16	3.64	2.8618
	04b RPT	0.08	3.55	237.8	59.2	9.27	2.29	1.7238
	08VJ04c	0.04	2.52	108.2	22.2	4.33	0.85	0.8958
	08VJ04d	0.06	3.45	126.9	19.7	4.54	0.72	0.5112
	08VJ04e	0.05	2.57	173.5	40.6	6.78	1.56	1.2715
	04e RPT	0.05	2.95	128.0	29.5	5.29	1.17	1.2231
	08VJ04f	0.04	2.50	110.7	23.9	4.91	1.01	1.3979
	08VJ20a1	0.02	1.86	54.24	14.34	2.29	0.51	0.5717
	08VJ20a2	0.01	2.27	33.58	8.23	1.66	0.28	0.5984
	08VJ20a3	0.19	5.96	490.15	82.17	17.43	2.93	1.8663
	08VJ2a3 RPT	0.17	5.67	480.77	109.41	18.17	4.13	2.9042
	08VJ20a3 (2)	0.18	5.71	524.08	102.25	19.40	3.79	2.7631
	08VJ20b1	0.16	22.77	43.09	1.17	2.26	0.06	0.8902
	08VJ20b2	0.06	17.17	20.83	0.97	1.91	0.05	1.2533
	08VJ20b3	0.42	21.53	171.43	4.77	6.57	0.18	1.1288
	08VJ20b3 RPT	0.16	15.98	67.55	2.64	3.34	0.12	1.1908
Laramie Anorthosite Complex								(t=1435 Ma)
	LAC Ia	0.49	24.22	157.6	3.5	4.92	0.11	1.1088
	LAC Ib	0.56	22.97	203.5	5.0	5.82	0.15	0.8983
	LAC Ia RPT	0.70	22.25	311.4	11.8	8.13	0.32	0.5911
	LAC Ib RPT	0.62	21.74	259.5	9.0	7.02	0.24	0.7378
	LAC IIa	0.27	10.14	240.1	14.0	6.81	0.41	0.9937
	LAC IIb	0.23	8.50	234.8	15.4	6.36	0.42	0.6761
	LAC IIa RPT	0.16	5.66	268.6	36.5	7.30	0.98	0.7954
	LAC IIb RPT	0.24	8.29	264.1	23.7	7.20	0.64	0.8074

4.2

Table 4.2

Re-Os data for all of the samples with 2σ absolute errors. Initial Os isotope values are calculated using the geologically accepted ages for the systems.

unit has the largest grain size (>1mm) and few to no inclusions (the middle unit is intermediate between the other two layers). All of the layers of melt rock have remarkably uniform chemistry and are compositionally similar to a monzonite (Floran et al., 1978). The uniform chemical and isotopic composition of the melt

rock has led researchers to believe that radioactive isotope systems for the melt rock have all been reset by the impact event, and do not show signs of inheritance from the Labradorian target rock (Hodych and Dunning, 1992; Ramezani et al., 2005), or the meteorite.

The samples for this study were the same as those used by Ramezani et al. (2005) for U-Pb zircon and ^{39}Ar-^{40}Ar sanidine analysis. They were collected from the top of the upper layer of melt rock, as far away as possible from the contact between the melt sheet and the target rock and therefore are the least influenced by xenoliths. The minerals analyzed for ^{187}Re-^{187}Os isotopes were magnetite (± minor ilmenite) pyroxene (mostly augite with some ferroan-enstatite) and a whole rock powder. Pyroxene and whole rock separates were used because magnetite did not produce any range in Re/Os on a Re-Os isochron diagram, which is possibly due to homogenization during analysis of large sample aliquots (>0.4 g).

4.2.2 Great Bear Magmatic Zone (GBMZ)

The GBMZ is interpreted as a Paleoproterozoic calc-alkaline volcanic arc formed during subduction of an oceanic plate and corresponding oceanic ridge (1875-1840 Ma, Hoffman and Bowring, 1984; Gandhi et al. 2001). The magmatic zone is located in the centre of the Wopmay orogen which is an accreted terrain on the west of the Slave craton in northern Canada. To the east of the GBMZ is the Hottah terrain which is the oldest of the Wopmay orogen and comprises amphibolite facies sedimentary and volcanic rocks intruded by calc alkaline plutons (1914-1902 Ma, Hildebrand et al., 1987). It is interpreted as a volcanic arc assemblage

101

originally located on the western border of the Slave craton. To the west of the GBMZ is the Coronation Supergroup which is allochthonous on the western margin of the Slave craton and on the eastern edge of the Hottah terrain (Hoffman and Bowring 1984). The Coronation Supergroup is comprised of submarine volcanics, siliciclastics and carbonates formed in a marginal basin during a short period of extension (1900-1878 Ma, Hildebrand et al., 1987) before the formation of the GBMZ. The marginal basin became shortened and was thrust to its current position as an accretionary wedge during the onset of subduction to the west of the Hottah terrain. The GBMZ grew as the marginal basin closed and thrust the Coronation Supergroup towards the east as subduction occurred under the Hottah terrain. The magmatic zone comprises volcanic and intrusive rocks ranging in composition from mafic to felsic, but all with high alkalis and low TiO_2 contents similar to arc magmas in the Andes and western North America (Hildebrand et al., 1987). The alkali content of the magmas ranged from sodic-rich granites during the onset of magmatism, and changed to more potassic rich towards the end (Gandhi et al., 2001). Arc volcanism stopped at around 1860 Ma and the arc rocks became folded at an angle oblique to the overall trend of the zone due to changes in the direction of subduction (Hildebrand et al., 1987). During and after folding, large potassic granite and diorite plutons were intruded into the GBMZ until ~1843 Ma when magmatism ceased in the area. Associated with the felsic intrusives throughout the GBMZ are large Fe rich (magnetite and hematite) mineral veins interpreted to be related to Na and K alteration of the plutons. Two of these magnetite veins have been sampled for investigation by this study.

Both magnetite samples were collected from massive magnetite veins in the GBMZ during the Northwest Territories Geoscience Office 2008 field season. The first sample (08VJ04) is from a magnetite-actinolite-apatite vein associated with sodium altered quartz monzonite intrusions (Gandhi et al., 2001). The mineralization is similar to that found in the Olympic Dam in Australia and Kiruna deposits of Sweden (Hitzman et al., 1987). Sodium alteration indicates that the mineralization is related to the early stages of magmatism in the GBMZ although no direct dating has been made (Gandhi et al., 2001). The second sample (08VJ20a-b) is from granite-magnetite veins thought to be syntectonic. Some sulphide and uranium mineralization is also present in the veins (molybdenite, chalcopyrite, pyrite and uraninite) although none was found within the magnetite vein the sample was taken from. ^{187}Re-^{187}Os geochronology using molybdenite and U-Pb dating of zircons in the granite indicate that the veining is ~1875 Ma (Ootes et al., 2008). The geochronology indicates that the second sample is also related to the onset of magmatism in the GBMZ, the presence of dravitic tourmaline ($NaMg_3Al_6Si_6O_{18}(BO_3)_3(OH)_4$) within the magnetite-granite veins indicates that sodium alteration may be present, as with 08VJ04.

The formation processes of the iron oxide mineralization associated with the GBMZ is not fully understood, although it is most likely related to hydrothermal fluids, both magmatic and meteoric in origin (Hitzman et al., 1987). However, the limited amount of sulphide mineralization and large volumes of iron oxide indicate that the process may be different from typical Phanerozoic porphyry deposits.

4.2.3 Laramie Anorthosite Complex (LAC)

The LAC (1440-1430 Ma, Scoates and Chamberlain, 2003) is exposed over an area of ~800 km^2 at the border between Wyoming and Colorado and is one of the most well studied anorthosite complexes in the world. The LAC intrudes the Cheyenne belt, which is a structural feature separating the Archean Wyoming Craton in the north, and the Proterozoic Colorado province in the south. The belt is interpreted to represent the boundary between an Archean continent and accreted Proterozoic island arc terrains (Duebendorfer and Houston, 1987). The anorthosite complex is surrounded by satellite intrusions of a more chemically evolved monzonitic composition which were intruded during the last stages of LAC emplacement. The Sybille monzosyenitic intrusion (~1435 Ma Scoates and Chamberlain, 2003) is one such satellite and is located to the north of the LAC. It is interpreted to have crystallized from a ferrodiorite parent magma thought to be a residual liquid phase left behind during the crystallization of the contemporaneous anorthosite (Scoates et al., 1996). The parent ferrodiorite is also exposed as discrete pods and dykes in the centre of the Sybille intrusion and associated with the ferrodiorite, are Fe-Ti oxide rich dykes of ferrodiorite composition. Oxide rich deposits such as these are commonly found associated with anorthosites (e.g., Rogaland in NW Norway, and Suwałki NW Poland, Mitchell et al. 1996; Morgan et al. 2000). The origin for these deposits is unclear, although the currently favored hypothesis is formation as an immiscible liquid in the presence of a P_2O_5, which may lower the solidus of iron oxide melts (Bolsover, 1986; Hitzman et al., 1987; Mitchell et al., 1996).

The magnetite samples used for ^{187}Re-^{187}Os analysis in this study were

from the oxide rich melts of the Sybille intrusion, and were originally collected by J. Farquhar and T. Chacko for high temperature oxygen isotope thermometry (Farquhar et al. 1993). The major oxide mineral is massive titanomagnetite with ilmenite lamellae, apatite, pyrite and pyrrhotite. Inclusions are also common in some areas, and no sulphides were found in the titanomagnetites analyzed in this study. The oxide rich ferrodiorite host rocks commonly display alternating feldspar and olivine, augite, and Fe-Ti oxide rich bands, which are interpreted as high density cumulate crystal settling (Mitchell et al., 1996). No geochronology has been attempted on the oxide rich ferrodiorites directly, although isotopic tracing using Sr and Nd isotopes has shown that the rocks are products of a crustal melt variably contaminated by the overlying Archean basement (Mitchell et al., 1996; Scoates and Chamberlain, 2003).

4.3. Analytical techniques

The GBMZ and LAC samples were both separated from individual hand samples containing massive magnetite. The massive magnetite was cut into 6-8 30g pieces using a rock saw. The edges of the samples were ground to avoid contamination from the saw blade, and were then crushed to a coarse powder using an agate pestle and mortar. The magnetite was then purified using magnetic separation and demagnetization techniques described in Chapter 2 Section 2.2. Once the magnetite had been purified, it was inspected using a binocular microscope, and had a visual purity of >95% (it is extremely difficult to obtain a 100% pure magnetite separate due to the high magnetism of the mineral). The magnetite was then powdered using an agate pestle and mortar before Re-Os extraction and analysis.

105

The Manicouagan magnetite, pyroxene and whole rock samples were received pre-separated and crushed. They were inspected for purity using a binocular microscope and were considered to be of a similar purity to the mineral separates obtained at the University of Alberta.

The Re-Os characteristics of the samples were investigated at the University of Alberta Radiogenic Isotope Facility, using the procedures described in Chapter 2, Section 2.3 and Chapter 3, Section 3.3, with some modifications described below. 800-1000 mg of finely crushed sample powder was added to borosilicate Carius tubes along with an accurately weighted double spike of isotopically enriched ^{190}Os and ^{185}Re. Concentrated HCl was also added to the magnetite samples whereas inverse aqua regia was added to pyroxene and whole rock samples before sealing the Carius tubes and heating to 240ºC for 48 hours. The magnetite was dissolved using a double dissolution technique similar to that of Chesley et al. (1999) where an initial dissolution using concentrated HCl dissolves the magnetite, and then concentrated HNO_3 is added to create inverse aqua regia which is used to ensure sample and spike homogenization.

Once the samples were dissolved, Re and Os were chemically extracted from the acid mix using a solvent extraction for Os and anion exchange column chemistry for Re. The solvent extraction followed the methods of Cohen and Waters (1996) although chloroform was used as the solvent rather than carbon tetrachloride. This was followed by 2 micro-distillations (e.g. Birck et al., 1997),

106

which further purified the Os aliquot. Before Re could be separated by anion exchange column chemistry, much of the solubilized iron from the magnetite needed to be removed. Excess Fe causes saturation of the resin adsorption sites and limits Re retention. Fe was removed from the evaporated sample using 3 ml 0.2N HNO_3 to mobilize the Re aliquot and precipitate Fe^{3+}. The precipitate was then removed using a centrifuge and 0.1 μm filter. The remaining liquid was evaporated to dryness and the procedure repeated 2 more times before the sample was passed through the anion exchange column using the traditional Re separation techniques (Morgan et al., 1991). The Re aliquot was then further purified using single bead anion chromatography (Selby and Creaser, 2003).

The purified Re and Os fractions were analyzed by conventional negative thermal ionization mass spectrometry (NTIMS) (Creaser et al., 1991; Volkening et al., 1991) using a Micromass Sector 54. Isotopic ratios were corrected for isobaric interferences, mass fractionation, oxygen isotopes, and spike and blank contributions. Total procedural blanks ranged from 10 to 3 pg for Re and 2 to 0.3 pg for Os, the average $^{187}Os/^{188}Os$ ratio of the blank changed throughout analysis from 0.49 to 1.2. The reason for the change in the isotopic composition of the blank is unclear, although the results are not significantly affected using either composition.

Trace element data for the magnetite samples was obtained using a Perkin Elmer Elan6000 quadrupole ICP-MS in solution mode. 30 mg of sample powder was dissolved in glass beakers using 6N HCl on a hotplate for 12 hours. The solution was then evaporated to dryness and re-suspended in 0.2N HNO_3 for analysis. 63

elements were analyzed, and normalized to the chondrite reference for comparison and interpretation.

4.4 Results

Re-Os isotopic data and trace element data for the samples analyzed are presented in Tables 4.1 and 4.2, and plotted in the following figures. In total, 39 samples have been analyzed in this study.

4.4.1 Manicouagan Impact melt rock

Re and Os contents and ^{187}Re-^{187}Os ratios for all of the MIM samples are low in comparison to values reported from sulphide minerals (e.g. Morelli et al., 2004; 2005) although they are generally consistent with previously reported magnetite Re-Os contents from Washington State volcanics (Hart et al., 2003). Six magnetite samples from MIM show high ^{187}Re/^{188}Os ratios (>1000) but they do not show any spread in Re/Os ratio or Os isotopes. The lack of isotopic spread is a common feature of the MIM minerals, only the whole rock values do not plot as a point on an isochron diagram. Regression of the MIM data on an isochron diagram shows that the minerals define a Model 3 age of 290 ± 64 Ma (Figure 4.1), which is effectively a 2-point isochron. This age is older than the age of the impact as defined by U-Pb zircon analysis (Hodych and Dunning, 1992; Ramezani et al. 2005).
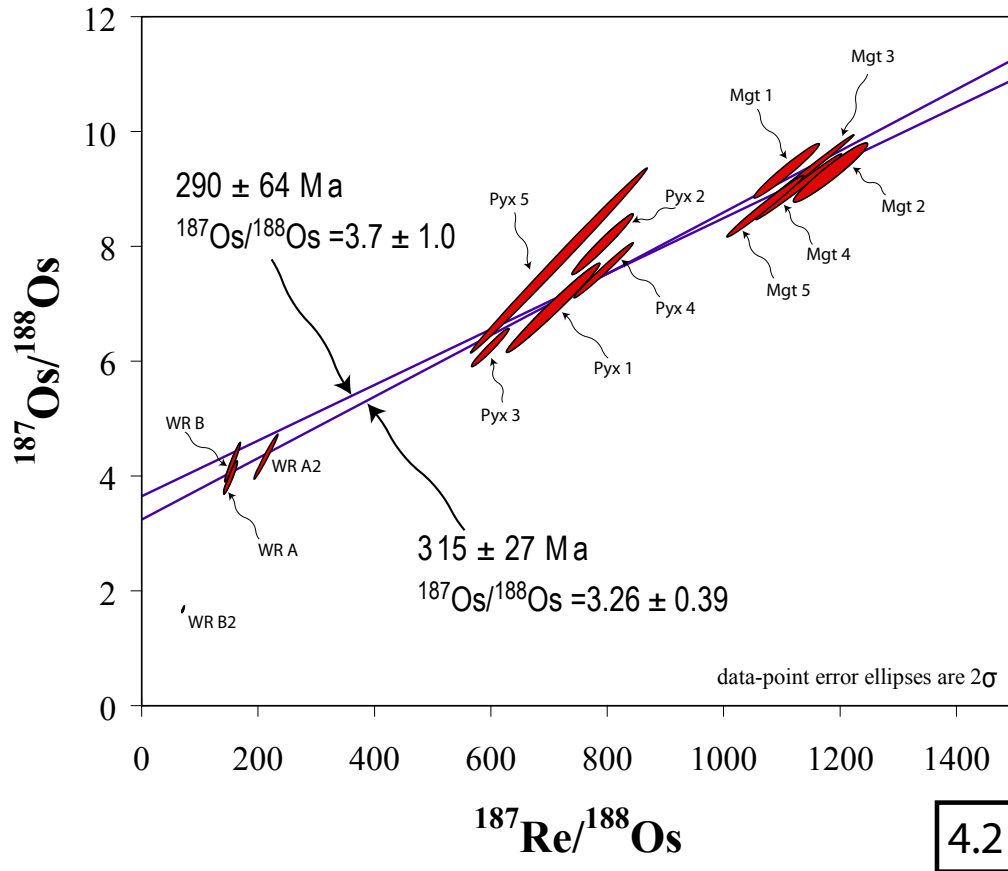
Figure 4.2

Isochron diagram for the Manicouagan impact melt rock. The younger isochron is calculated using the mineral separates (pyroxene and magnetite), the older isochron is calculated using all analyses. Sample WRB2 was not used in either isochron and is shown for reference only.

The whole rock samples contain lower γOs and initial Os isotopes than the mineral separates suggesting that they could contain a different component. If the whole rock values are plotted with the minerals on an isochron diagram, the age produced is 315 ± 27 Ma (Figure 4.1), indicating that the whole rock possibly contains an older (inherited and non-homogenized) component. The whole rock Re-Os isotopic values are also interesting in that they are not an average of the mineral

data, which suggests that there is an unidentified (probably high Os) low Re/Os phase not sampled in this dataset. The precise mineralogy of the whole rock is not known because the sample was received pre-crushed as a powder; therefore the composition of the high Os phase cannot be determined. The only indicator of the high Os phase is sample WR-B2, which plots below any of the calculated isochrons and contains 15ppt Os (it is not included in the 315 Ma regression). This Os content is approximately twice that of the other whole rock samples, and the $^{187}Os/^{188}Os$ ratio of the sample is 1.5 rather than ~4 for the other whole rock values. A repeat analysis from the same powder (WR-B) produced isotopic compositions in line with the WR-A and WR-A2 values, possibly indicating that the WR-B2 value is an anomaly, or that the high Os phase presumably present in WR-B2 has extremely low abundance.

4.4.2. Great Bear Magmatic Zone

The GBMZ magnetites contain the lowest Re and Os contents analyzed in this study and due to the low contents, they are adversely effected by blank contributions. The samples are also dominated by radiogenic osmium, $^{187}Os*$ (>80% of total Os for 08VJ04) which means that the stable isotopes of Os are in extremely low abundance. Stable isotopes of Os are important for plotting isochron diagrams because ^{187}Re and ^{187}Os isotopes are plotted relative to stable ^{188}Os. The blank contribution to ^{188}Os is between 14-25% for sample 08VJ04 and 1-22% for sample 08VJ20, which correlates to large uncertainties in $^{187}Re/^{188}Os$ vs. $^{187}Os/^{188}Os$ space. Low abundances of stable Os isotopes are also found within some sulphide minerals (Stein et al., 2000; Morelli et al., 2005) although these minerals have

110
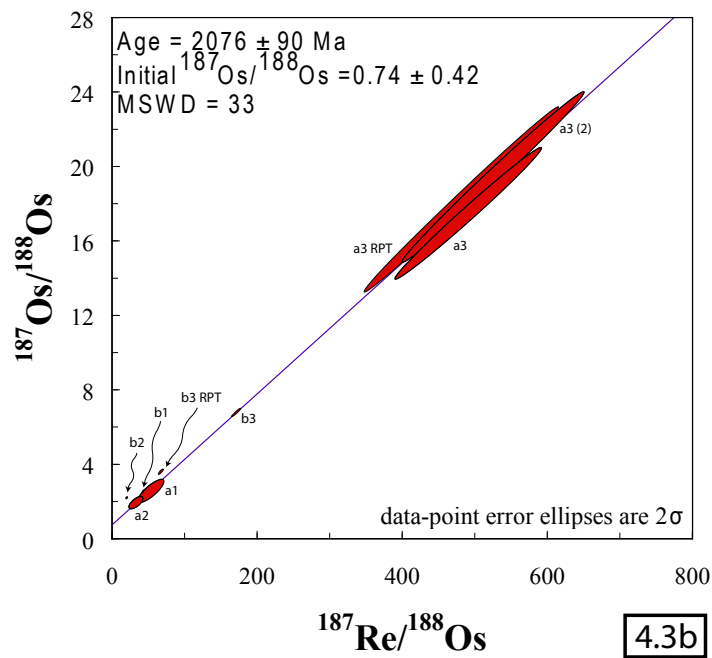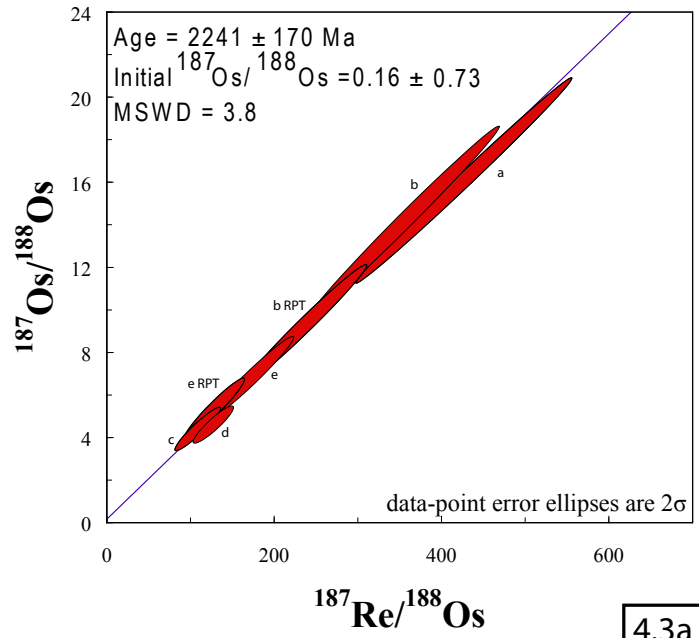
Figure 4.3a and b

Isochron diagrams for the two Great Bear magmatic zone samples. Both isochrons are Model 3

regressions and the large error ellipses are due to large blank corrections.

high Re contents and high (>5000) $^{187}Re/^{188}Os$ ratios, which is not the case with the magnetite samples. High Re contents and $^{187}Re/^{188}Os$ ratios allow the accurate calculation of model ages using single samples or using ^{187}Re vs. $^{187}Os*$ diagrams so that the effects of the ^{188}Os blank contribution can be removed. Techniques such as these can not be used on the GBMZ data because of the low abundances of both Os and Re, and so isochron diagrams necessarily contain large error ellipses.

Isochron diagrams for both of the GBMZ samples do not produce the known ages of the GBMZ (1875-1840 Ma). Using all of the analyses, 08VJ04 produces an age of 2241 ± 170 Ma (Figure 4.2a) and 08VJ20 produces an age of 2076 ± 90 Ma (Figure 4.2b). Both of these ages are Model 3 ages, which indicate that there is variation in initial Os isotopes of the samples. If the Os initial isotopic composition of the samples are calculated individually (assuming an age of 1875 Ma based on the Re-Os molybdenite age for the veins (Ootes et al., 2008)) the values range from 0.5 to 3.5 (Figure 4.3). The spread in initial Os isotopes suggests that the ages produced from the samples are most likely geologically meaningless, and that the source of Os has changed during crystal growth. (Figure 4.3) also indicates that the more radiogenic the initial Os isotope value, the greater the error is, which is related to the low abundance of ^{188}Os, and the large blank contribution to that measurement.

Figure 4.3 shows that there are four aliquots of sample 08VJ20 that have higher Os contents, and therefore lower blank contributions than all of the other analysis. If these samples are plotted on an isochron diagram, they produce an imprecise Model 3 age of 1878 ± 420 Ma (Figure 4.4) which is consistent with
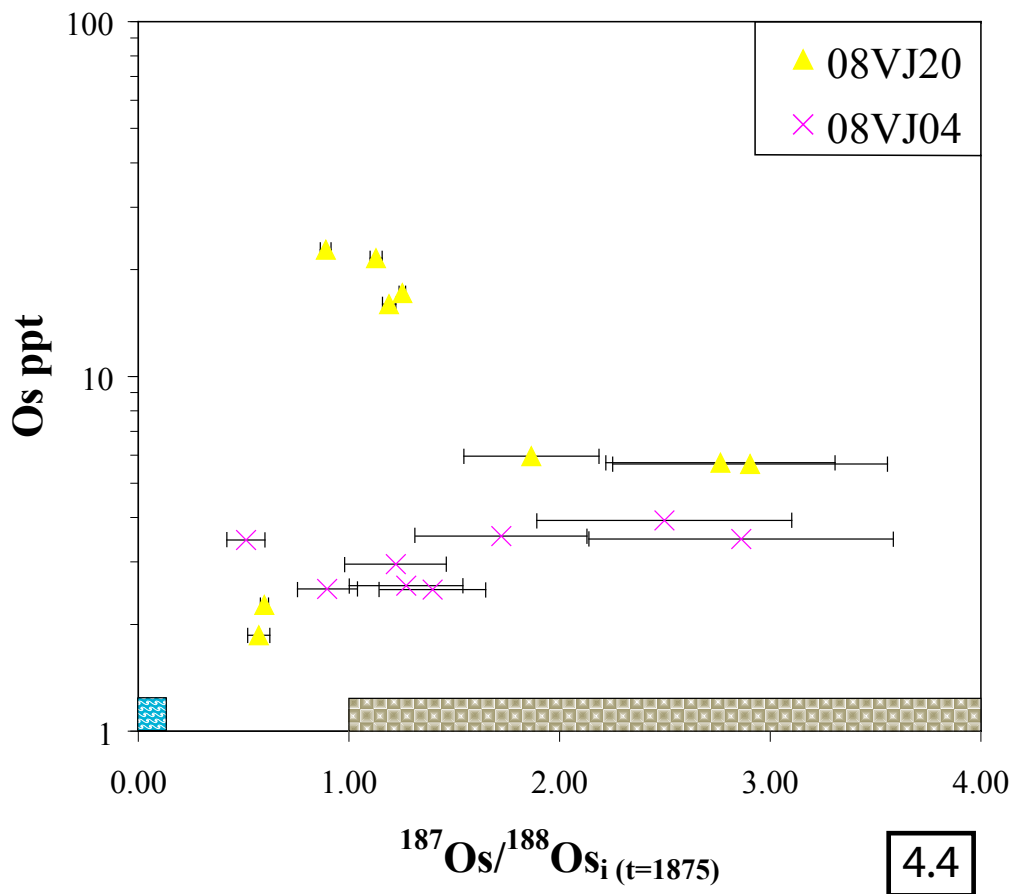
Figure 4.4

Initial Os content of the Great Bear magmatic zone samples calculated assuming an age of 1875 Ma

plotted against Os content. The bars at the bottom of the graph represent the average composition of

continental crust - brown squares (Shirey and Walker, 1998) and seawater during the Paleoproterozoic

(Kendall et al., 2009)

the known age. All of the high Os aliquots originate from sample 08VJ20b

which appears to have different trace element chemistry to the other magnetites.

Sample 08VJ20b has a similar composition to the other GBMZ samples regarding

siderophile and chalcophile elements (those that would be associated with a spinel

mineral phase), but the rare earth, and lithophile elements are distinctly different

(Figure 4.5) 08VJ20b is highly enriched in light rare earth elements (La/Lu >225) and also Sr, Zr, P, Ti and Y relative to the other samples.
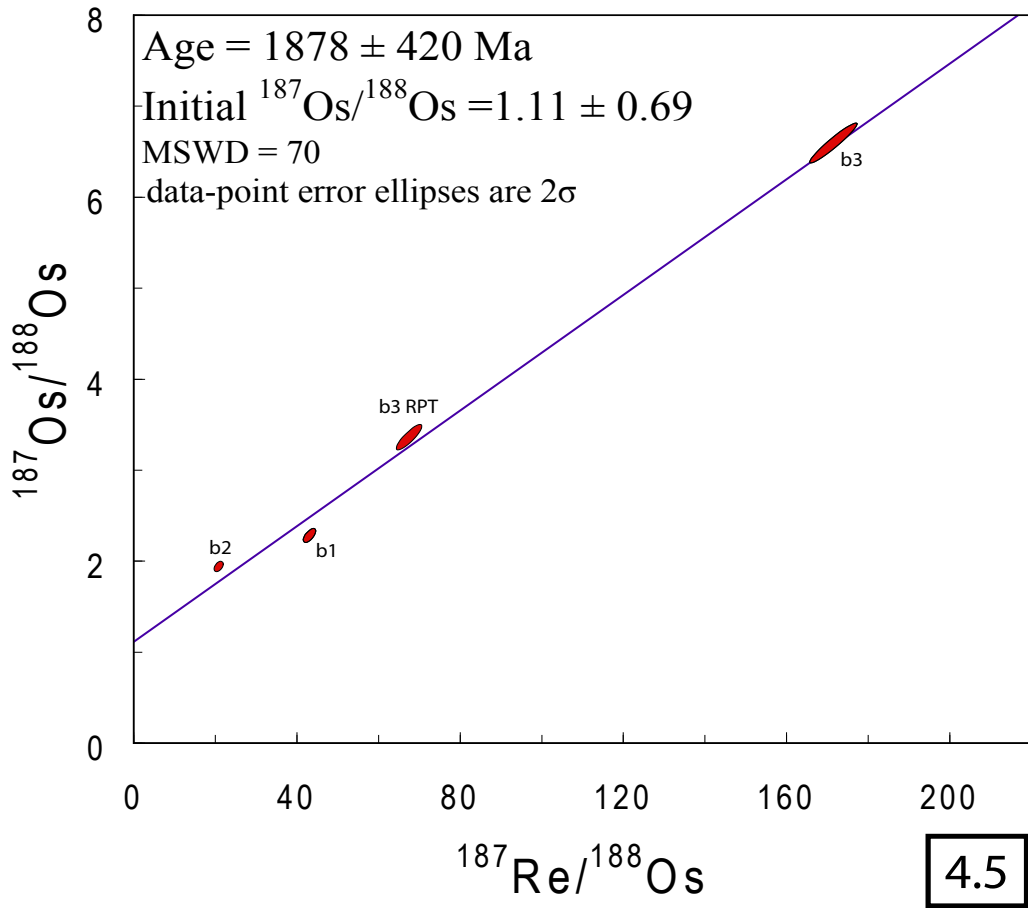
Figure 4.5

Isochron diagram using GBMZ samples with high Os content.

The veins which host the magnetite for this study also contain dravitic tourmaline which is likely to be a dominant host for these elemental anomalies (e.g. Hellingwerf et al., 1994) along with actinolite and apatite. No known studies have suggested a link between tourmaline, apatite, actinolite and Re or Os, although sulphide minerals associated with tourmaline in veins have been shown to have high Re-Os contents (e.g. Morelli et al., 2005).
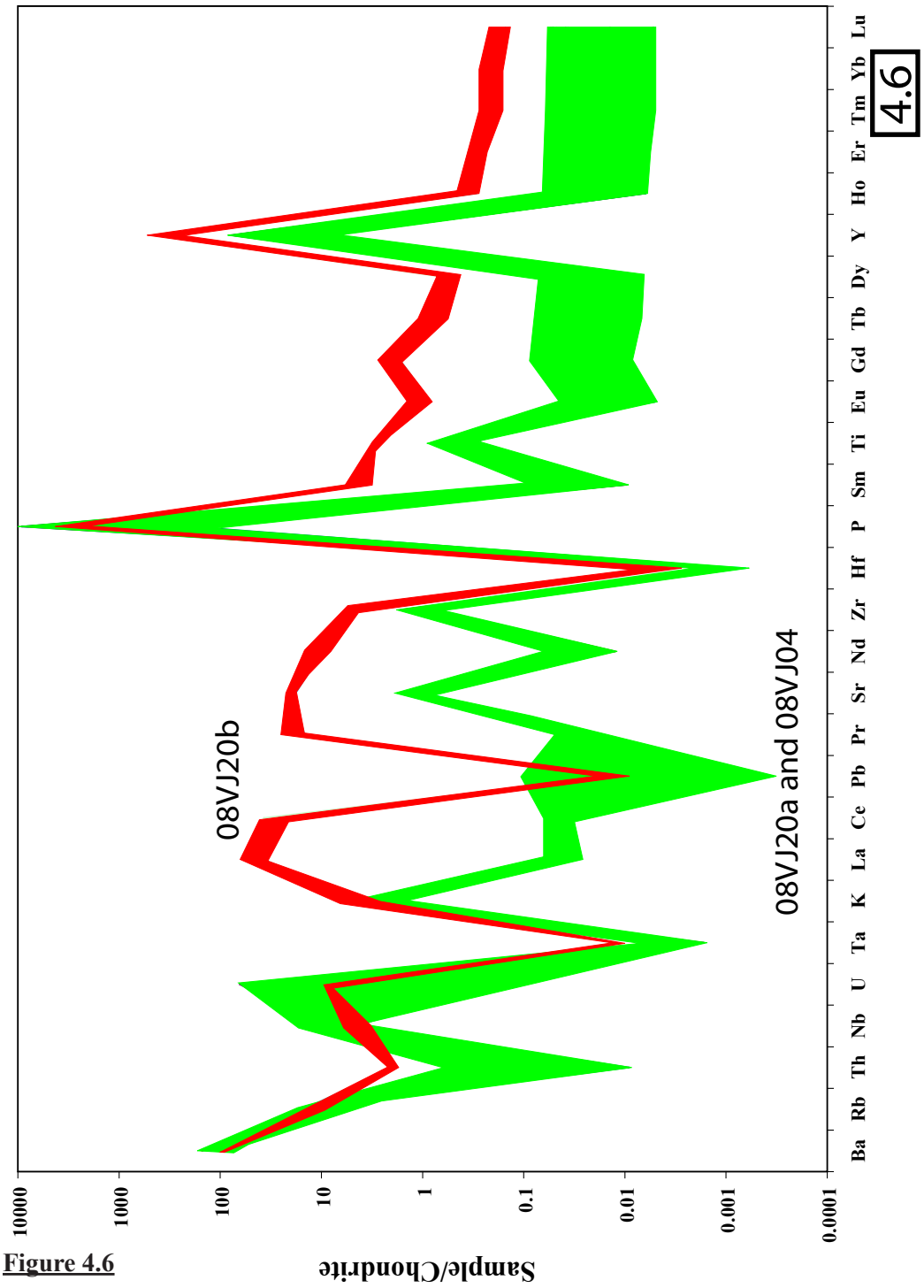
Figure 4.6

Spider diagram showing the difference in trace element content between high and low Os samples from the Great Bear magmatic zone. Values are normalized to carbonaceous chondrite.

The presence of molybdenite in some of the veins indicates that the Re and Os may be controlled by micro MoS_2 possibly within the tourmaline. However, Figure 4.6 indicates that there is no link between Mo content and Os in the samples, although there is a possible link with Arsenic, a main constituent of arsenopyrite (FeAsS) which is known to partition Re, and therefore Os into its structure (Morelli et al., 2005). Arsenopyrite has not been identified in the area however, and due to the lack of correlation between Os and Mo, the magnetite is considered to be the dominant host for the Re and Os.
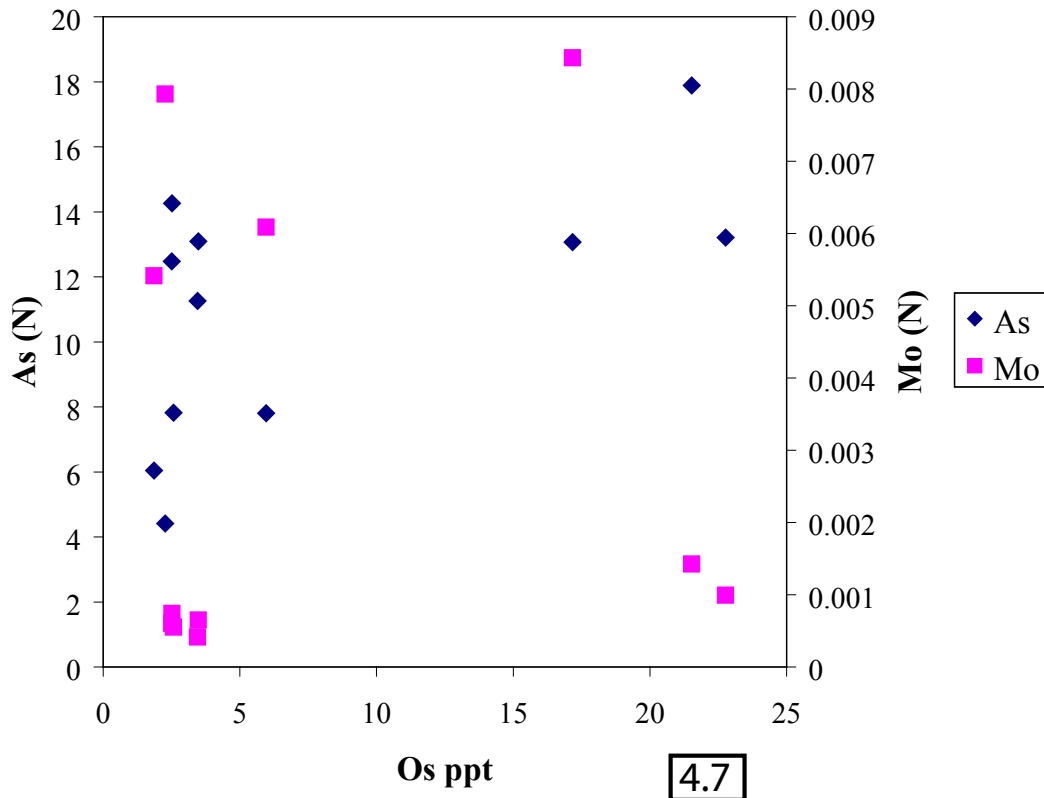
Figure 4.7

Arsenic and Molybdenum vs Os content of the Great Bear magmatic zone samples. The As and Mo values are normalized to carbonaceous chondrite.

4.4.3. Laramie Anorthosite Complex

The Re and Os contents in the LAC magnetites are intermediate between the GBMZ and MIM values. They are not as affected by blank contributions to the stable or radiogenic isotopes, with a maximum of 13% blank contribution for ^{188}Os (although only 1 sample is above 8%) and <1% for ^{187}Os. The samples are also dominated by radiogenic Os with all samples containing >83% ^{187}Os*. When the LAC data are plotted on an isochron diagram they produce a model 3 age of 1246 ± 100 Ma which is not within error of the 1440-1430 Ma age of Scoates and Chamberlain (2003) for the Sybille intrusion. The Re-Os analyses were obtained from two pieces of magnetite from the LAC, the isochron is entirely controlled by LAC I which can be plotted on its own to produce a Model 1 age of 1231 ± 41 Ma (Figure 4.7). The more precise age produced using LAC I is still not within error of the true age, but the Model 1 isochron suggests that the age may have some geological relevance, however it only contains 4 data points. The age produced from LAC II is 1423 ± 1400 Ma which is largely related to the large blank correction for LAC IIa R (13% blank contribution to ^{188}Os) due to low Os abundance and limited sample spread along the isochron. There is no evidence for trace element control to Os abundance within the LAC magnetite samples. Normalized trace element spider diagrams (Figure 4.7) show no differences in the trace element patterns of the two magnetite samples. Peaks in Sr, P and Y and a high La/Lu ratio (13-19) suggests however, that there may be small amounts of apatite within the magnetite. The magnetite dykes from the Sybille intrusion are known to contain up to 30% apatite (Bolsover 1986), and only a very small quantity would be needed to produce to trace element anomalies. The Re and Os abundances are very unlikely to be

related to apatite contamination due to the lack of correlation between Sr, P, Y and

Re or Os.
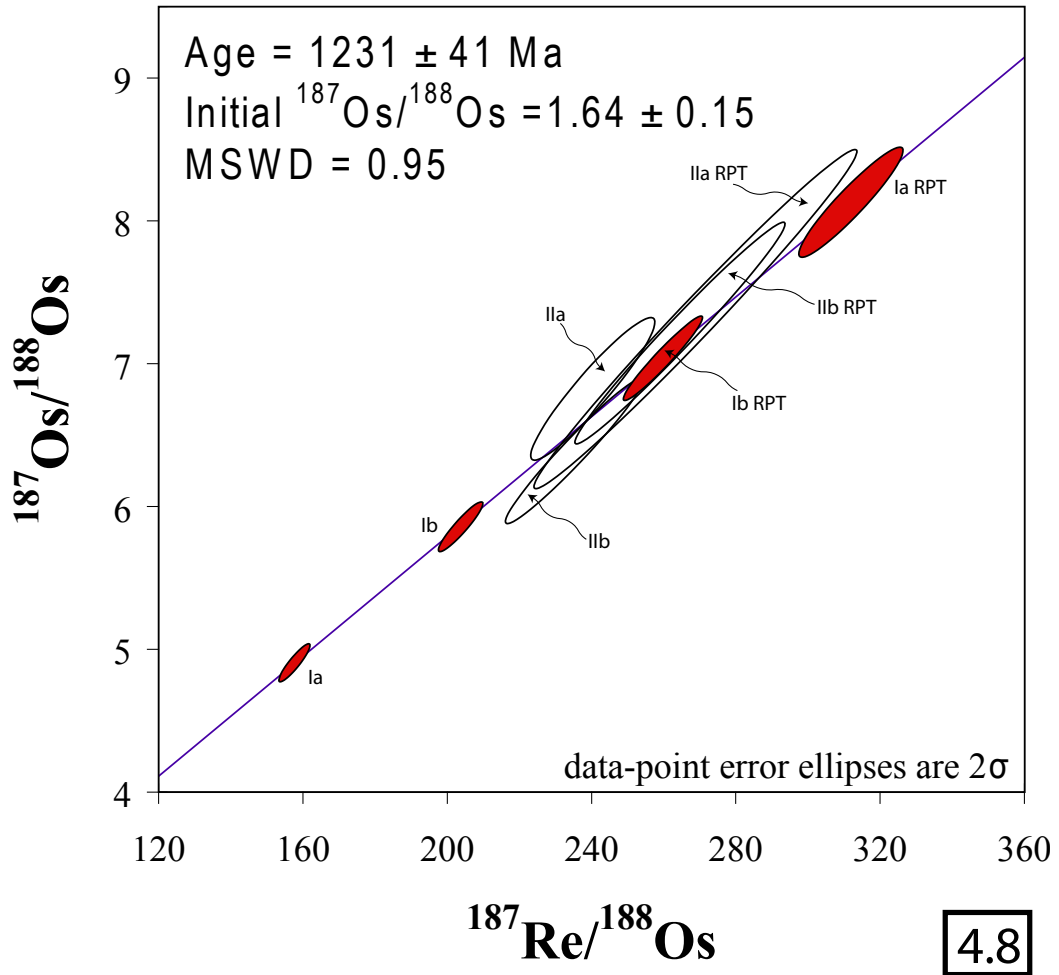
Figure 4.8

Isochron diagram for the Laramie anorthosite complex magnetite samples. Only the samples shaded

red are included in the Model 1 age regression.

4.5 Discussion

4.5.1. Interpretation of magnetite ^{187}Re-^{188}Os ages and initial isotopic composition.

Our results indicate that ^{187}Re-^{188}Os ages produced from magnetite in all of the geological settings studied are either inconsistent with previously reported ages, or not acceptable for precise geochronology. However, the ages produced show some degree of concordance with the known ages, and first order distinctions between Paleozoic, Proterozoic and Archean can be made. Interpretations regarding the ages produced from each of the study areas are given below.
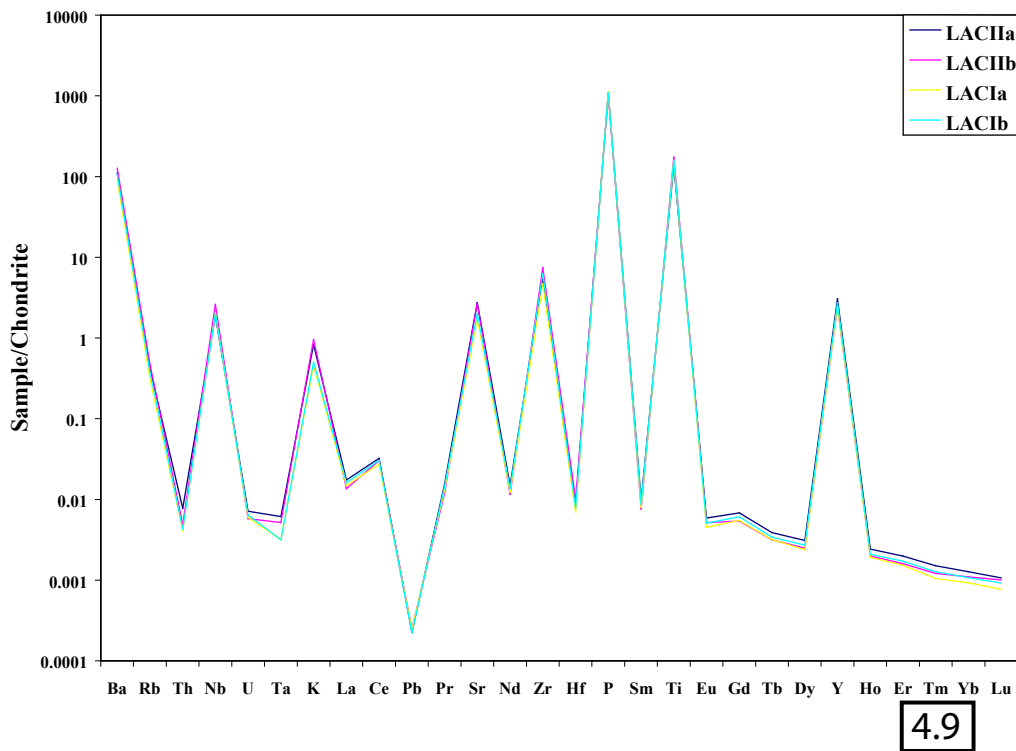
Figure 4.9

Spider diagram for Laramie anorthosite complex samples. Values are normalized to carbonaceous chondrite and show very little inter-sample variation.

4.5.1.1 Manicouagan Impact Melt rock.

Previous studies investigating the MIM have found no evidence of isotopic inheritance from the impacted country rock or meteorite. The ^{40}Ar-^{39}Ar system is well suited to trace isotopic inheritance due to the step heating method accessing information on both the younger and older domains of a mineral at different stages in the process. Also U-Pb analysis of zircons by Ramezani et al. (2005) reports no zircon analysis outside the 2 sigma error of the 215.5 Ma which would suggest inheritance. Therefore it seems difficult to explain the 290 ± 64 Ma ^{187}Re-^{188}Os mineral isochron with inheritance. However, the 315 ± 27 Ma older age produced when the whole rock analyses are added to the isochron may indicate inheritance on a micro scale.

The Manicouagan meteorite impacted predominantly the Tshenukutish and Lelukual terrains, which comprise mostly granites, anorthosites, diorites and gabbros (Jordan et al., 2006). Mafic and ultramafic rocks are a well known source for PGE mineralization (Garuti et al., 1997; Hoatson and Sun, 2002; Desharnais et al., 2004) and can contain tiny PGE nodules on their own or within sulphides (Liu et al., 2005). It is possible that a very small amount of sulphide, or PGE alloy could be entrained from the gabbro during impact into the melt rock, and retain its isotopic composition. Such PGE or sulphide grains are known to survive large melting events in the mantle unperturbed (e.g. Pearson et al., 2007).

Mass balance equations indicate that the total Os budget of sample WR-B2 (the whole rock sample with the highest Os content) could be accounted for by 2

120

Os rich alloy/sulphide grains of 0.5 μm in diameter (this would mean however, that the remainder of the sample was devoid of Os). The number of grains required to account for the Os budget increases if the diameter is reduced, but if the grains are hypothesized to be ≤1μm in diameter, it is likely that they would be very rare, and possibly not homogeneously distributed in the rock powder. The model age produced by sample WR-B2, assuming a chondritic Os initial at Grenvillian time (0.12) produces an age of 1172.6 ± 83 Ma which is congruous with the 1170 Ma age for the gabbro (Indares and Dunning, 2004), the other whole rock samples produce similar ages with the same initial, whereas the minerals produce Paleozoic ages. Model ages however can only be effectively used as a guide when Re/Os ratios are >5000 due to the large influence of the unknown initial Os ratio. Even though the old model ages of the whole rock analysis can not be used to prove inheritance, in conjunction with the older isochron, and missing high Os reservoir, they strongly suggest that the Re-Os isotopic system was not entirely reset by the Manicouagan impact.

If the whole rock analyses are showing evidence of isotopic mixing and the 315 Ma age is a mixing isochron, there are two possible older phases that could be involved, the meteorite, or the Proterozoic country rock. Isotopic mixing models using the meteorite as the contaminant do not produce realistic results due to the high Os content of meteorites. To produce the 315 Ma isochron age, there needs to be a 2.5% meteorite component (assuming a chondritic composition and an age similar to the earth) which would increase the Os content of the rock to 172 ppb which is ~11,000 times greater than the Os content of the whole rock, therefore this

model is unrealistic. A 10% addition of Proterozoic country rock is needed to create the 315 Ma isochron (assuming a 1170 Ma age for the gabbro, and a $^{187}Re/^{188}Os =$ 50 (Shirey and Walker, 1998)), which also produces a $^{187}Re/^{188}Os$ for the whole rock of 157 which is consistent with the analysis. The required inheritance appears large, but could be accounted for by a very small number of Os rich alloy grains, whereas the majority of the country rock could be located in a lower, more xenolith rich area of the melt sheet. The mixing models therefore suggest that inheritance from the Proterozoic basement is more consistent with the data and is the preferred model.

It is possible that the U-Pb and ^{40}Ar-^{39}Ar systems did not experience the same inheritance due to the subject minerals crystallizing directly from the melt rock which would have had its isotopic systems reset rather than using whole rock analysis. ^{40}Ar-^{39}Ar ages have been attempted from a whole rock sample, with poor quality late Triassic ages produced (Ramezani pers com., 2008) hinting at the possibility of inheritance.

4.5.1.2. Great Bear Magmatic Zone

^{187}Re-^{187}Os geochronology using magnetite in the GBMZ is negated by the range in $^{187}Os/^{188}Os_i$ for all of the samples. The initial isotope values can potentially be used however to trace the origin of the fluids the magnetite crystallized from if the Re-Os system in magnetite is robust. The iron oxide deposits in the GBMZ are thought to be related to Na and K rich brines associated with subduction zone magmatism beneath the Hottah arc (Hitzman et al., 1987), but this theory is unproven. Initial

122

Os isotopes are well suited to discovering the origin of the fluid, as they reflect the isotopic composition of the source. The variation in initial Os isotopes of the samples analyzed in this study suggest that the source for the fluid may have changed over time, either from an extremely high Os initial composition (~3) to a low (~0.5) or vice versa. It is likely that magnetite crystallized in equilibrium with the fluid, and therefore the trace element composition of magnetite may also reflect any provenance changes (Carew et al., 2006) and help constrain the source. Unfortunately, the provenance of the fluid is difficult to investigate for two reasons; Firstly, the samples are variably contaminated with trace mineral phases which produce unexpected peaks in elements not usually associated with magnetite. Secondly, repeat analysis of the same sample produces different $^{187}Os/^{188}Os_i$, which are not within error.

The variable contamination of magnetite with trace mineral phases most likely tourmaline, actinolite and apatite causes problems when interpreting trace element data (the magnetite is estimated to be >95% pure). Trace elements in magnetite, e.g. rare earth elements, large ion lithophile elements and high field strength elements are much more compatible in tourmaline (Jiang et al., 2004) and apatite (Prowatke and Klemme, 2006) than magnetite (Carew et al., 2006). Elements commonly present in spinel minerals, such as Al, and Mg can also be found in tourmaline, and therefore can not be used to determine fluid compositional changes.

The main problem in characterizing the fluid source for the magnetite is the

variable $^{187}Os/^{188}Os_i$ values produced from repeat sample analysis. Large sample sizes were used in an attempt to limit nugget effects and sample heterogeneity, however the calculated initial Os isotopes at 1875 Ma for repeat analysis of sample 08VJ20a3 and sample 08VJ20a3 produce similar results and vary outside of the error (which is very large, at 17-25%). The simplest explanation for the variation in initial isotopes is that the samples did not have their $^{187}Re-^{187}Os$ isotopes reset at 1875 Ma. However, regression of the two samples produces an age of 1980 $\pm$ 350 Ma with an $^{187}Os/^{188}Os_i$ =1.7 $\pm$ 2.6. This age is concurrent with the known age but the large uncertainty of the initial Os isotope value means that the value can not be used to help constrain the fluid origin. Variations in repeat analysis of magnetite samples have been documented previously. Hart et al., (2003) report γOs values of 184 and 95 for sample "ahv (mt)" and 203 and 122 for sample "dol (mt)", they indicate that the associated errors are large, but do not discuss them further. Variations in repeat analysis are not common using sulphide minerals, and may indicate that Re-Os system behaves differently in magnetite than sulphide. However, repeat analyses of the same black shale samples have been known to produce different initials. These variations have been explained by incomplete sample powder homogenization and post depositional disturbance (Kendall et al., 2009), both of these processes may have affected the GBMZ samples.

Similar spreads in $^{187}Os/^{188}Os_i$ have been found with sulphide minerals in ore settings (Lambert et al., 1998; 2000; Yang et al., 2008) and various interpretations have been used to explain the variations. Lambert et al. (1998; 2000) indicate that variable $^{187}Os/^{188}Os_i$ values can be produced from a single magmatic event due

124

to sulphides crystallizing from a continually evolving sulphide liquid, immiscible with the host magma. As the host magma assimilates the crust through which it is passing, it scavenges the Re and Os, most likely from crustal sulphides. These crustal sulphides can have very radiogenic $^{187}Os/^{188}Os_i$ and this is then transferred to the immiscible sulphide liquid from which the crystallizing sulphides originate via an equilibrium R process (where R is the effective mass of silicate magma which a mass of sulphide magma has equilibrated) (Campbell and Naldrett, 1979). Another hypothesis is presented by Yang et al. (2008) who indicate that Os diffusion can account for initial isotope variations in some magmatic sulphides. They suggest that massive sulphide grains have a greater chance of achieving Os equilibrium if R processes are occurring, because Os can diffuse under moderate temperatures (400ºC) across sulphide grain boundaries to maintain equilibrium between grains. Disseminated sulphide can not reach equilibrium because the grains are surrounded by silicate phases which block Os diffusion, therefore these minerals are more likely to retain the variable $^{187}Os/^{188}Os_i$ of the sulphide liquid.

Both of these scenarios require mafic magmatism and the crystallization of ore minerals from immiscible sulphide liquids, which is not the case for the GBMZ samples. The magnetite collected in this study is massive although hydrothermal rather than magmatic in origin (Ootes et al., 2008). Fluid inclusion studies have shown that the mineralizing temperatures were >400ºC indicating that Os diffusion could have been possible, although the initial Os variations do not support this theory. The hydrothermal nature of the crystallizing fluid indicates that that the scavenging of crustal Os was not an assimilation process such as Lambert et al.

125

(1998; 2000) but more likely a metasomatic process or a leaching of the country rock (Hedenquist and Lowenstern, 1994). Figure 4.3 shows that some crustal Os must have been involved to create the Os initials, and if the extreme radiogenic initials are ignored, the variation can be explained by mixing between seawater and average continental crust Os. $\delta^{18}O$ isotope work on the magnetites could help to indicate if multiple fluids are involved in the creation of the $^{187}Os/^{188}Os_i$ variations, and also help constrain the origin of the fluids (Hedenquist and Lowenstern, 1994). Osmium isotopes have indicated that variation is present, but are unsuitable for precisely locating the source, or identifying the components.

4.3.1.3 Laramie Anorthosite Complex

The LAC data appears the least complicated of all of the magnetite data with all the data points falling on one isochron. The problem is that the model 1 age of 1231 ± 41 Ma with $^{187}Os/^{188}Os_i$ =1.64 ± 0.15, is not within error of the known age of its host, the Sybille intrusion. The age also does not correlate with any dated event in the surrounding area and therefore is difficult to explain by isotopic resetting (Whitmeyer and Karlstrom, 2007). There are detrital zircon grains found in a quartz arenite of 1.2 Ga age close to the Idaho Wyoming boarder (Stewart et al., 2001). Paleocurrent directions indicate that the zircons most likely originated from the East, therefore there may be unidentified 1.2 Ga felsic intrusions close to the LAC. The Pike Peaks granitic batholith is late Grenvillian in age ~1.08 Ga (Smith et al., 1999) and is relatively close, in central Colorado. But there is no associated deformation or large thermal aureole associated with the intrusion and so is unlikely to have an effect on the Re-Os isotopes in magnetite 200 miles

126

away. The magnetite age is also similar to that of the Laurentian 1.2-1.1 Ga mid continental rift (Figure 3.1), although the rifting mostly took place far to the East of the LAC, large extensional faulting occurred in SW Colorado associated with the event (Whitmeyer and Karlstrom, 2007) but these are not thought to affect Re-Os isotopes. Fluids associated with the faulting could affect the magnetite Re-Os isotopes however; the major and trace element chemistry of the LAC samples does not suggest fluid alteration. It is also possible that the 1231 ± 41 Ma age produced by the magnetite reflects the true age of the Fe-Ti ferrodiorite dykes. No independent age dating has been conducted directly on the dykes, the age is assumed to be contemporaneous with the Sybille intrusion due to its proposed origin as an Fe-Ti rich immiscible liquid produced from the ferrodiorite parent magma. Geochemical modeling and major and trace element analysis suggests a genetic link between the Sybille monzosyenite and the ferrodiorite (Scoates et al., 1996; Scoates and Chamberlain, 2003), therefore it seems unlikely that magnetite from the ferrodiorite crystallized 200 Ma after the intrusion, but it can not be ruled out until precise dating of the Fe-Ti dykes takes place.

An alternative explanation for the young age is that the Re-Os system in magnetite has a low closure temperature and reflects a long cooling history of the LAC. Ar-Ar and U-Pb analyses of mineral separates from a granitic intrusion within the LAC have been used to reconstruct the cooling history of the complex (Harlan et al., 1994; Scoates and Chamberlain 2003). The geochronology and associated closure temperatures to Pb and Ar diffusion within the minerals suggests that the LAC cooled at a rate of 20-25°C/Myr for the first 30 million years until the intrusion
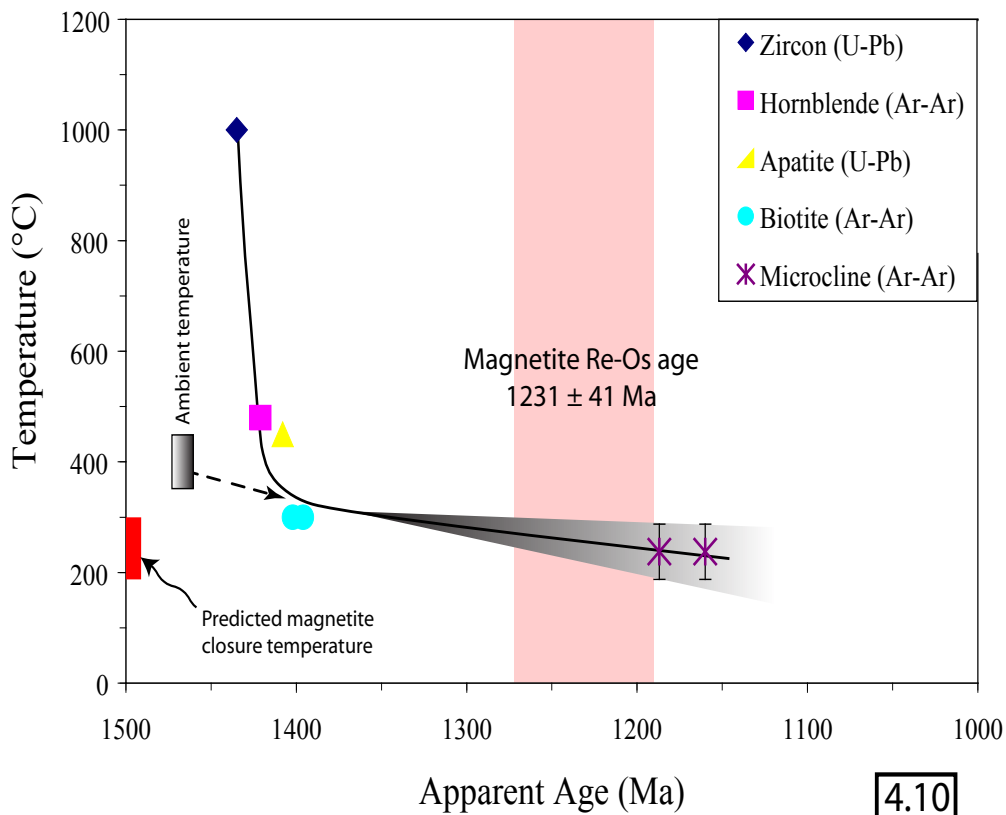
Figure 4.10

Cooling profile for the Laramie anorthosite complex as defined by the closure temperatures of various minerals, values are taken from Harlan et al. (1994) and Scoates and Chamberlain, (2003). Ambient geothermal temperature is taken from Harlan et al. (1994). Error estimates for the closure temperature of microcline to Ar diffusion are taken from Warnock and Zeitler, (1998) and are considered to be minimum error estimates.

reached an ambient temperature of ~400ºC. The final cooling stage is reported to be much slower with a rate of ~6ºC/Myr (Harlan et al., 1994). Figure 4.10 shows that the young Re-Os magnetite age for the intrusion may be explained by magnetite having a low closure temperature (~250ºC) to Os diffusion. Similar low

closure temperatures to Os diffusion have been found for some sulphide minerals e.g. pyrrhotite which has a closure temperature of 300-400ºC (Brenan et al., 2000). Re-Os geochronology using pyrrhotite and magnetite indicates that both minerals behave similarly in regards to Os diffusion (Yang et al., 2008) adding support to the low closure temperature theory for both minerals.   The implication of this finding is that magnetite may only be useful for geochronology in systems which cool quickly, and have not undergone metamorphism; therefore, magnetite from MORB or flood basalts could potentially be an ideal system for Re-Os magnetite geochronology. Magnetite analyses from Ferrar flood basalts, Tasmania, (Brauns et al., 2000) and the Fankeng flood basalts, SE China, (Zhou et al., 2005) produce precise and accurate analysis and neither have been effected by post depositional metamorphism.

4.5.2. Comparison between the results of this study and previous $^{187}Re/^{188}Os$ magnetite studies

Only two previous studies of Re and Os isotopes in magnetite have produced single mineral isochrons. Table 4.3 indicates that Brauns et al. (2000) and Zhou et al. (2005) were able to produce isochrons because of the high Re and Os content of their magnetite. No other study has found Re contents as high as these, which is presumably related to geological setting. High Re and Os contents indicate that samples were produced from high degree partial melting (>25%) of the residual mantle after all of the sulphide has been consumed. Under these conditions, platinum group element nodules are mobilized and can become concentrated into

129

spinel phases (Righter et al., 1998; Luguet et al,. 2007) which can be analyzed to find the age of the event. Other magnetite analyses from different settings do not concentrate Re and Os and are therefore less suitable for geochronology.

			Re (ppb)	Os (ppt)	Age (Ma)
Magnetite Isochron	Brauns et al., 2000	Flood Basalt	0.8-17	8-313	177.3
	Zhou et al., 2005	Flood Basalt	0.9-7	47-690	175.4
Magnetite No isochron	Hart et al., 2002	Volcanics	0.1-1	7-169	Quat
	Hart et al., 2003	Volcanics	0.3-1	2.6-44	Quat
	Chesley and Ruiz, 1998	Flood Basalt	0.5-3	39-670	17-16
	Ripley et al., 2008	Altered BIF	0.1-3.4	10-48000	1878
	Mathur et al., 2005	Ore	1.5-2	6.0-51	3
	This study	Ore	0.04-0.7	1.8-24	1875, 1231
Mixed isochron involving magnetite	Mathur et al., 2002	Ore	0.3-6	6.0-76	110
	Morgan et al., 2000	Ore	0.3-1.4	36-114	1159
	Graham et al., 2004	Kimberlite and related rocks	0.1-0.8	35-8000	2025
	This study	Impact melt rock	3.2-3.6	30-33	215

4.3

Table 4.3

Compilation of all of the published geochronology using the [187]Re-[187]Os system in magnetite, and the geological settings the magnetite originated from. The data is separated into groups based on the success of the geochronology and whether other minerals were needed to create an isochron.

Experimental data has suggested that Re and Os can be concentrated in magnetite (e.g. Righter et al., 1998), however, due to the low abundances of both of these elements in the crust (<1 ng/g Re and 0.05 ng/g Os (Shirey and Walker, 1998)), magnetite abundance becomes very important. In an ore environment (e.g. the oxide dykes in the LAC where magnetite content can be up to 75%), even if the Re and Os budgets for the intrusion are entirely constrained by magnetite, the large abundance of the mineral dilutes the Re-Os contents. Sulphide minerals are also commonly present in many ore settings (e.g. GBMZ) and they are known to have greater partition coefficients for Re and Os than magnetite (Fonseca et al., 2007), further limiting the abundance of the elements in the spinel phase.

4.4 Summary of results and conclusions regarding the ^{187}Re-^{187}Os magnetite geochronometer

Magnetite from the MIM has shown that the Re-Os system is extremely sensitive to crustal mixing and contamination. The presence of isotopic mixing was mostly controlled by whole rock analysis, whereas magnetite appeared to crystallize from a primary melt. The lack of isotopic spread caused problems with magnetite geochronology, although an imprecise age of 290 ± 64Ma was obtained from magnetite and pyroxene separates, which is close to, but not within error of the accepted age.

The GBMZ results show that magnetite could potentially be used as a tool for analysis of fluid provenance in hydrothermal ore deposits. Magnetite analysis would need to be in conjunction with another isotope system to provide robust

131

information. The initial isotopes in magnetite could in some instances be a useful tracer. The low Re-Os contents of the GBMZ data created blank issues, and large errors. The samples with the highest Re-Os contents were able to imprecisely reproduce the age of the event at 1878 ± 420 Ma.

The model 1 age produced from the LAC samples indicates that magnetite can produce spread on an isochron, and therefore the mineral has the potential for dating. The 1231 ± 41 Ma age produced by the magnetite is 200 Ma younger than the LAC, but can not be completely ruled out as a crystallization age for the magnetite until more precise and accurate dating can take place. The young age produced suggests that magnetite has a low closure temperature to Os diffusion ($\sim$200-300ºC) and is therefore not suitable to date the crystallization of systems which have cooled slowly, or have been metamorphosed.

If no other technique is available, Re-Os analysis of magnetite is capable of providing imprecise ages, but magnetite can be used in conjunction with other minerals to produce more precise crystallization ages. The low closure temperature for Os diffusion in magnetite indicates that the mineral may be useful for geochronology in un-metamorphosed MORB and flood basalts where other methods of geochronology are not possible. Also, the abundance of magnetite relative to the Re-Os content of the source has been shown to be important and should be considered when attempting geochronology.

4.6. References

Aulbach, S., Shirey, S. B., Stachel, T., Creighton, S., Muehlenbachs, K., and Harris, J. W., 2009. Diamond formation episodes at the southern margin of the Kaapvaal Craton: Re-Os systematics of sulfide inclusions from the Jagersfontein Mine. Contributions to Mineralogy and Petrology, 157(4): 525-540.

Birck, J.L., RoyBarman, M. and Capmas, F., 1997. Re-Os isotopic measurements at the femtomole level in natural samples. Geostandards Newsletter-the Journal of Geostandards and Geoanalysis, 21(1): 19-27.

Bolsover, L.R., 1986. Petrogenesis of the Sybille iron-titanium oxide deposit, Laramie anorthosite complex, Laramie Mountains, Wyoming, MSc Thesis (Unpublished) Stony Brook, New York, 78 pp.

Brauns, C.M., Hergt, J.M., Woodhead, J.D. and Maas, R., 2000. Os isotopes and the origin of the Tasmanian dolerites. Journal of Petrology, 41(7): 905-918.

Brenan, J.M., Cherniak, D.J. and Rose, L.A., 2000. Diffusion of osmium in pyrrhotite and pyrite: implications for closure of the Re-Os isotopic system. Earth and Planetary Science Letters, 180(3-4): 399-413.

Campbell, I.H. and Naldrett, A.J., 1979. Influence of silicate - sulfide ratios on the geochemistry of magmatic sulfides. Economic Geology, 74(6): 1503-1506.

Carew, M.J., Mark, G., Oliver, N.H.S. and Pearson, N., 2006. Trace element geochemistry of magnetite and pyrite in Fe oxide (+/- Cu-Au) mineralised systems: Insights into the geochemistry of ore-forming fluids. Geochimica Et Cosmochimica Acta, pp. A83-A83.

Chesley, J.T., Rudnick, R.L. and Lee, C.T., 1999. Re-Os systematics of mantle xenoliths from the East African Rift: Age, structure, and history of the Tanzanian craton. Geochimica Et Cosmochimica Acta, 63(7-8): 1203-1217.

Cohen, A.S. and Waters, F.G., 1996. Separation of osmium from geological materials by solvent extraction for analysis by thermal ionisation mass spectrometry. Analytica Chimica Acta, 332(2-3): 269-275.

Creaser, R.A., Papanastassiou, D.A. and Wasserburg, G.J., 1991. Negative thermal ion mass spectrometry of osmium, rhenium and iridium. Geochimica Et Cosmochimica Acta, 55(1): 397-401.

Desharnais, G., Peck, D.C., Scoates, R.F.J. and Halden, N.M., 2004. The KO zone: A new model for PGE-Cu-Ni mineralization in the Marginal Zone of the Fox River sill, northern Manitoba, Canada. The Canadian Mineralogist, 42: 291-302.

Duebendorfer, E.M. and Houston, R.S., 1987. Proterozoic accretionary tectonics at the southern margin of the Archean Wyoming Craton. Geological Society of America Bulletin, 98(5): 554-568.

Eggins, S.M., 1993. Origin and Differentiation of picritic arc magmas, Ambae (AOBA), Vanuatu. Contributions to Mineralogy and Petrology, 114(1): 79-100.

Farquhar, J., Chacko, T. and Frost, B.R., 1993. Strategies for high-temperature oxygen-isotope therometry - a worked example from the Laramie Anorthosite complex, Wyoming, USA. Earth and Planetary Science Letters, 117(3-4): 407-422.

Floran, R. J., Grieve, R. A. F., Phinney, W. C., Warner, J. L., Simonds, C. H.,

Blanchard, D. P., and Dence, M. R., 1978. Manicouagan impact melt, Quebec, 1, Stratigrapy, Petrology, and Chemistry. Journal of Geophysical Research, 83(NB6): 2737-2759.

Fonseca, R.O.C., Mallmann, G., O'Neill, H.S.C. and Campbell, I.H., 2007. How chalcophile is rhenium? An experimental study of the solubility of Re in sulphide mattes. Earth and Planetary Science Letters, 260(3-4): 537-548.

Gandhi, S.S., Mortensen, J.K., Prasad, N. and van Breemen, O., 2001. Magmatic evolution of the southern Great Bear continental arc, northwestern Canadian Shield: geochronological constraints. Canadian Journal of Earth Sciences, 38(5): 767-785.

Gangopadhyay, A. and Walker, R.J., 2003. Re-Os systematics of the ca. 2.7-Ga komatiites from Alexo, Ontario, Canada. Chemical Geology, 196(1-4): 147-162.

Garuti, G., Fershtater, G., Bea, F., Montero, P., Pushkarev, E. V., and Zaccarini, F., 1997. Platinum-group elements as petrological indicators in mafic-ultramafic complexes of the central and southern Urals: Preliminary results. Tectonophysics, 276: 181-194.

Graham, S., Lambert, D. and Shee, S., 2004. The petrogenesis of carbonatite, melnoite and kimberlite from the Eastern Goldfields Province, Yilgarn Craton. Lithos, 76(1-4): 519-533.

Harlan, S.S., Snee, L.W., Geissman, J.W. and Brearley, A.J., 1994. Paleomagnetism of the Middle Proterozoic Laramie anorthosite complex and Sherman Granite, southern Laramie Range, Wyoming and Colorado Journal of Geophysical Research-Solid Earth, 99(B9): 17997-18020.

135

Hart, G.L., Johnson, C.M., Shirey, S.B. and Clynne, M.A., 2002. Osmium isotope constraints on lower crustal recycling and pluton preservation at Lassen Volcanic Center, CA. Earth and Planetary Science Letters, 199(3-4): 269-285.

Hart, G.L., Johnson, C.M., Hildreth, W. and Shirey, S.B., 2003. New osmium isotope evidence for intracrustal recycling of crustal domains with discrete ages. Geology, 31(5): 427-430.

Hedenquist, J.W. and Lowenstern, J.B., 1994. The role of magmas in the formation of hydrothermal ore-deposits. Nature, 370(6490): 519-527.

Hellingwerf, R.H., Gatedal, K., Gallagher, V. and Baker, J.H., 1994. Tourmaline in the central Swedish ore district. Mineralium Deposita, 29(2): 189-205.

Hildebrand, R.S., Hoffman, P.F. and Bowring, S.A., 1987. Tectonomagmatic evolution of the 1.9 Ga Great Bear Magmatic Zone, Wopmay orogen, Northwestern Canada. Journal of Volcanology and Geothermal Research, 32(1-3): 99-118.

Hitzman, M.W., Oreskes, N. and Einaudi, M.T., 1992. Geological characteristics and tectonic setting of Proterozoic iron-oxide (Cu-U-Au-REE) Deposits. Precambrian Research, 58(1-4): 241-287.

Hoatson, D.M. and Sun, S.S., 2002. Archean layered mafic-ultramafic intrusions in the West Pilbara Craton, Western Australia: A synthesis of some of the oldest orthomagmatic mineralizing systems in the world. Economic Geology and the Bulletin of the Society of Economic Geologists, 97(4): 847-872.

Hodych, J.P. and Dunning, G.R., 1992. Did the Manicouagan impact trigger end-of-Triassic mass extinction. Geology, 20(1): 51-54.

136

Hoffman, P.F. and Bowring, S.A., 1984. Short-lived 1.9 Ga Continental-Margin and its destruction, Wopmay orogen, Northwest Canada. Geology, 12(2): 68-72.

Indares, A. and Dunning, G., 2004. Crustal architecture above the high-pressure belt of the Grenville Province in the Manicouagan area: new structural, petrologic and U-Pb age constraints. Precambrian Research, 130(1-4): 199-228.

Jiang, S.Y., Yu, J.M. and Lu, J.J., 2004. Trace and rare-earth element geochemistry in tourmaline and cassiterite from the Yunlong tin deposit, Yunnan, China: implication for migmatitic-hydrothermal fluid evolution and ore genesis. Chemical Geology, 209(3-4): 193-213.

Jicha, B. R., Johnson, C. M., Hildreth, W., Beard, B. L., Hart, G. L., Shirey, S. B., and Singer, B. S., 2009. Discriminating assimilants and decoupling deep-vs. shallow-level crystal records at Mount Adams using U-238-Th-230 disequilibria and Os isotopes. Earth and Planetary Science Letters, 277(1-2): 38-49.

Jordan, S.L., Indares, A. and Dunning, G., 2006. Partial melting of metapelites in the Gagnon terrane below the high-pressure belt in the Manicouagan area (Grenville Province): pressure-temperature (P-T) and U-Pb age constraints and implications. Canadian Journal of Earth Sciences, 43(9): 1309-1329.

Kendall, B., Creaser, R.A., Gordon, G.W. and Anbar, A.D., 2009. Re-Os and Mo isotope systematics of black shales from the Middle Proterozoic Velkerri and Wollogorang Formations, McArthur Basin, northern Australia. Geochimica Et Cosmochimica Acta, 73(9): 2534-2558.

137

Lambert, D.D., Foster, J.G., Frick, L.R., Ripley, E.M. and Zientek, M.L., 1998. Geodynamics of magmatic Cu-Ni-PGE sulfide deposits: New insights from the Re-Os isotope system. Economic Geology and the Bulletin of the Society of Economic Geologists, 93(2): 121-136.

Lambert, D.D., Frick, L.R., Foster, J.G., Li, C.S. and Naldrett, A.J., 2000. Re-Os isotope systematics of the Voisey's Bay Ni-Cu-Co magmatic sulfide system, Labrador, Canada: II. Implications for parental magma chemistry ore genesis, and metal redistribution. Economic Geology and the Bulletin of the Society of Economic Geologists, 95(4): 867-888.

Liu, Q., Hou, Q.L., Zhou, X.H. and Xie, L.W., 2005. The distribution of platinum-group elements in gabbros from Zhujiapu, Dabie orogen. Acta Petrologica Sinica, 21(1): 227-239.

Luguet, A., Shirey, S.B., Lorand, J.P., Horan, M.F. and Carlson, R.W., 2007. Residual platinum-group minerals from highly depleted harzburgites of the Lherz massif (France) and their role in HSE fractionation of the mantle. Geochimica Et Cosmochimica Acta, 71(12): 3082-3097.

Mallmann, G. and O'Neill, H.S.C., 2007. The effect of oxygen fugacity on the partitioning of Re between crystals and silicate melt during mantle melting. Geochimica Et Cosmochimica Acta, 71(11): 2837-2857.

Marques, J.C., Ferreira, C.F., Carlson, R.W. and Pimentel, M.M., 2003. Re-Os and Sm-Nd isotope and trace element constraints on the origin of the chromite deposit of the Ipueira-Medrado sill, Bahia, Brazil. Journal of Petrology, 44(4): 659-678.

Mathur, R. et al., 2002. Age of mineralization of the candelaria Fe oxide Cu-Au

deposit and the origin of the Chilean iron belt, based on Re-Os isotopes. Economic Geology and the Bulletin of the Society of Economic Geologists, 97(1): 59-71.

Mathur, R., Titley, S., Ruiz, J., Gibbins, S. and Friehauf, K., 2005. A Re-Os isotope study of sedimentary rocks and copper-gold ores from the Ertsberg District, West Papua, Indonesia. Ore Geology Reviews, 26(3-4): 207-226.

Mitchell, J.N., Scoates, J.S., Frost, C.D. and Kolker, A., 1996. The geochemical evolution of anorthosite residual magmas in the Laramie Anorthosite Complex, Wyoming. Journal of Petrology, 37(3): 637-660.

Mondal, S.K., Frei, R. and Ripley, E.M., 2007. Os isotope systematics of mesoarchean chromitite-PGE deposits in the Singhbhum Craton (India): Implications for the evolution of lithospheric mantle. Chemical Geology, 244(3-4): 391-408.

Morelli, R. M., Creaser, R. A., Selby, D., Kelley, K. D., Leach, D. L., and King, A. R., 2004. Re-Os sulfide geochronology of the Red Dog sediment-hosted Zn-Pb-Ag deposit, Brooks Range, Alaska. Economic Geology, 99(7): 1569-1576.

Morelli, R.M., Creaser, R., Selby, D., Kontak, D.J. and Horne, R.J., 2005. Rhenium-osmium geochronology of arsenopyrite in Meguma group gold deposits, Meguma terrane, Nova Scotia, Canada: Evidence for multiple gold-mineralizing events. Economic Geology, 100(6): 1229-1242.

Morgan, J.W., Golightly, D.W. and Dorrzapf, A.F., 1991. Methods for the separation of Rhenium, Osmium and Molybdenum applicable to isotope geochemistry Talanta, 38(3): 259-265.

139

Morgan, J.W., Stein, H.J., Hannah, J.L., Markey, R.J. and Wiszniewska, J., 2000. Re-Os study of Fe-Ti-V oxide and Fe-Cu-Ni sulfide deposits, Suwalki Anorthosite Massif, northeast Poland. Mineralium Deposita, 35(5): 391-401.

Ootes, L., Goff, S., Gleeson, S., Jackson, V., Creaser, R., Evensen, N., Samson, I., Corriveau, L., and Mumin, A.H., 2008. Field relationships, petrography, chronology, and fluid character or the Nori/RA Cu-Mo-U (± REE & W) prospect: An 'early' OPCG example in the Great Bear Magmatic Zone? Northwest Territories Yellowknife Geoscience Forum, Yellowknife.

Pearson, D.G., Parman, S.W. and Nowell, G.M., 2007. A link between large mantle melting events and continent growth seen in osmium isotopes. Nature, 449(7159): 202-205.

Prowatke, S. and Klemme, S., 2006. Trace element partitioning between apatite and silicate melts. Geochimica Et Cosmochimica Acta, 70(17): 4513-4527.

Ramezani, J., Bowring, S.A., Pringle, M.S., Winslow, F.D. and Rasbury, E.T., 2005. The Manicouagan impact melt rock: A proposed standard for the intercalibration of U-Pb and Ar-40/Ar-39 isotopic systems. Geochimica Et Cosmochimica Acta, 69(10): A321-A321.

Richardson, S.H. and Shirey, S.B., 2008. Continental mantle signature of Bushveld magmas and coeval diamonds. Nature, 453(7197): 910-913.

Righter, K., Chesley, J.T., Geist, D. and Ruiz, J., 1998. Behavior of Re during magma fractionation: an example from Volcan Alcedo, Galapagos. Journal of Petrology, 39(4): 785-795.

Righter, K. and Downs, R.T., 2001. The crystal structures of synthetic Re- and

PGE-bearing magnesioferrite spinels: Implications for impacts, accretion and the mantle. Geophysical Research Letters, 28(4): 619-622.

Righter, K., Chesley, J.T., Calazza, C.M., Gibson, E.K. and Ruiz, J., 2008. Re and Os concentrations in arc basalts: The roles of volatility and source region fO(2) variations. Geochimica Et Cosmochimica Acta, 72(3): 926-947.

Selby, D. and Creaser, R.A., 2003. Re-Os geochronology of organic rich sediments: an evaluation of organic matter analysis methods. Chemical Geology, 200(3-4): 225-240.

Scoates, J.S. and Chamberlain, K.R., 2003. Geochronologic, geochemical and isotopic constraints on the origin of monzonitic and related rocks in the Laramie anorthosite complex, Wyoming, USA, pp. 269-304.

Scoates, J.S., Frost, C.D., Mitchell, J.N., Lindsley, D.H. and Frost, B.R., 1996. Residual-liquid origin for a monzonitic intrusion in a mid-Proterozoic anorthosite complex: The Sybille intrusion, Laramie anorthosite complex, Wyoming. Geological Society of America Bulletin, 108(11): 1357-1371.

Shirey, S.B. and Walker, R.J., 1998. The Re-Os isotope system in cosmochemistry and high-temperature geochemistry. Annual Review of Earth and Planetary Sciences, 26: 423-500.

Smith, D. R., Noblett, J., Wobus, R. A., Unruh, D., Douglass, J., Beane, R., Davis, C., Goldman, S., Kay, G., Gustavson, B., Saltoun, B., and Stewart, J., 1999. Petrology and geochemistry of late-stage intrusions of the A-type, mid-Proterozoic Pikes Peak batholith (Central Colorado, USA): implications for petrogenetic models. Precambrian Research, 98(3-4): 271-305.

Stein, H.J., Morgan, J.W. and Schersten, A., 2000. Re-Os dating of low-level highly

radiogenic (LLHR) sulfides: The Harnas gold deposit, southwest Sweden, records continental-scale tectonic events. Economic Geology and the Bulletin of the Society of Economic Geologists, 95(8): 1657-1671.

Sun, W.D., Bennett, V.C., Eggins, S.M., Kamenetsky, V.S. and Arculus, R.J., 2003. Enhanced mantle-to-crust rhenium transfer in undegassed arc magmas. Nature, 422(6929): 294-297.

Volkening, J., Walczyk, T. and G. Heumann, K., 1991. Osmium isotope ratio determinations by negative thermal ionization mass spectrometry. International Journal of Mass Spectrometry and Ion Processes, 105(2): 147-159.

Walker, R.J., Prichard, H.M., Ishiwatari, A. and Pimentel, M., 2002. The osmium isotopic composition of convecting upper mantle deduced from ophiolite chromites. Geochimica Et Cosmochimica Acta, 66(2): 329-345.

Walker, R.J. and Nisbet, E., 2002. Os-187 isotopic constraints on Archean mantle dynamics. Geochimica Et Cosmochimica Acta, 66(18): 3317-3325.

Warnock, A.C. and Zeitler, P.K., 1998. Ar-40/Ar-39 thermochronometry of K-feldspar from the KTB borehole, Germany. Earth and Planetary Science Letters, 158(1-2): 67-79.

Whitmeyer, S.J. and Karlstrom, K.E., 2007. Tectonic model for the Proterozoic growth of North America. Geosphere, 3(4): 220-259.

Yang, S.H., Qu, W. J., Tian, Y. L., Chen, J. F., Yang, G., and Du, A. D., 2008. Origin of the inconsistent apparent Re-Os ages of the Jinchuan Ni-Cu sulfide ore deposit, China: Post-segregation diffusion of Os. Chemical Geology, 247(3-4): 401-418.

142

Zhou, J.C., Jiang, S.Y., Wang, X.L., Yang, J.H. and Zhang, M.Q., 2005. Re-Os isochron age of Fankeng basalts from Fujian of SE China and its geological significance. Geochemical Journal, 39(6): 497-502.

5 Conclusion

The ^{187}Re-^{187}Os system has been investigated in magnetite and other oxide minerals from a range of well dated geological settings to test the potential for geochronology. Magnetite and oxide minerals from Drybones Bay, Kyle Lake and Iron Mountain kimberlites and Whitefish Lake, Pele and Torngat lamprophyres from North America and Premier kimberlite South Africa have shown that the ^{187}Re-^{187}Os system is not suitable for geochronology. The reason for this is that the oxide minerals contain different initial Os isotopic compositions and therefore do not plot as a straight line on an isochron diagram. Chromite content of the oxide mineral phases appears to control the Os abundance within the samples, although it is not clear whether the Os is located within the crystal structure, or is contained within micro PGE alloys. Back scattered electron imaging of a selection of oxide minerals from each sample did not identify PGE alloys, which may not be surprising as mass balance calculations suggest that the entire Os budget for the sample may be taken up by one 2μm diameter nugget in some cases. The initial Os isotopic composition of the samples back corrected for ^{187}Os added since emplacement suggests that the host magmas for Kyle Lake, Iron Mountain, Torngat and Premier intrusions, were from depleted portions of the CLM which had remained isolated from the convecting mantle for long periods of time. Whitefish Lake, Pele and Drybones Bay contained radiogenic Os isotopes and evidence of post emplacement alteration and therefore interpretations regarding their source region could not be made. T_{RD} and T_{MA} ages calculated from the unaltered samples are in general agreement with previously published depletion ages where they are available, and appear to correlate well with

the timing of major crustal events proximal to the intrusions. The results suggest Re-Os isotopes in oxide minerals from kimberlites and lamprophyres can be used to study the age of the CLM and the timing of crustal formation events. Previously, the only samples amenable to this type of study were mantle xenoliths or xenocrysts. Magmatic oxide minerals from kimberlites and lamprophyres are much more abundant than mantle xenoliths/xenocrysts because they are a major magmatic phase rather than a geological hitchhiker. Further tests need to be conducted before oxide minerals can be used systematically to investigate the CLM as only four out of seven samples produced meaningful results in this study. However, due to the large and increasing database of well dated kimberlites and related rocks, there are numerous opportunities for further analysis.

As well as investigating the ^{187}Re-^{187}Os system in oxide minerals from mantle derived magmas, magnetite crystallized from crustal sources was also examined in order to assess its potential for precise and accurate ^{187}Re-^{187}Os geochronology. The areas chosen for study were the Manicouagan impact melt rock, massive magnetite veins from the Great Bear magmatic zone and the Laramie anorthosite complex. All of the areas have been previously dated using U-Pb zircon dating amongst other isotope systems. The results suggest that the ^{187}Re-^{187}Os system in magnetite can not systematically be used for precise and accurate dating. The Re and Os contents of the magnetite analyzed were very low (1-33 ppt Os) and therefore were subject to large blank associated errors. The magnetite from Manicouagan plotted as a single point on an isochron and therefore was not suitable for geochronology. When a pyroxene mineral separate was added, an age of 290 ± 64 Ma was produced, which

145

is close to the known age (215 Ma) although not within error. Magnetite from the Great Bear magmatic zone contained the lowest Os abundances (1-22 ppb) and was therefore the most affected by the blank contribution. Precise and accurate geochronology was not possible from these samples either, but the initial Os isotopes of the magnetite could be used to show that the source for the Os changed over time, and was most likely a mixture of Os from Paleoproterozoic seawater and continental crust. The magnetite from the Laramie anorthosite complex produced a model 1 isochron age of 1231 ±41 Ma, which is not within error of the known age (1440-1430 Ma). However, when this result plotted on a cooling curve of the anorthosite complex produced from Ar-Ar and U-Pb analysis of mineral separates with different closure temperatures, it is shown that magnetite has a low (200-300ºC) closure temperature to Os diffusion. The low closure temperature of magnetite to Os diffusion, and the very low Os contents suggest that, in the future, magnetite should only be used as a geochronometer in areas which have not experienced metamorphism, or where other techniques are available. Possible areas for future research using the ^{187}Re-^{187}Os system in magnetite are, banded iron formations, mid ocean ridge basalt and flood basalt provinces.

The ^{187}Re-^{187}Os system in magnetite and other oxide minerals can provide valuable information regarding the depletion ages of continental lithospheric mantle where errors of ± 0.4 Ga are acceptable. Whereas, as a tool for precise and accurate crustal level geochronology, magnetite should be used to only provide an estimate of the age. The low closure temperature of magnetite to Os diffusion also indicates that ^{187}Re-^{187}Os isochrons involving magnetite in areas which have

undergone metamorphism should be interpreted with caution.

Appendix

Spinel microprobe data

Spinel ID	TiO_2	MgO	MnO	Cr2O3	Al_2O_3	Fe_2O_3	FeO	Total
WFL-3	21.3	4.9	1.0	0.6	3.1	26.0	42.6	100.1
WFL-5	21.8	4.5	0.9	0.6	3.3	24.2	43.9	99.8
WFL-6	18.4	7.1	0.3	2.1	14.3	16.1	38.7	97.4
WFL-7	17.7	8.6	0.6	3.8	15.1	15.3	35.5	97.0
WFL-9	20.9	6.4	1.3	0.5	3.0	27.3	39.5	99.5
WFL-12	21.6	6.3	1.2	1.1	4.2	24.0	40.5	99.5
WFL-14	20.8	6.9	1.1	0.9	4.8	25.0	38.8	99.0
WFL-17	19.8	7.5	1.4	1.5	2.9	29.0	36.4	99.0
WFL-18	21.6	8.5	1.5	0.7	4.5	25.6	37.1	99.8
WFL-20	20.1	4.5	1.0	0.7	1.0	30.1	41.6	99.4
WFL-23	20.9	5.1	1.6	0.9	2.4	26.1	40.7	98.3
KL-1	8.2	9.1	0.5	9.4	2.3	45.5	24.6	99.8
KL-2	2.8	11.9	0.6	48.3	8.1	10.6	17.0	99.8
KL-3	2.8	12.0	0.6	48.4	9.5	9.2	17.2	100.2
KL-4	2.9	9.6	0.5	49.2	8.9	5.5	19.8	96.8
KL-5	9.0	8.1	0.5	5.7	2.0	47.5	26.7	99.8
KL-6	9.4	7.8	0.5	3.9	2.0	47.8	27.4	99.2
KL-7	9.8	7.7	0.5	3.4	2.0	47.3	27.8	98.8
KL-8	6.8	4.6	0.7	0.1	0.3	57.0	29.2	99.2
KL-9	7.8	5.0	0.6	0.1	0.6	54.6	29.7	98.9
KL-10	9.5	6.6	0.6	2.1	2.0	47.8	28.8	97.8
KL-11	9.2	6.7	0.6	2.5	1.8	47.5	28.0	96.8
KL-12	2.6	8.3	0.5	47.0	8.4	7.9	21.5	96.6
KL-13	8.9	7.8	0.6	6.4	2.3	46.2	27.1	99.7
KL-14	9.5	4.4	0.5	4.9	2.0	44.2	32.6	98.6
KL-15	2.5	7.9	0.5	47.2	8.2	7.8	22.0	96.5
KL-17	9.1	7.4	0.5	2.9	1.8	49.3	27.5	98.9
KL-18	5.6	8.2	1.2	42.8	6.5	11.0	24.0	100.0
KL-19	9.6	6.7	0.4	3.4	1.9	46.5	29.1	98.0
KL-20	9.6	7.4	0.6	4.8	2.0	45.9	27.8	98.6
KL-21	10.0	4.1	0.6	2.9	1.6	45.4	33.1	98.0
KL-22	8.7	4.3	0.4	4.9	2.0	45.9	32.3	99.1
KL-23	9.2	3.4	0.4	2.9	1.9	46.0	33.8	98.2
KL-24	11.7	4.0	0.6	4.8	1.4	41.5	35.2	99.8
P-1	9.8	2.1	0.7	0.1	1.9	48.4	36.4	99.9
P-2	9.5	2.6	0.7	0.0	1.8	49.4	35.4	99.9

P-3	19.5	6.0	1.2	0.9	9.3	21.6	39.8	98.6
P-4	18.2	7.5	0.9	1.2	10.3	23.4	36.9	98.9
P-6	17.9	3.7	0.9	0.2	8.8	23.3	41.6	96.9
P-lt-1	21.2	2.3	1.5	3.9	6.2	15.7	46.1	97.4
P-lt-2	21.1	2.7	1.3	1.7	5.7	17.7	45.1	97.3
P-lt-3	23.3	2.9	1.2	2.1	5.8	15.3	47.4	98.6
P-lt-4	31.7	6.4	1.1	1.2	5.2	2.2	49.7	98.3
P-lt-5	21.4	4.3	1.2	1.3	9.0	16.6	44.1	98.4
P-lt-6	20.6	4.6	1.1	1.1	9.7	17.5	43.0	98.3
P-lt-7	16.3	3.4	0.8	1.0	3.8	32.2	40.1	98.3
P-lt-8	15.7	4.2	0.8	0.7	4.0	33.4	38.3	97.7
P-9	22.3	2.0	0.8	10.4	6.5	8.4	49.0	100.0
P-11	28.6	1.8	1.3	2.0	6.1	4.3	54.1	98.8
P-12	19.2	2.0	1.1	1.1	9.4	19.3	45.8	98.4
P-13	16.3	2.7	0.7	1.1	7.2	28.2	42.3	99.2
P-14	17.1	3.8	0.7	0.6	5.5	28.7	40.5	97.3
P-17	20.1	4.8	0.9	1.6	6.8	20.9	41.6	97.3
P-19	15.8	3.8	0.8	0.8	4.0	34.1	39.5	99.2
P-20	11.7	1.6	0.4	0.7	1.2	40.7	39.1	96.7
P-21	7.6	12.1	0.3	31.3	15.1	11.4	22.5	100.8
P-22	6.6	12.6	0.3	31.4	17.3	11.0	21.4	101.1
P-24	6.5	12.3	0.3	33.0	16.3	10.9	21.5	101.4
P-25	6.4	12.0	0.3	32.8	16.5	10.4	21.8	100.8
P-26	18.1	3.0	0.8	1.8	11.0	19.0	43.9	98.3
P-31	20.1	2.8	1.2	0.5	9.3	18.9	45.4	98.7
P-32	17.7	3.0	0.9	0.3	8.3	24.3	42.8	97.9
P-33	10.5	14.2	0.4	15.5	18.1	19.0	21.9	100.1
P-34	20.3	3.0	1.5	0.9	9.7	16.8	44.5	97.3
TL-1	5.7	9.5	0.5	26.9	9.0	25.5	23.6	101.3
TL-2	4.2	7.0	0.4	26.2	8.0	28.7	25.6	100.7
TL-3	8.9	6.3	0.8	8.8	2.0	44.6	29.6	101.3
TL-7	5.7	5.9	0.6	0.2	0.5	60.6	26.7	100.9
TL-11	12.7	7.3	0.9	0.1	2.0	46.1	31.2	100.6
TL-12	14.1	7.2	0.8	0.7	1.9	42.3	32.5	99.7
TL-13	13.2	7.7	0.9	0.4	1.9	45.2	31.3	101.0
TL-14	12.2	7.4	1.0	6.1	2.0	40.2	30.3	99.5
TL-16	18.6	4.9	2.7	1.5	0.6	32.5	37.7	99.2
TL-18	17.2	7.7	0.9	1.5	1.2	36.7	34.0	99.9
TL-19	14.4	7.5	0.8	1.2	1.8	42.7	32.5	101.3
TL-23	15.0	7.3	0.9	1.0	1.7	41.2	33.5	101.0
TL-24	16.1	8.1	1.0	1.1	1.7	38.9	32.9	100.3

149

TL-28	12.9	7.5	0.9	0.2	1.7	45.6	31.0	100.2
TL-29	14.9	8.6	0.8	22.4	2.5	18.0	31.2	99.1
TL-31	20.3	9.5	1.0	5.4	1.6	26.6	34.6	99.5
TL-34	11.3	6.9	1.0	0.1	1.8	48.6	30.3	100.6
TL-35	13.5	7.8	1.0	5.5	1.7	39.5	31.0	100.5
TL-36	14.3	7.7	0.9	1.2	1.7	42.9	32.0	101.1
TL-38	14.4	8.0	0.9	1.6	2.1	41.7	31.9	100.9
TL-40	15.8	8.4	1.0	0.7	1.7	40.7	32.5	101.4
TL-41	16.0	8.2	1.0	0.7	1.8	40.1	32.8	101.1
IM-1-1	1.2	10.8	0.5	61.8	1.4	7.6	16.1	99.6
IM-1-2	5.6	16.0	0.6	45.8	5.8	13.8	13.0	100.9
IM-2-1	5.6	14.8	0.7	45.6	7.4	11.2	14.9	100.4
IM-2-2	5.9	17.3	0.7	14.6	12.5	38.2	12.2	101.7
IM-3-1	5.8	17.1	0.7	16.1	12.3	37.2	12.4	101.8
IM-3-2	4.7	14.5	0.8	38.9	6.6	19.6	13.8	99.1
IM-3-3	5.9	12.0	0.8	0.2	4.8	58.2	18.0	100.3
IM-4-1	6.2	16.3	0.7	41.8	6.1	16.7	12.9	101.1
IM-4-2	7.1	12.4	0.8	0.5	3.5	57.4	18.7	100.6
IM-4-3	5.7	11.6	0.7	0.5	3.4	59.4	18.5	100.2
IM-4-4	7.5	16.4	0.6	32.0	6.3	23.5	13.8	100.4
IM-5-1	6.9	16.8	0.6	30.4	6.4	26.5	12.3	100.9
IM-5-3	15.0	17.5	0.7	0.3	6.2	42.4	18.7	101.4
IM-5-4	7.2	12.4	0.8	0.3	5.9	54.4	19.1	100.4
IM-5-5	5.5	12.7	0.7	0.4	3.1	61.7	16.8	101.4
IM-6-1	0.2	12.7	0.4	43.1	17.5	9.3	14.3	97.7
IM-6-2	0.2	13.1	0.4	43.3	17.3	9.9	13.7	98.0
IM-6-3	1.1	16.0	0.5	41.3	17.7	12.6	10.6	100.2
IM-6-4	0.2	12.3	0.4	43.2	18.1	8.4	15.1	98.1
IM-np-1	7.0	13.1	0.8	0.4	4.7	56.4	18.0	101.0
IM-np-2	12.7	17.0	0.7	1.9	7.9	42.9	18.0	101.4
IM-np-3	5.1	9.1	1.1	0.3	1.5	60.8	21.1	99.6
IM-np-4	6.0	14.3	0.7	45.6	5.5	12.4	15.7	100.4
IM-np-5	6.6	12.5	0.9	0.5	4.3	57.6	18.0	100.7
IM-np-6	4.5	11.9	0.7	0.3	5.4	46.5	23.1	97.6
IM-np-7	6.5	13.1	0.8	0.6	4.2	56.8	17.1	99.5
IM-np-8	0.1	12.6	0.4	50.3	17.2	4.4	15.3	100.6
IM-np-9	5.8	13.4	0.6	0.4	5.5	47.5	20.6	97.9
IM-np-10	6.0	16.1	0.7	40.3	6.6	17.8	12.7	100.8
IM-np-11	5.1	15.7	0.7	45.2	5.6	14.2	12.3	99.0
IM-np-12	5.4	9.6	0.9	0.4	4.8	57.0	21.2	99.6
IM-np-13	5.8	13.0	0.7	0.7	5.5	55.5	17.4	99.5

150

IM-np-14	6.8	16.5	0.6	39.1	6.9	16.1	12.8	99.4
IM-np-15	6.2	16.0	0.7	39.5	7.3	16.4	13.1	99.5
IM-np-16	11.8	16.8	0.7	0.5	9.1	43.8	17.2	100.2
IM-np-17	6.6	12.5	0.8	0.4	4.1	57.4	18.0	100.0
IM-np-18	6.3	14.6	0.6	40.2	8.8	13.8	16.3	100.9
IM-np-19	5.8	13.0	0.8	0.5	4.6	59.6	17.0	101.5
IM-np-20	6.6	12.9	0.8	0.4	4.5	58.3	17.9	101.6
Prem 3-1	0.3	7.8	0.4	44.2	13.9	11.4	22.2	100.6
Prem 3-2	0.3	7.8	0.4	44.1	13.8	11.4	22.2	100.4
Prem 3-3	0.2	7.4	0.4	47.1	11.5	10.3	21.9	99.2
Prem 3-4	0.2	7.8	0.4	46.5	12.2	10.8	21.7	99.8
Prem 3-5	2.1	2.1	1.0	25.6	3.8	33.4	29.0	97.4
Prem 5-1	16.0	4.3	1.7	8.2	10.5	17.8	38.8	98.1
Prem 5-2	12.4	3.9	1.6	11.8	12.2	18.8	36.3	97.8
Prem 5-3	14.3	4.0	1.7	9.7	11.2	18.5	37.7	98.0
Prem 5-5	1.8	0.3	0.4	1.5	0.8	61.5	32.4	99.7
Prem 5-6	14.9	4.2	1.7	8.8	10.9	18.8	37.9	97.9
Prem 9-3	6.0	5.9	1.6	25.6	2.8	23.0	31.5	100.4
Prem 9-15	0.3	8.2	0.4	44.1	13.8	11.8	21.6	100.5

Ilmenite microprobe data

Ilmenite ID	TiO_2	MgO	MnO	Cr_2O_3	Al2O3	Fe_2O_3	FeO	Total
WFL-16	50.9	13.7	0.8	1.4	1.3	10.5	20.5	99.2
WFL-19	53.6	13.2	1.2	1.0	0.6	7.2	23.2	100.3
P-lt-1	48.3	14.1	0.4	2.7	1.2	15.0	17.8	99.6
P-lt-2	48.7	13.4	0.4	3.0	0.9	13.7	19.3	99.6
P-lt-3	49.9	13.7	0.5	1.9	0.7	12.4	19.8	99.1
P-8	48.9	11.6	0.3	4.6	1.3	9.6	23.0	99.5
P-10	49.0	12.9	0.4	3.5	1.0	13.3	20.5	100.8
P-15	48.5	12.6	0.4	4.4	1.0	12.0	20.8	99.9
P-16	48.2	12.3	0.4	4.8	1.1	12.0	21.0	99.9
P-18	51.3	12.5	0.4	2.5	0.8	8.5	23.5	99.7
P-23	53.1	5.8	1.3	1.2	0.0	2.4	36.1	100.1
P-29	48.8	0.7	0.9	0.0	0.1	3.4	41.2	96.8
P-30	47.7	12.0	0.4	5.9	1.1	11.1	21.1	99.3
TL-21	47.3	11.8	0.8	1.6	0.1	16.1	20.8	98.7
TL-22	46.7	11.4	0.8	1.1	0.3	16.4	21.1	98.3
TL-30	44.7	10.4	0.5	4.3	0.4	16.0	21.1	97.5

TL-32	45.0	11.0	0.6	4.3	0.3	16.6	20.2	98.1
DB-3	41.3	5.4	0.2	0.5	0.2	23.5	27.3	98.5
DB-4	41.0	5.5	0.2	0.5	0.2	24.4	26.8	98.8
DB-5	42.0	5.9	0.2	0.6	0.2	23.2	27.0	99.3
DB-6	50.5	12.1	0.6	3.2	0.1	10.1	23.1	99.8
DB-7	50.3	11.6	0.6	3.3	0.1	9.3	23.9	99.2
DB-8	40.3	4.1	0.2	0.7	1.3	19.7	28.7	95.1
DB-9	41.9	6.5	0.2	0.5	1.0	22.1	26.0	98.4
DB-10	49.1	10.9	0.5	3.8	0.1	9.7	24.2	98.3
DB-11	36.7	4.1	0.1	0.6	0.2	31.1	25.5	98.4
DB-12	36.4	4.2	0.2	0.7	0.2	31.4	25.1	98.2
DB-13	37.4	4.5	0.2	0.7	0.2	29.7	25.6	98.2
DB-14	40.0	5.2	0.2	0.6	0.2	25.5	26.6	98.3
DB-15	39.9	5.3	0.2	0.5	0.2	25.6	26.2	98.1
DB-16	37.9	4.6	0.2	0.7	0.2	28.8	25.7	98.2
DB-17	37.5	4.4	0.2	0.5	0.2	30.2	25.8	98.8
DB-18	36.7	4.0	0.2	0.7	0.2	31.5	25.6	98.9
DB-19	36.5	4.0	0.2	0.6	0.2	31.1	25.6	98.3
DB-20	37.9	4.7	0.2	0.7	0.2	29.1	25.6	98.4
DB-21	38.2	4.6	0.2	0.7	0.2	28.7	25.9	98.4
DB-22	38.1	4.7	0.2	0.7	0.2	29.2	25.7	98.8
DB-23	38.1	4.6	0.2	0.6	0.2	28.9	25.9	98.6
DB-24	37.7	5.2	0.2	0.7	0.2	29.6	24.4	98.1
DB-25	41.9	6.4	0.2	1.1	0.3	22.3	26.1	98.4
DB-26	39.2	5.0	0.2	0.5	0.2	27.0	26.1	98.3
DB-27	39.3	5.0	0.2	0.6	0.2	26.9	26.2	98.5
DB-28	39.4	5.1	0.2	0.6	0.2	26.7	26.3	98.6
Prem 1-2	48.6	0.9	7.0	0.5	0.3	6.3	35.0	98.7
Prem 1-3	52.8	12.5	0.3	0.7	0.4	6.8	24.8	98.4
Prem 2-1	50.9	11.4	0.4	0.8	1.3	8.9	25.2	99.0
Prem 2-2	47.7	0.9	6.6	0.5	0.2	8.2	34.7	98.9
Prem 2-3	46.7	0.9	6.2	0.5	0.2	8.6	34.2	97.5
Prem 2-4	51.4	11.1	0.4	0.6	0.5	8.7	26.1	98.9
Prem 2-5	48.3	2.7	4.8	0.5	0.2	8.3	33.8	98.6
Prem 2-6	51.4	10.8	0.3	0.5	0.3	8.6	26.7	98.7
Prem 7-1	50.9	14.8	0.4	2.5	1.1	8.1	18.3	97.2
Prem 7-2	54.0	14.3	0.7	0.6	0.2	6.0	21.8	98.2
Prem 7-3	47.1	3.5	5.3	2.5	1.4	8.4	30.1	99.1
Prem 7-4	48.5	1.9	5.7	0.8	0.1	6.2	34.0	97.9

152

Prem 8-6	49.1	0.8	7.5	0.5	0.6	5.9	35.2	99.8
Prem 8-7	48.2	0.4	8.8	0.5	0.4	5.5	34.4	98.8
Prem 9-9	52.0	13.9	0.3	0.9	2.0	7.0	21.7	98.0
Prem 9-10	52.4	11.4	1.1	0.4	0.2	6.7	25.8	98.0
Prem 9-13	49.8	9.4	0.4	0.6	0.2	10.5	27.8	98.8
Prem 9-14	47.0	2.0	8.1	0.4	0.5	7.0	32.8	99.7
Prem 9-19	49.6	7.2	2.0	1.1	0.3	9.3	29.8	99.4
Prem 9-20	52.9	15.1	0.3	1.3	0.9	7.7	20.4	98.6
Prem 9-21	52.5	12.7	0.5	1.0	0.8	6.8	24.2	98.7
Prem 9-23	46.2	1.2	7.8	1.4	0.7	8.5	32.3	98.9
Prem 9-24	51.1	11.4	0.4	0.5	0.2	9.0	25.2	97.9
Prem 9-25	51.2	11.6	0.4	0.5	0.2	9.2	25.0	98.2